

February 8, 2020

# THE PHYSICS OF A SEXTET QUARK SECTOR\*

Alan. R. White<sup>†</sup>

Argonne National Laboratory  
9700 South Cass, IL 60439, USA.

## Abstract

Electroweak symmetry breaking can be a consequence of color sextet quark chiral symmetry breaking, with sextet pions producing the longitudinal components of the electroweak vector bosons. If so, a special solution of QCD is involved, for which the high-energy S-Matrix can be constructed “semi-perturbatively” via the chiral anomaly and reggeon diagrams. An infra-red fixed point and the starting point of color superconductivity are crucial components of the construction of the massless theory. The spectrum is consistent with, but is more limited than is required by, confinement and chiral symmetry breaking. Infinite momentum physical states contain both quarks and a universal “anomalous wee gluon” component. The pomeron is approximately a regge pole and the Critical Pomeron describes asymptotic cross-sections.

Because the electroweak mass scale is related to the wee gluon coupling to sextet quarks, the pomeron couples strongly to the electroweak sector. This coupling could produce large  $x$  and  $Q^2$  events at HERA, and vector boson pairs at Fermilab. Further evidence for the sextet sector at Fermilab would be a large  $E_T$  jet excess due, in part, to the non-evolution of  $\alpha_s$ , and other phenomena related to the possibility that top quark production is due to the  $\eta_6$ .

The sextet proton and neutron are the only new baryonic states, with masses that are  $\gtrsim 500$  GeV. Sextet states will dominate high energy hadronic cross-sections and, since sextet neutrons are absolutely stable, they could produce the dominance of dark matter in the universe and also, perhaps, ultra high energy cosmic rays. Other cosmic ray phenomena, particularly the spectrum knee, suggest that the effective sextet sector threshold is between Fermilab and LHC energies. If this is the case, then large cross-section effects are to be expected at the LHC. Jet and vector boson cross-sections will be very much larger than expected and sextet baryons should also be produced. Double pomeron produced states could provide definitive evidence for the existence of the sextet sector in the initial low luminosity running of the LHC.

---

\*Work supported by the U.S. Department of Energy under Contract W-31-109-ENG-38

<sup>†</sup>arw@hep.anl.gov

## 1. INTRODUCTION

The initial pursuit[1, 2], nearly thirty years ago, of a particular solution of supercritical Reggeon Field Theory (RFT) has led us to first associate the Critical Pomeron[3] with a special high-energy solution of QCD, then to connect this QCD solution to a very particular form of electroweak symmetry breaking[4, 5]. If this is the symmetry breaking and solution of QCD chosen by nature then, as outlined in [6] and [7], we anticipate that there is a major change in the strong interaction above the electroweak scale. A new color sextet sector appears, with electroweak scale masses, that at high enough energies should become responsible for the major part of the total cross-section. The existence of this sector offers a natural explanation for the dominance of dark matter and in fact, an interaction change of just this kind could be responsible for the apparent “knee” in the cosmic ray spectrum that occurs just above the Tevatron energy. Other cosmic ray phenomena that occur above the knee energy, also appear to be clear evidence for the same interaction change. That the knee is associated with the effective energy threshold for the sextet sector would be natural if inclusive pomeron exchange has to be involved when sextet states are produced, with large cross-section, from initial triplet states.

We should emphasize that it could well be that the knee is not associated with sextet physics. If it is, however, then large cross-section effects have to appear very rapidly as the energy increases and they should be apparent at the LHC, with dramatic and exciting physics involved. In particular, jet cross-sections and electroweak vector boson cross-sections will be overwhelmingly large and pomeron exchange cross-sections will be of particular interest. Some indication of this physics could be observable at the Tevatron, or even at HERA. Hints, that may already have been seen, are the large  $E_T$  jet excess at the Tevatron and large  $x$  and  $Q^2$  events at HERA.

We will use  $QCD_S$  to denote<sup>‡</sup> QCD with six color triplet and two color sextet quarks. Within  $QCD_S$ , sextet chiral symmetry breaking gives a triplet of “sextet pions” ( $\Pi^\pm, \Pi^0$ ) and a “higgs-like” particle - the  $\eta_6$ . When the electroweak sector of the Standard Model is added, the “sextet higgs mechanism” takes place. By “eating” the  $\Pi$ ’s, the  $W^\pm$  and  $Z^0$  acquire masses that are a manifestation of the QCD sextet chiral scale. Thus, electroweak symmetry breaking is accomplished without any new interaction being added to the established  $SU(3) \otimes SU(2) \otimes U(1)$  gauge interactions of the Standard Model. (A short-distance  $SU(2) \otimes U(1)$  anomaly can be avoided by, for example, also adding heavy leptons.) Furthermore, the electroweak scale is a new

---

<sup>‡</sup>The suffix can be thought of as denoting special, or sextet, or saturated - the asymptotic freedom constraint is “saturated”.

QCD scale and the symmetry breaking is connected, as discussed above, with a major change in the strong interaction above this scale.

Even though  $QCD_S$  has a special solution, with some distinct properties relative to conventional QCD, we anticipate that all the established properties of QCD below the electroweak scale will be obtained. A particularly significant property of  $QCD_S$  is, however, the limitation on the spectrum of states compared to what would be anticipated from just color confinement and chiral symmetry breaking. The high energy solution of  $QCD_S$  is constructed as a critical phenomenon by starting within the color superconducting phase and, as a result, all the physical states correspond to Goldstone bosons in the superconducting theory. This implies that, in the normal hadronic sector, both glueballs and quark resonances (such as the  $\rho$ ) are clearly excluded as asymptotic states. A related consequence is that there is no BFKL pomeron and there is no odderon.

The spectrum of states involving sextet quarks is, perhaps, the deepest consequence of the construction of the the spectrum of  $QCD_S$  via the superconducting phase. Because there are no chiral symmetries involving both sextet and triplet quarks, there are no hybrid sextet/triplet states and the only new sextet states, in addition to the sextet pions and the  $\eta_6$ , are a “sextet proton” (the  $P_6$ ) and the “sextet neutron” (the  $N_6$ ), both of which will have electroweak scale masses that are, perhaps, as low as 500 GeV. Because of the conservation of sextet quark baryon number, one of the sextet nucleons must be absolutely stable. The absence of sextet current quark masses implies that the stable state must be the  $N_6$ . Therefore, at the ultra-high energies relevant for the early universe, the production of stable, neutral, sextet neutrons will dominate over the production of stable, charged, triplet protons. Consequently, we have a very natural explanation for the dominance of dark matter formed (as nuclei, clumps, etc.) from sextet neutrons. Furthermore, because neutral, massive,  $N_6$ ’s will avoid the GZK cut-off they could also be the mysterious, ultra-high energy, cosmic rays. Since they would simply be very high energy dark matter, their origin would, presumably, no longer be a mystery.

The purpose of this paper is two-fold. Firstly, we want to lay out what we now know about  $QCD_S$  and how we know it. Secondly, we will outline experimental consequences that we expect from the combination of  $QCD_S$  with the sextet higgs mechanism. While we have discussed high-energy phenomena that  $QCD_S$  could produce in the past[8, 9], we did not have the detailed understanding that we now have of how the chiral anomaly produces high-energy states and amplitudes. As a result, the emphasis in this paper will be very different to that of our earlier papers<sup>§</sup>. Particularly important will be the strong coupling of the pomeron to the electroweak sector that follows from the anomaly pole method that we develop to estimate cross-sections for

---

<sup>§</sup>Most notably we believe our discussion of instanton interactions and dynamical masses is irrelevant in the, infinite momentum, S-Matrix formulation within which we now work.

the hard diffractive production of electroweak vector bosons. Predictions can then be made for soft diffraction by combining the hard diffractive estimates with pomeron regge theory. Finally, we observe that if pomeron exchange amplitudes are large then cut-pomeron amplitudes should also be large. We then arrive at the prediction of large inclusive cross-sections for sextet states, across most of the rapidity axis, that we expect to be the major characteristic of  $QCD_S$  physics above the electroweak scale. There will also be “non-diffractive” consequences of the sextet sector that we will discuss, including the non-evolution of  $\alpha_s$  above the electroweak scale and the possibility that top production is due to the  $\eta_6$ .

While our papers have suggested a link for some time, we believe that the arguments presented in this paper make it clear that the sextet higgs mechanism is inextricably tied to the pomeron and infinite momentum hadron states that have emerged from our work on the regge limit of QCD. If this were not the case, as we discuss again below, the  $\eta_6$  would be[10] a light axion-like state that is ruled out experimentally. Indeed, it may well be that the left-handed vector nature of the electroweak sector of the Standard Model plays an important role with respect to inducing the special (S-Matrix) solution of  $QCD_S$  that is involved. We should emphasize that, because our construction of this solution is dependent on infra-red effects of the chiral anomaly, it is crucial that, initially, all quarks, including the sextet sector, are massless.

In this paper, we will discuss only how vector boson masses are generated by the sextet higgs mechanism. This mass generation is responsible for raising all effects of the sextet sector to momenta at or above the electroweak scale. This is crucial for obtaining normal QCD at low energies since, within massless  $QCD_S$ ,  $\alpha_s$  remains less than it’s fixed point value ( $\approx 1/34$ ). The familiar, larger, value of  $\alpha_s$  is obtained only after an effective low-energy theory is obtained by integrating out the sextet sector. In addition, to be physically applicable, triplet quark effective masses must of course, be added to the S-Matrix of  $QCD_S$ . We will not consider whether or not the origin of effective quark masses is directly related to the sextet higgs mechanism. This is likely to be a subtle issue that could, perhaps, involve some form of Gribov confinement[11] via distortion of the Dirac sea. Fortunately, for most of our discussion, only vector boson masses are relevant and so the issue can be avoided.

Our high-energy solution of  $QCD_S$  is very close to perturbation theory in that it is derived via perturbative reggeon diagrams, albeit very complicated multiparticle diagrams in which there is an elaborate phenomenon of cut-off dependent infra-red divergences coupled to (effective) triangle diagram anomalies. As a result, within this framework, both confinement and chiral symmetry breaking have a diagrammatic description. The primary reason that the physics involved stays perturbative is the existence of the infra-red fixed point (referred to above) in the massless theory, due to the large number of quarks. By preventing the infra-red growth of  $\alpha_s$ , the infra-red fixed point produces infra-red scaling properties for reggeon interaction kernels that

are vital for the emergence of physical scattering amplitudes via infra-red divergences.

The most crucial property of  $QCD_S$  is that, as we have already noted, the high-energy behavior can be constructed by starting from  $CSQCD_S$ , the “color superconducting” version of the theory, in which the  $SU(3)$  color symmetry is broken to  $SU(2)$ . The original motivation for this starting point came from a correspondence between supercritical pomeron RFT and  $CSQCD_S$ . This correspondence is referred to indirectly above and the arguments for it are described in Appendix D - where we review our full multi-regge program. There is, however, an important technical reason why the construction can be carried through. Again because of the particular quark content,  $CSQCD_S$  can be obtained from  $QCD_S$  by introducing an asymptotically free scalar field. The asymptotic freedom implies that, in the ultra-violet region, this field can be smoothly decoupled. In the infra-red region the only remnant of the decoupling is the “anomaly contribution” of unphysical longitudinal wee gluons that, as we discuss below, provides the all important mechanism that produces a non-perturbative spectrum out of perturbative diagrams.

When massive gluons are present, as in  $CSQCD_S$ , triangle diagram anomalies appear[12, 13, 14] in the effective vertices of reggeon diagrams. The contribution of the anomalies is strongly dependent on ultra-violet and infra-red cut-offs and so different “solutions” of the theory can be obtained depending on how such cut-offs are handled. The essential part of the reggeon diagram analysis described in Appendix D is the initial imposition of a transverse momentum cut-off. This cut-off produces a violation of gauge invariance Ward identities for the anomaly generating vertices. As a result, infra-red transverse momentum divergences appear which, when the quarks involved are massless, produce residue amplitudes that contain “anomaly poles” resulting from infra-red chirality transitions. (An anomaly pole is produced, in part, by a pinching of massless particle and antiparticle poles in the same zero momentum propagator and so, automatically, involves a chirality transition.) Since an anomaly pole can be identified as a Goldstone boson particle pole associated with chiral symmetry breaking, this provides a crucial mechanism for both a bound-state, Goldstone boson, confining, spectrum and the appropriate amplitudes, to appear via the contribution of anomalies and transverse momentum infra-red divergences.

As we implied above, the infra-red anomaly contributions persist, via the contribution of longitudinal wee gluons, after the removal of the large  $k_\perp$  cut-off and the restoration of  $SU(3)$  gauge symmetry. It is well-known that the contribution of longitudinal wee gluons is an, a priori unresolved, ambiguity in the infinite momentum quantization of  $QCD$  which is closely related to the well-known Gribov problem[15] and, therefore, the choice of vacuum at finite momentum. In effect, therefore, we resolve this ambiguity in  $QCD_S$  by constructing the high-energy behavior via  $CSQCD_S$ .

The transition from  $CSQCD_S$  to  $QCD_S$  is to be achieved via supercritical

RFT and the phase transition appearance of the Critical Pomeron[3]. If this can be carried through in full detail, the regge behavior of  $QCD_S$ , together with the infinite momentum hadron states, will be obtained from the much simpler infra-red divergence and anomaly structure that appears in  $CSQCD_S$ . In particular, within (infinite momentum)  $QCD_S$ , confinement and chiral symmetry breaking will be understood as resulting from dynamical infra-red chirality transitions produced by wee gluon interaction anomalies. However, as we already emphasized above, the spectrum of physical states will be significantly limited compared to that normally anticipated. Only states that correspond to Goldstone bosons in  $CSQCD_S$  will be present. These states (and only these) have, as a consequence of the flavor anomaly, a wee gluon content that produces the infra-red divergent amplitudes giving the, eventual, physical amplitudes. Pions and nucleons are included amongst such states, but flavor singlet Goldstone bosons, unstable resonances and glueballs, are all excluded (as asymptotic states). Because there are no chiral symmetries that couple the triplet and sextet quark sectors, there are no corresponding Goldstone bosons in  $CSQCD_S$ . This is why there are no hybrid baryons in  $QCD_S$ . A fact that is crucial for the stability of the  $N_6$  and, hence, for our explanation of the origin of dark matter.

Usually it is assumed that the solution of QCD is such that the only non-conserved axial U(1) charge is that coupling to the short-distance topological anomaly. If this were the case in  $QCD_S$ , the U(1) symmetry (essentially the sextet symmetry) associated with the  $\eta_6$  would be unbroken. As a consequence, in addition to being the analog of the usual higgs scalar, the  $\eta_6$  would also be, as we noted earlier, a light axion of the kind that is ruled out experimentally. In our solution of  $QCD_S$  the anomaly vertices, that are responsible for the dynamical “wee gluon” component of infinite momentum physical states, break both the sextet and triplet U(1) symmetries and so there is no light axion. (At infinite momentum “wee partons” play the role of the vacuum.) Although the  $\eta_6$  appears, initially, to be a Goldstone boson of the appropriate kind to appear as a physical state, there is a multigluon regge exchange (a daughter of the pomeron) that mixes with it. This mixing, presumably, generates a large (electroweak scale) mass for the  $\eta_6$ . The  $\eta_6$  also couples to the triplet sector via the gluon intermediate state and if it has an electroweak scale mass the mixing will be primarily with the  $t\bar{t}$  state. Consequently, as we will discuss, the  $\eta_6$  could actually be responsible for top production at the Tevatron.

In general, because anomaly couplings dominate, only a very limited subset of the color zero gluon degrees of freedom contribute to the  $QCD_S$  high-energy S-Matrix. (Presumably, there is a corresponding limitation in the finite energy S-Matrix.) This is why there is no BFKL pomeron and no odderon. We are not aware of any experimental evidence against this. Rather, strong experimental evidence that this should be the case is, surely, provided by the (almost total) absence of glueballs in the resonance spectrum, the absence of the odderon[16] in experiments at HERA,

and the lack[16] of any definitive evidence for the BFKL pomeron.

It is well-known that, in general, both  $s$ -channel and  $t$ -channel unitarity (via reggeon unitarity) impose very strong constraints on the behavior of a theory in multi-regge limits. A solution of QCD in all such limits necessarily determines how unitarity, the physical spectrum, and the validity of perturbation theory all coexist. Obtaining such a solution is, therefore, likely to be almost as difficult as solving the full theory. As we have said, according to our arguments the multi-regge limits of  $QCD_S$  are described by the Critical Pomeron[3], which is known to satisfy all unitarity requirements. In addition, we are able to give a diagrammatic construction in which the connection between perturbation theory, the pomeron, and the physical bound state spectrum is clear. If everything goes through as we describe, it will be apparent that  $QCD_S$  is a version of QCD that, perhaps uniquely, satisfies all general requirements.

On the lattice, it would be very difficult, if not impossible, to see the co-ordinated infra-red dynamical fluctuations of longitudinal wee gluons and the Dirac sea that provide the anomaly couplings, and consequent infra-red divergences, in infinite momentum  $QCD_S$ . Not surprisingly, perhaps, within the lattice framework, the infra-red fixed-point that we have discussed is generally believed[17] to be associated with a non-confining continuum theory and the confining “anomaly-driven” S-Matrix that we have discovered is not seen.

Section 2 is devoted to the high-energy solution of  $CSQCD_S$ . Our essential aim is to focus on the physics that underlies this solution. To this end, we keep the discussion at a fairly broad level and supplement it with a number of Appendices. In Appendix A we describe the formal infra-red and ultra-violet  $\beta$ -function properties that are needed to connect  $CSQCD_S$  to  $QCD_S$ . In Section 2, we do not use the full multi-regge theory that is necessary to actually derive the solution that we describe. Instead, we use the anomaly-pole vertex method developed in [13]. Needed properties of the triangle anomaly and the contribution of the anomaly pole are described in detail in Appendix B and we give a summary of the background multi-regge theory in a further pair of Appendices. Appendix C gives a basic description of the properties of the reggeon diagrams that appear in elastic scattering amplitudes. This is a well-known formalism that we need summarized in order to describe our full multi-regge program in Appendix D. As part of our description of the full program, we include the historical development which led to our association of the Critical Pomeron with  $QCD_S$ . Since many of the details of how the transition from  $CSQCD_S$  to  $QCD_S$  is described by the Critical Pomeron have still to be worked out we give, in Section 3, only a brief outline of the features that are relevant for the purposes of this paper.

We begin the process of combining the electroweak sector with  $QCD_S$  in Section 4. In particular, we show how masses for the electroweak bosons are generated by anomaly interactions that result from the presence of wee gluons in infinite mo-

mentum physical states. This is the infinite momentum analog of vacuum generation of the masses. Most importantly, we see that the mass scale is determined by the coupling of wee gluons to sextet quarks. We can then carry the knowledge of this coupling over to the coupling of the pomeron to sextet quark states and, in particular, to multiple  $Z^0$  and  $W^\pm$  states.

We begin our discussion of the hard diffractive production of  $W$ 's and  $Z$ 's, via sextet pions, in Section 6. In Sections 6 and 7 we discuss processes that might be seen (or may have already been seen) at current accelerators and could provide evidence for the existence of the sextet sector. Although diffractive processes are usually a relatively small fraction of total cross-sections, the strong coupling of the sextet sector to wee gluons enhances their significance. The strong coupling can be directly exploited by utilising the generation of a sextet pion as an anomaly pole. In Section 6 we discuss diffractive deep-inelastic scattering. Because the photon couples to sextet quarks, it can be diffractively excited to a  $Z^0$ , via sextet pion production. Very similarly, a  $Z^0$  component of the neutral current, or a  $W^\pm$  component of the charged current, can also produce an on-shell, massive, vector meson via diffractive scattering. At HERA, although large  $x$  and  $Q^2$  is required, it may just be possible to see these processes. The fast, longitudinal,  $Z^0$  produced by a sextet pion has a higher probability (than a transverse  $Z^0$ ) for decay to a jet (or lepton) pair that are sufficiently close together, in phase space, to appear as a single massive jet. Although such a jet is likely to be particularly difficult to identify in the kinematical situation at HERA, we suggest nevertheless that, in the most dramatic large  $x$  and  $Q^2$  event presented[18] by ZEUS, a  $Z^0$  may indeed have been produced.

Sextet quark physics that might be seen at the Tevatron is the focus of Section 6. We describe a number of small cross-section effects that might be seen in diffractive, and diffractive related, processes involving  $W^\pm$  and  $Z^0$  vector bosons. However, the “close together” decay properties of fast, longitudinal, bosons produced by sextet pions could again be a problem. Probably, the most important feature that could be decisively established is that the production cross-section for  $W^+W^-$  and  $Z^0Z^0$  pairs has an anomalous component with event characteristics different from the Standard Model. This would be the first indication of what should become a dominant, very large, cross-section at the LHC. If the sextet quark dynamical mass scale is well above the top quark mass, then the production properties of  $W$ 's and  $Z$ 's could be the only new physics visible at the Tevatron scale. If this scale is lower the situation could be more subtle. The observed  $t\bar{t}$  events could originate from the  $\eta_6$ , even though they can be understood perturbatively. The interpretation of the top quark mass would, however, be different and non-perturbative decay modes should also be seen. A jet excess at large  $E_T$  would provide supporting evidence for this picture, since  $\alpha_s$  evolution should stop at  $E_T \sim m_{top}$ .

If the sextet sector exists, the LHC will most probably be the discovery ma-

chine. Sections 7 and 8 are devoted to explaining why we expect that dramatic effects will be seen. In Section 7 we discuss dark matter and the cosmic ray phenomena that tell us that the sextet sector could appear at the LHC. We first discuss how the  $P_6$  -  $N_6$  mass difference tells us that the  $N_6$  is stable. The dominance of dark matter in the universe can then be viewed as confirmation of the dominance of sextet states at high energy. We then describe the well-known knee in the cosmic ray spectrum and discuss how, if it is associated with sextet physics, the scale at which sextet physics appears is consistent with the expectation that pomeron couplings to the sextet sector should be involved. We also note that there is a large catalogue of cosmic ray phenomena that have been seen at energies above the knee that collectively provide very significant support for the theoretical picture that we are advocating. We specifically discuss the observation of large transverse momenta “dijet” events as well as the potential appearance of  $N_6$ ’s as ultra high-energy cosmic rays.

We discuss the specifics of what we expect to see at the LHC in Section 8. The major evidence for the sextet sector is likely to be that, in general, jet cross-sections and cross-sections for multiple vector boson production are orders of magnitude larger than expected. Although the fact, referred to above, that large momentum longitudinal vector bosons have a relatively high probability to decay to jet and lepton pairs that are close together in phase space, may well complicate the detailed observation of these cross-sections. However, the double pomeron cross-section for electroweak vector boson pairs, which can be studied (in part) during the initial low luminosity running, may well be the most definitive early evidence that is seen. There could be spectacular events in which the forward protons are tagged and only large  $E_T$  leptons are seen in the central detector. It could even be that “dark matter”, in the form of a sextet neutron/antineutron pair, can be produced in double pomeron exchange. If so, this would be really dramatic. It could also be the most realistic way to detect the  $N_6$  at the LHC.

A priori,  $N_6$  and  $P_6^\pm$  pairs (and also  $\eta_6$  pairs) are too massive to be detected in double pomeron exchange. Although, given the increased magnitude of sextet cross-sections, this might not actually be the case. We expect, in any case, that central region inclusive cross-sections for the production of such states will be sufficiently large that, if they can be detected, they will surely be seen.

## 2. COLOR SUPERCONDUCTING $QCD_S$

In this Section we will describe the physics that produces the  $CSQCD_S$  high-energy S-Matrix.

### 2.1 Symmetry Breaking, Reggeization and Infinite Momentum States

As we discuss further in Appendix A, the breaking of the  $SU(3)$  color symmetry of  $QCD_S$ , that gives  $CSQCD_S$ , can be achieved with an asymptotically free scalar field that is a complex color triplet. As a consequence of the symmetry breaking,  $CSQCD_S$  contains an  $SU(2)$  triplet of massless gluons, plus two  $SU(2)$  doublets (with mass  $\frac{2}{\sqrt{3}}M$ ) and one singlet (with mass  $M$ ) of massive gluons. Each  $SU(3)$  triplet quark gives one  $SU(2)$  doublet and one singlet quark. Each  $SU(3)$  sextet quark gives one  $SU(2)$  triplet, one doublet, and one singlet quark.

We will assume that the scalar field couples to the quarks and so gives a mass to all of the  $SU(2)$  singlets and to the  $SU(2)$  doublets originating from the sextet quarks. Therefore, in the massless sector, the quarks that (before the symmetry breaking) were  $SU(3)$  triplets, carry different  $SU(2)$  color from those that were sextets. Consequently, the two kinds of quarks can not combine to form color zero, massless, bound states in  $CSQCD_S$ . For reasons that will become clear, it is important that this correctly reflects the fact that there is no chiral symmetry mixing sextet and triplet quarks in either  $QCD_S$  or  $CSQCD_S$ .

All quarks and gluons (massive or not) are reggeized, but only the  $SU(2)$  singlets have infra-red finite regge trajectory functions. The infra-red scaling behavior of various “transverse momentum kernels” that describe the interactions of reggeized quarks and gluons will be an essential ingredient of the following analysis. The scalar particle produced by the scalar field does not reggeize and so at the non-leading power level  $CSQCD_S$  is, presumably, a non-unitary theory. (A feature that does not interfere with the construction of the leading high-energy behavior of  $QCD_S$  via  $CSQCD_S$ .)

The current status of the program that we have developed to construct the multi-regge behavior of  $CSQCD_S$  is outlined in Appendix D. We believe that this program, as it is now formulated, would give the high-energy behavior of  $QCD_S$  unambiguously if pursued to completion. However, we can arrive much more simply at the physics involved if we utilise the approach that we developed in [13]. In that paper, we introduced a procedure that was designed to bypass the multi-regge construction and instead obtain directly the  $CSQCD_S$  scattering amplitudes for infinite momentum states. This procedure is, essentially, what we now describe.

If the high-energy states and amplitudes of  $QCD_S$  can be derived from perturbative reggeon diagrams, then the parton model should have a broad validity, well beyond leading-twist perturbation theory. For this to be the case, the “naive” validity of the perturbative vacuum at infinite momentum must hold for deeper reasons. This can be so if infinite momentum states have a universal “wee parton” component that carries the finite momentum “properties of the vacuum”. (Note that, although it is not directly relevant at this point, regge pole factorization properties for the pomeron are, most probably, a pre-requisite for a universal wee parton distribution in hadrons.) As we shall see, it is indeed a universal wee gluon component of infinite momentum states that determines our solution of  $CSQCD_S$ .

## 2.2 Pion Anomaly Pole Vertices

The primary assumption in [13] was that the wee gluon properties of the physical states could be obtained from properties of the chiral anomaly and “anomaly pole” vertices<sup>¶</sup>. It is well-known that an anomaly pole appears, in particular kinematic circumstances, in a three-point vertex of local currents when the triangle diagram anomaly is present and when the fermions producing the anomaly are massless. When the vertex involves an axial current that is the generator of a chiral symmetry that is spontaneously-broken, this pole can be directly interpreted as a Goldstone boson particle pole associated with the symmetry breaking.

The invariant functions of a triangle diagram depend on the invariants  $k_1^2$ ,  $k_2^2$ , and  $q^2$ , where, as shown in Fig. 1(a),  $k_1$ ,  $k_2$  and  $q$  are the momenta entering at each of the vertices.

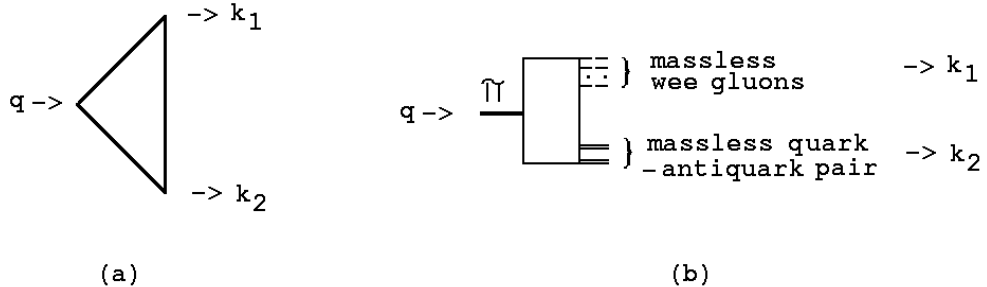


Fig. 1 (a) Triangle momenta (b) How wee gluons give a pion anomaly pole.

The pole is present when either

$$k_1^2 = k_2^2 = 0, \quad q^2 \rightarrow 0, \quad \text{or} \quad k_1 = 0, \quad k_2^2 = q^2 \rightarrow 0 \quad (2.1)$$

<sup>¶</sup>We expect this to be an outcome of the full multi-regge program and we emphasized in [13] that if the assumptions made appeared to be ad-hoc this was, in large part, because of our deliberate efforts to avoid the obscurity of multi-regge theory.

and the residue is determined by the anomaly. (Some details of how the pole is generated are given in Appendix B.)

We anticipate that the occurrence of anomaly poles in regge limit effective triangle diagrams will be a widespread phenomenon in the full multi-regge analysis of  $CSQCD_S$ . They appear whenever components of the relevant currents (not the full currents) appear as effective vertices in a triangle diagram. Poles associated with a flavor anomaly current component are Goldstone boson particle poles that are, in effect, dynamically generated. As illustrated in Fig. 1(b), the kinematics producing a Goldstone (pion) pole can occur when a set of wee gluons produces a divergence at  $k_1^2 = 0$  and couples via an effective triangle diagram to a quark-antiquark pair that carries a light-like momentum  $k_2$ . In this Section, we will refer to all quark/antiquark (triplet or sextet) Goldstone bosons in  $CSQCD_S$  as “pions” and, when we need to, will refer to quark/quark or antiquark/antiquark Goldstone bosons[19] as “nucleons”. Effectively, all of our discussion of pions will also apply to nucleons, even though we will not usually say so explicitly. Poles associated with the  $U(1)$  anomaly do not contribute as particle poles but instead contribute as  $\delta$ -functions that conserve wee gluon transverse momenta during an interaction.

In the initial analysis that follows, the underlying calculations needed to demonstrate the existence of the appropriate anomaly pole vertices, effectively, already exist. In particular, in the calculations of [12], that were carried out after [13] was published, we obtained results that essentially derive what was assumed in [13]. However, as we develop a complete dynamical picture in the following, we will introduce a variety of anomaly pole effective vertices whose existence is a natural extrapolation of existing vertices but, for which, the underlying (very complicated) multi-regge calculations still need to be performed. In [12] we showed explicitly how, in the scattering of electroweak vector bosons, effective vertices containing a triangle diagram are generated, in the channel with pion exchange quantum numbers, by the contraction of larger loop diagrams. As a result, we can anticipate that in general scattering processes involving an infinite momentum vector boson, if a transverse momentum cut-off is imposed, a pion anomaly pole will indeed appear with the wee gluon couplings we assumed to exist. Our specific assumption was that a massless on-shell pion carrying light-cone momentum  $k_+$  has a coupling to wee gluons (carrying total light-cone momentum  $k_-$ , with  $k_-/k_+ \rightarrow 0$ ) given by the anomaly pole residue of a triangle diagram that is generated as illustrated in Fig. 2. The coupling is to a massless quark-antiquark pair that has a vector-like helicity and any number of “wee gluons”, that are also in a vector-like state. The dashed line in the triangle diagram is a zero momentum quark propagator that, as discussed in Appendix B, generates the anomaly pole and also produces a chirality transition.

As we will discuss at length shortly, it is important that it is the longitudinal

component of the massive gluon that is responsible for the quark/antiquark vertex of the triangle diagram that is formed in Fig. 2. That the scattering state involved (denoted by an arrow) is an electroweak vector boson is not important in the present discussion. What matters is that according to (B.17), in an “infinite momentum” frame reached via a boost  $a_3(\zeta)$ , the momentum dependence of the anomaly pole coupling is

$$[ k_+ k_- \sinh \zeta ] \quad (2.2)$$

which is finite when  $k_- \rightarrow 0$ , if  $k_- \cosh \zeta$  is kept finite.

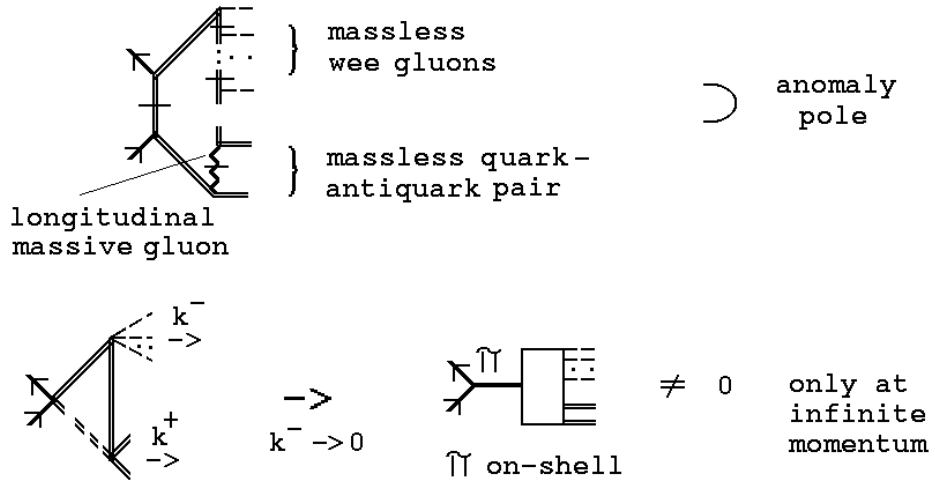


Fig. 2 Anomaly pole generation in an effective triangle diagram. (The hatched lines are on mass-shell.)

### 2.3 Transverse Momentum Kernels and Infra-Red Divergences

In [13] we also argued that, because the anomaly pole is generated by a light-cone internal momentum region within the triangle diagram, we could use transverse momentum diagrams to discuss wee gluon interactions within the infinite momentum pion state. (This is straightforwardly the case in the multi-regge framework of Appendix D.) The coupling (2.2) is defined at  $k_\perp = 0$ , where  $k_\perp$  is the transverse momentum of the wee gluons. That it is non-zero is correlated with the fact that, for  $k_\perp \neq 0$ , the anomaly pole contribution to the effective triangle diagram violates the wee gluon Ward identity (for reasons discussed in Appendix B). A direct consequence is that infra-red divergences appear in the transverse momentum diagrams and dominate the physical pion scattering amplitude. (In the multi-regge framework, a transverse momentum cut-off is initially responsible for the failure of Ward identities that then leads to the occurrence of divergences and the correlated appearance of anomaly pole couplings.)

To describe the infra-red divergences that occur, we must first describe the infra-red properties of the transverse momentum kernels that are involved. These kernels are defined in more detail in Appendix C. We begin with the kernels  $K_N^I(\underline{k}, \underline{k}')$  that involve only the SU(2) triplet of massless gluons. ( $I$  denotes SU(2) color.) When the color of the multigluon state is non-zero, infra-red divergences give (in a sense explained in Appendix C)

$$\Omega \left\{ \begin{array}{c} \underline{k}_1 \cdots \\ \cdots \\ \underline{k}_N \cdots \end{array} \right\} \boxed{K_N^I} \left\{ \begin{array}{c} \cdots \underline{k}'_1 \\ \cdots \\ \cdots \underline{k}'_N \end{array} \right\} = K_N^I(\underline{k}, \underline{k}') \rightarrow \infty, \quad Q^2, I \neq 0 \quad (2.3)$$

As a result, the sum of all gluon transverse momentum diagrams in any colored channel exponentiates to zero, as illustrated in Fig. C1.

When  $I = 0$  and  $Q^2 \neq 0$ , the kernels  $K_N^0(\underline{k}, \underline{k}')$  are finite and have an important scaling property as described in Appendix C (before and after (C.9)). As a result, there is no exponentiation of divergences in color zero gluon channels. However, the disappearance of all colored multigluon states is not confinement since gluon poles remain in the color zero diagrams. Confinement is produced when the remaining  $Q^2 = 0$  singularity in color zero channels is absorbed into a “condensate”, as we describe below.

The most important contribution of the  $K_N^0$  kernels comes when a color zero set of massless gluons accompanies another SU(2) color zero transverse momentum state, as can be the case in states produced by the pion anomaly pole couplings. In Fig. 3 we show the kernel  $K_R(\hat{k}, \underline{k}, \hat{k}', \underline{k}')$  describing the interactions of massless gluons with the massive (SU(2) singlet) reggeized gluon and the kernel  $K_Q(\hat{k}, \underline{k}, \hat{k}', \underline{k}')$  describing the analogous interaction with an SU(2) singlet quark-antiquark pair.

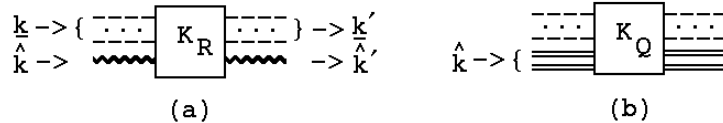


Fig. 3 Kernels for massless gluon interactions with (a) a massive reggeized gluon (b) a quark-antiquark pair.

Ward identities require that both  $K_R$  and  $K_Q$  vanish when either  $\underline{k} \rightarrow 0$  with  $\underline{k}'$  fixed or when  $\underline{k}' \rightarrow 0$  with  $\underline{k}$  fixed. But, because these kernels have a dimension of [momentum]<sup>2</sup> and additional non-zero mass and momentum scales (i.e.  $M^2$  and  $\hat{k}^2$ ) are present, we expect that these kernels neither vanish, nor have an infra-red scaling property, when  $\underline{k} \sim \underline{k}' \rightarrow 0$ . As a result, whenever the interactions of Fig. 3 exist,

infra-red divergences should again cause the sum of all diagrams to exponentiate to zero.

However, as illustrated in Fig. 4(a), because of helicity conservation in the massless quark and gluon sector, there is no transverse momentum kernel describing the interaction of negative signature, color zero, massless gluons with the massive reggeized gluon. This is because a multigluon state containing an odd number of gluons and carrying SU(2) color zero necessarily has “anomalous color charge parity”, i.e. the color charge parity is necessarily positive and can not be equal to the negative signature. Similarly, as illustrated in Fig. 4(b), for a massless quark-antiquark state that carries negative signature, color zero, and normal color charge parity, there is also no interaction.

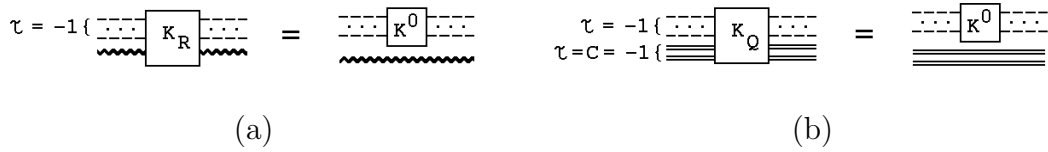


Fig. 4 Reggeon states without interaction kernels.

Related to the lack of interactions, transverse momentum states of the kind shown in Fig. 4 will couple only through anomalies. As a result, there will be no exponentiation of divergences in reggeon channels with these quantum numbers. Instead, the scaling property of the massless gluon kernels will lead to an overall divergence, as illustrated in Fig. C5.

## 2.4 Pion Scattering Amplitudes Via Infra-Red Divergences

In [13] we considered feynman diagram contributions to the particular transverse momentum diagram shown in Fig. 5, in which there are three wee gluons in each of the pion channels and also in the pomeron channel.

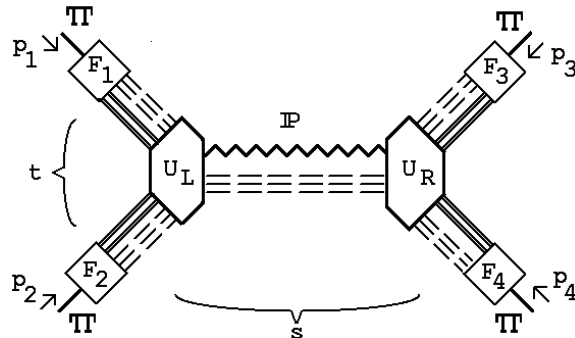


Fig. 5 A transverse momentum diagram for pion scattering.

(The notation in Fig. 5 is the same as for Fig. 2.) Because of the foregoing discussion, this diagram is amongst the simplest, describing pion scattering, that contain a transverse momentum divergence that does not exponentiate to zero. In [13] we carried out a detailed infra-red analysis to extract the resulting amplitude.

We will not reproduce the analysis of [13] here but, rather, will elaborate on features of the underlying physics that we did not discuss in [13]. For this purpose we need to describe, briefly, the kinematics involved in the analysis. The kinematics were chosen so that each of the initial and final state pions was in an infinite momentum frame, reached by an appropriate boost, such that an anomaly pole residue corresponding to (2.2) could give the contribution of each of the four external pion couplings  $F_i$ . To also produce internal triple-regge anomaly interactions, the wee gluons in the outgoing pions were associated with light-cones whose space direction is orthogonal to that of the incoming wee gluon light-cones. We, therefore, introduced distinct Lorentz frames as follows. We calculated the left-hand part of Fig. 5 in a “left-hand finite momentum frame” in which  $p_1$  and  $p_2$  have the form<sup>||</sup>

$$\begin{aligned} p_1 &= k^{1+} + q^{1-} = k_{1-} + q_{1+} \\ &= \left( \frac{k}{\sqrt{2}}, \frac{k}{\sqrt{2}}, 0, 0 \right) + \left( \frac{q}{\sqrt{2}}, -\frac{q}{\sqrt{2}}, 0, 0 \right) \end{aligned} \quad (2.4)$$

$$\begin{aligned} p_2 &= -k^{2+} - q^{2-} = -k_{2-} - q_{2+} \\ &= -\left( \frac{k}{\sqrt{2}}, 0, \frac{k}{\sqrt{2}}, 0 \right) - \left( \frac{q}{\sqrt{2}}, 0, -\frac{q}{\sqrt{2}}, 0 \right) \end{aligned} \quad (2.5)$$

where  $q^{1-}$  and  $q^{2-}$  are, respectively, the wee gluon momenta in  $F_1$  and  $F_2$ . For simplicity, we took the scale of the light-cone momenta for all on-shell pions to be  $k$  and the scale of all wee gluon (longitudinal) momenta to be  $q$  although, as we discuss further below, this is clearly not essential. Since

$$p_1^2 = p_2^2 = 2kq \quad (2.6)$$

$q$  is both the wee gluon scale and the scale which puts pions on-shell as it vanishes.

The right-hand part of Fig. 5 was calculated in a “right-hand finite momentum frame” in which

$$\begin{aligned} p_3 &= k^{2+} + q^{2-} \\ &= \left( \frac{k}{\sqrt{2}}, 0, \frac{k}{\sqrt{2}}, 0 \right) + \left( \frac{q}{\sqrt{2}}, 0, \frac{-q}{\sqrt{2}}, 0 \right) \end{aligned} \quad (2.7)$$

---

<sup>||</sup>The notation is straightforward in that  $k^{1+}$  is a vector with raised index component along the light-cone defined by the positive  $\{1\}$  - axis (and all other orthogonal components are zero). Similarly  $q^{1-}$  is a vector with raised index component along the light-cone defined by the negative  $\{1\}$  - axis. The same vectors can be labeled via lowered index components as usual.

$$\begin{aligned}
p_4 &= -k^{1^+} - q^{1^-} \\
&= -\left(\frac{k}{\sqrt{2}}, \frac{k}{\sqrt{2}}, 0, 0\right) - \left(\frac{q}{\sqrt{2}}, -\frac{q}{\sqrt{2}}, 0, 0\right)
\end{aligned} \tag{2.8}$$

and so we also have

$$p_3^2 = p_4^2 = 2kq \quad (2.9)$$

The full scattering amplitude for Fig. 5 was calculated in the “infinite momentum frame” in which

$$\begin{aligned}
 p_1 &= \left( C \frac{k+q}{\sqrt{2}}, \frac{k-q}{\sqrt{2}}, 0, S \frac{k+q}{\sqrt{2}} \right) \\
 p_2 &= - \left( C \frac{k+q}{\sqrt{2}}, 0, \frac{k-q}{\sqrt{2}}, S \frac{k+q}{\sqrt{2}} \right) \\
 p_3 &= \left( C \frac{k+q}{\sqrt{2}}, 0, \frac{k-q}{\sqrt{2}}, -S \frac{k+q}{\sqrt{2}} \right) \\
 p_4 &= - \left( C \frac{k+q}{\sqrt{2}}, \frac{k-q}{\sqrt{2}}, 0, -S \frac{k+q}{\sqrt{2}} \right)
 \end{aligned} \tag{2.10}$$

where  $C = \cosh \zeta$ ,  $S = \sinh \zeta$ , and so

$$\begin{aligned}
 s &= (p_1 + p_3)^2 \xrightarrow[q \rightarrow 0]{} (C^2 + S^2)k^2 \xrightarrow[C \rightarrow \infty]{} 2C^2k^2 \\
 t &= (p_1 + p_2)^2 \xrightarrow[q \rightarrow 0]{} -k^2
 \end{aligned} \tag{2.11}$$

We combined the mass-shell limit  $q \rightarrow 0$  and the regge limit  $s/t \rightarrow \infty$  by taking

$$q \sim 1/C \rightarrow 0 \quad (2.12)$$

Note that, as is apparent from (2.10), the wee gluon momentum  $q$  is exchanged only as a zero transverse momentum contribution in the infinite momentum frame.

The internal couplings  $U_L$  and  $U_R$  appearing in Fig. 5 are anomaly pole contributions from effective vertices of the form shown in Fig. 6

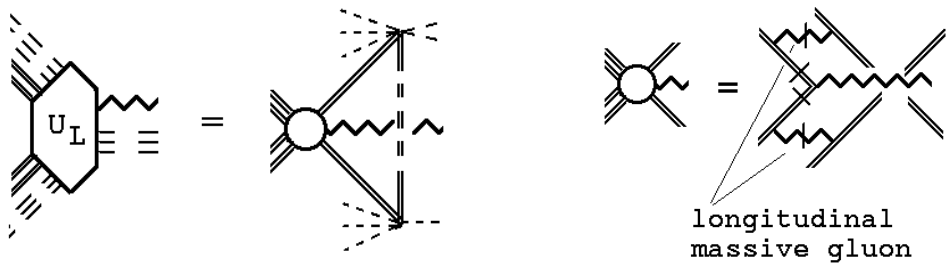


Fig. 6 An anomaly pole coupling.

(These vertices are illustrated in more detail in Fig. D7). Because the anomaly poles are integrated over in this case, they contribute as “anomaly  $\delta$ -functions” that produce a separate conservation of transverse momentum for the massless gluon interactions, allowing these interactions to be factorized off from the remaining “hard interaction”. As a result, the diagram of Fig. 5 has an overall logarithmic divergence from the region where the transverse momenta of all massless gluons are scaled uniformly to zero. After this divergence is factorized off (as a zero transverse momentum reggeon condensate) and the pion poles in each channel are also extracted, the amplitude obtained has the form

$$\begin{aligned}
A_{\pi\pi\pi\pi} &\sim \prod_i \{F_i \text{ anomaly pole coupling}\} \{\text{quark } k_{i\perp} \text{ integrals}\} \\
&\times \prod_{j=L,R} \{U_j \text{ anomaly amplitude}\} \{\text{massive gluon propagator}\} \\
&\sim \left\{ \frac{k C q}{M^2} \right\}^4 \left\{ \frac{(kC)}{M^2} \frac{(kCq)}{M^2} \right\}^2 \left\{ C q \right\}^4 \left\{ \frac{1}{t + M^2} \right\}
\end{aligned} \tag{2.13}$$

Writing  $t \sim k^2$  and  $s \sim C^2 k^2$ , (2.13) can be rearranged to give

$$A_{\pi\pi\pi\pi} \sim \left[ \frac{C q}{M} \right]^8 \left[ \frac{s q^2}{M^4} \right] \left[ \frac{t}{M^2} \right]^2 \left[ \frac{s}{t + M^2} \right] \tag{2.14}$$

Since the first two square brackets in (2.14) are finite constants when the limit (2.12) is taken, the kinematic structure of the pion scattering amplitude we obtain is, essentially, that of massive gluon exchange, i.e.

$$A_{\pi\pi\pi\pi}(s, t) = \left[ \frac{t}{M^2} \right]^2 \left[ \frac{s}{t + M^2} \right] \tag{2.15}$$

(Note that this result is obtained for  $t \gg M^2$ .) In higher-orders the massive gluon will reggeize, with an infra-red finite trajectory  $\alpha_g(t)$  that satisfies  $\alpha_g(M^2) = 1$ . But, since the exchange of four reggeized gluons is involved, as we add all diagrams and go to higher-orders, only the even signature amplitude will survive. As a result, reggeization of the massive gluon will give

$$\left[ \frac{s}{t + M^2} \right] \rightarrow \left[ \frac{s^{\alpha_g(t)} + (-s)^{\alpha_g(t)}}{t + M^2} \right] \tag{2.16}$$

That is, reggeized gluon exchange will provide the leading contribution to the pomeron but there will be no gluon pole at  $-t = M^2$ .

## 2.5 Momentum Flows and Wee Gluon Couplings

The general dynamical structure of the diagrammatic contributions to  $A_{\pi\pi\pi\pi}$  is illustrated in Fig. 7. Where there is a broken quark line (and a  $T$ ) there is a chirality transition of a zero momentum massless quark. Wee gluon couplings, that we will discuss shortly, are denoted by a circle containing a  $w$ .

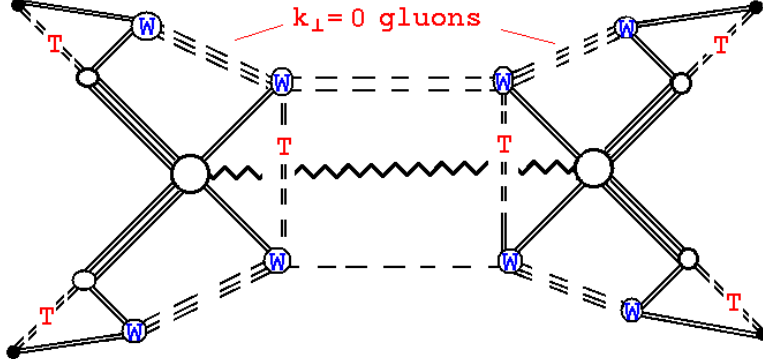


Fig. 7 Dynamical structure of the scattering amplitude.

Using the origin of the anomaly pole described in Appendix B, the scattering process can be interpreted as follows. A “pion” is created by the product of a physical quark field and a zero momentum “unphysical” antiquark field in which the Dirac sea is shifted. The antiquark becomes physical, via a chirality transition, that introduces an accompanying “semiclassical” anomalous wee gluon field (condensate) that effectively moves the sea back to its perturbative location. In the scattering process, the wee gluon field of an incoming pion is transformed into that of the outgoing pion by an anomaly coupling that involves a further rearrangement of the Dirac sea. The final state pions are created via a final shift of the Dirac sea that absorbs the anomalous wee gluon field.

The flow of large momentum ( $\sim k$  in the finite momentum frame) through the left side of Fig. 7 is shown in Fig. 8(a), while the flow of wee gluon longitudinal momentum ( $\sim Cq$  in the infinite momentum frame) is, as shown in Fig. 8(b), along an (almost) orthogonal set of lines. Note that, as is shown in Fig. 8(a), the large momentum flows along either the quark or the antiquark, but not both. The remaining momentum scale is the relative transverse momentum ( $\sim q_\perp$ ) of the quark-antiquark pair which simply flows around a loop, as illustrated in Fig. 8(c). In the finite momentum frame (“inside the pion”) the wee gluon limit  $q \rightarrow 0$  gives the zero momentum required for the first and last chirality transitions. In the infinite momentum frame  $Cq$  provides the light-cone momentum flowing around the triangle diagram giving the anomaly  $\delta$ -function. The “zero momentum” line in the  $\delta$ -function triangle therefore has momenta much smaller than  $q$  in the finite momentum frame.

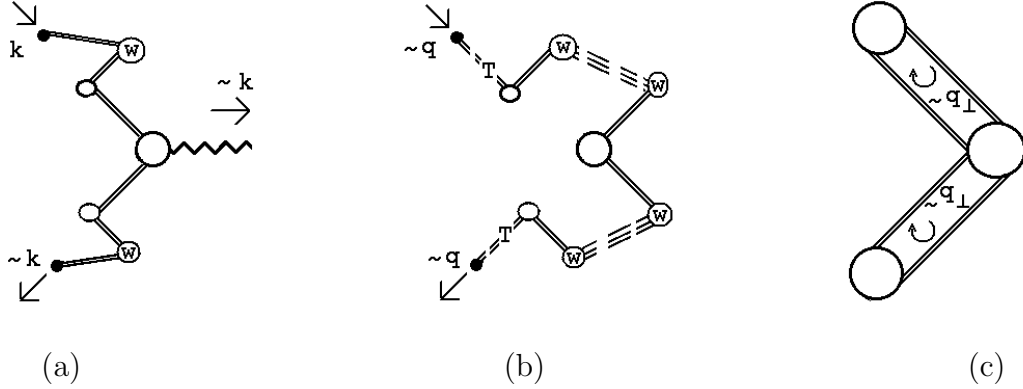


Fig. 8 Momentum flows.

There are eight wee gluon couplings that originate from the chirality transitions. As we already noted, they are denoted by a circle containing a  $w$  in Fig. 7. A factor of  $Cq$  for each wee gluon coupling gives the factor of  $[Cq/M]^8$  in (2.14). The other two factors in (2.14), apart from (2.16), arise from the integrations over the quark-antiquark relative transverse momenta. Clearly, all of the factors in (2.14), apart from (2.16), are scaled by the vector boson mass  $M$ . The overall factor of  $M^{-16}$  can be traced back to the eight contributions of longitudinal massive gluon exchange. Four appear via anomaly pole vertices of the form appearing in Fig. 2, and are represented by small circles in Fig. 7. The other four appear in the two vertices, of the form shown in Fig. 6, represented by large circles in Fig. 7. In each case the longitudinal contribution of the on-shell massive gluon gives a contribution of the form

$$\text{“} \frac{k_\mu k_\nu}{M^2} \text{”} \leftrightarrow [\text{wee gluon momentum}/M]_\mu [\text{quark transverse momentum}/M]_\nu \quad (2.17)$$

The existence of the amplitude (2.13) depends entirely on this interaction which, it is important to note, couples wee gluon related chirality transitions and small transverse momentum quark dynamics. Also, the appearance of a wee gluon momentum scale in the amplitude is crucially dependent on the presence of such transitions.

Clearly we need not have taken the wee gluon momentum scales of both scattering pions to be equal. In general the factor of  $[Cq/M]^8$  in (2.14) would be replaced by a separate factor of  $[(Cq)^2/M^2]^2$  for each scattering pion. Furthermore, we anticipate that if we were to carry through the complete multi-regge calculation of Appendix D, the wee gluon factor for each pion would be replaced by the (integrated) contribution

of a wee gluon distribution  $w(Cq/M)$  so that, in the pion amplitude,

$$\left[\frac{Cq}{M}\right]^8 \rightarrow \prod_{i=1,2} \left[ \int d(Cq_i/M) (Cq_i/M) w(Cq_i/M) \right]^2 \equiv \left[\frac{C}{M}\right]^8 \prod_{i=1,2} \left[ \int dq_i q_i w(q_i) \right]^2 \quad (2.18)$$

## 2.6 Higher-Order Diagrams

Consider now the higher-order diagrams that will add to that of Fig. 5. As we noted above, and discuss in more detail in Appendix C, adding interactions amongst the wee gluons will not change the nature of the overall divergence. Similarly there will be no change if the three wee gluons in the pomeron, and in each pion channel, are replaced by infinite sums over arbitrary (allowably different in each channel), odd, numbers of massless gluons that similarly have zero transverse momentum, carry overall SU(2) color zero, and have (anomalous) positive color charge parity. Again such wee gluons will have self-interactions but will not interact with the quark/antiquark pairs in the pions, or the SU(2) singlet reggeized, massive, gluon in the pomeron. The same discussion would also apply if the single massive gluon is replaced by any number of massive gluons (corresponding to multiple pomeron exchange).

## 2.7 Pomeron Production Vertices

In the remainder of this Section, and the following Sections, we will go far beyond the explicit calculations of [12] and [13]. We will introduce effective vertices for which the underlying (in general, multi-regge) calculations have not, as yet, been carried out but whose existence is a natural extrapolation of the vertices that we have already discussed. In particular, we consider here a set of effective vertices which are responsible for the vacuum production of pomerons that is one of the defining features of supercritical RFT.

A priori, it might appear that the anomaly  $\delta$  function vertex of Fig. 6 could give rise to simple ‘‘vacuum production’’ of massive reggeized gluon pairs by wee gluons, as illustrated in Fig. 9(a).

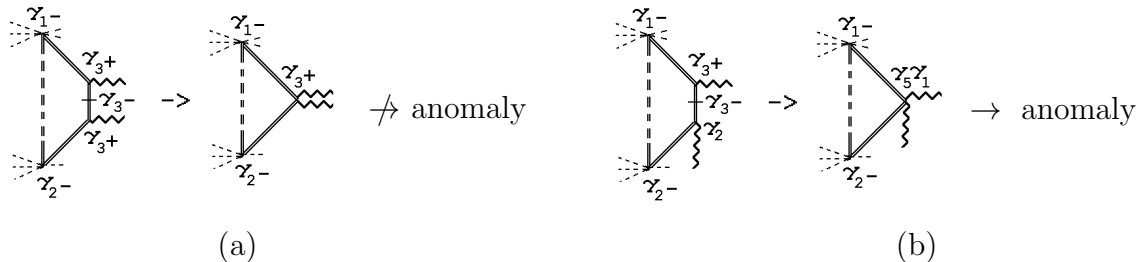


Fig. 9 Wee gluon vertices (a) that do not give an anomaly (b) that give an anomaly.

In fact, to have the axial vector structure for the anomaly, both gluons can not have the polarization needed to be exchanged in the scattering process. Instead, as illustrated in Fig. 9(b) one gluon must have a different polarization. Since the interaction can, nevertheless, take place some distance across the rapidity axis it leads to particle pole interactions within pomeron vertices.

The most general pomeron vacuum production vertices are generated as illustrated in Fig. 10. When these vertices are included, we reproduce the complete range of pomeron vertices that arise from the “vacuum production of pomerons” due to the pomeron condensate in the supercritical pomeron phase[20]. A more detailed study would be needed to determine whether the non-exchanged massive gluon in Figs. 9 and 10 is longitudinal.

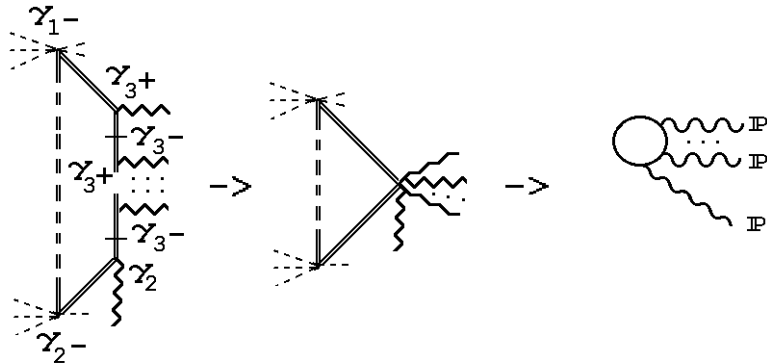


Fig. 10 Generation of pomeron vacuum vertices.

## 2.8 The Complete Set of Amplitudes and States

While it remains to be shown that the high-energy behavior of  $CSQCD_S$  maps completely on to supercritical RFT, we will assume, in this paper, that the connection is established. Our major purpose, here, has been to elaborate the physics that is involved. As we have seen, the essential physics of  $CSQCD_S$  is that a wee gluon condensate is produced by chirality transitions that are part of anomaly interactions introduced by the massive vector mesons. We can view the condensate as originating from a shift of the Dirac sea that produces states, and an S-Matrix, in which  $SU(2)$  color confinement and chiral symmetry breaking completely determine the spectrum. In our derivation at least, the wee gluon condensate has no connection with instantons. It is a “semi-classical” infra-red effect that, as we discuss in the next Section, becomes a dynamical effect in  $QCD_S$ . Note also that, since the anomalous wee gluons in a pion can not be produced from the perturbative quark/antiquark component by normal perturbative interactions (without an anomaly-related chirality transition), we can say that there is no simple quark/antiquark component in the infinite momentum pion “wave function” !

We expect the complete set of (infinite momentum) physical scattering amplitudes in  $CSQCD_S$  to be produced via a logarithmic divergence, as in our discussion of the amplitude obtained from Fig. 5. If this is the case, then any physical amplitude must involve initial and final scattering states that contain anomalous wee gluons. If such gluons appear only via anomaly pole vertices, as we have implied, then all physical states must be color zero Goldstone bosons. Unfortunately, we have only been able to study on-shell pion amplitudes. If we were to carry through the multi-regge program of Appendix D, then we would obtain amplitudes for off mass-shell reggeized pions to scatter. This would give us much more information about how a pion appears as an anomaly pole and would, perhaps, allow us to determine the role played by chiral symmetry in ensuring that such a pole is present. For the present we assume that an anomaly pole occurs if and only if there is a chiral symmetry that can be broken spontaneously. We will also have to be content with the anomaly pole mechanism as our only means to understand the dynamical formation of bound state Goldstone bosons.

We can refer to the Goldstone bosons as created by a product of quark/antiquark operators alone provided we remember that the wee gluon component can be eliminated only by a shift of the Dirac sea in one of the operators. If we denote color triplet quarks, generically, by  $q$  and color sextet quarks, generically, by  $Q$ , the Goldstone boson states of  $CSQCD_S$  include all flavor non-neutral  $q\bar{q}$  and  $Q\bar{Q}$  pseudoscalar mesons. In Section 5, we will discuss how the flavor neutral mesons (the  $\eta_6$  and the  $\eta_3$ ) mix with pure gluon states and, hence, do not appear as Goldstone bosons. Because of the equivalence of quark and antiquark representations when the gauge symmetry is  $SU(2)$ , there are  $qq$ ,  $\bar{q}\bar{q}$ ,  $QQ$ , and  $\bar{Q}\bar{Q}$  states that are Goldstone boson mesons in  $CSQCD_S$  but will become baryons, by acquiring an additional quark (or antiquark) in  $QCD_S$ . Such states reflect real chiral symmetries[19] of  $CSQCD_S$ .

We will not discuss the dynamics of baryon formation in this paper, although, we will briefly discuss the spectrum in the next Section. To discuss dynamics we need to know the full role of the  $SU(2)$  singlet quarks and gluons in  $CSQCD_S$ . According to the above argument, since they are not Goldstone bosons, they can not be physical states. If they are, nevertheless, “physical”, it must be that they appear as regge exchanges, without producing physical states. For example, within  $CSQCD_S$  there can be a regge exchange involving the combination of a Goldstone boson “nucleon” and an  $SU(2)$  reggeized quark that can become a normal, reggeized, nucleon in  $CSQCD$ , as  $SU(3)$  color is restored.

## 2.9 Background Wee Gluon Interactions

A more subtle question is the role played by the  $SU(2)$  singlet gluon. In particular, we can ask whether there is an odd-signature amplitude involving only exchange of the  $SU(2)$  singlet gluon reggeon. To obtain a divergent amplitude, there must be

a divergence produced by background wee gluon anomaly interactions, as illustrated in Fig. 11. In general, we would expect that there should be (multiple) chirality violating interactions that involve just wee gluons, accompanying all interactions and contributing to the overall divergence. As we will see in Section 5, the existence of wee gluon interactions of this kind is essential for adding the electroweak sector of the Standard Model to  $CSQCD_S$ . Nevertheless, to establish the existence and nature of such interactions surely requires elaborate multi-regge calculations that have yet to be carried out.

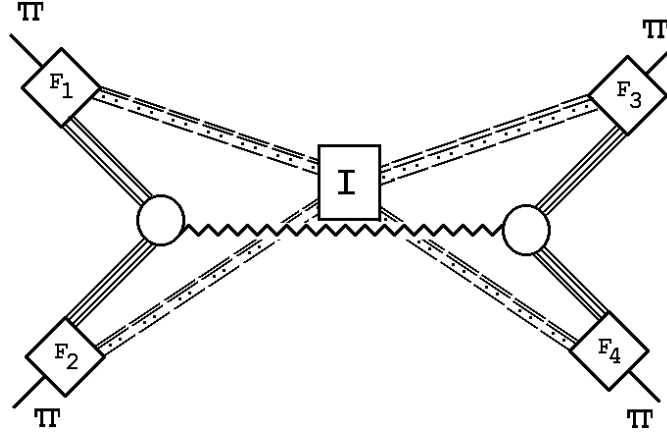


Fig. 11 Background Wee Gluon Interactions Accompanying Reggeon Exchange

The interaction of Fig. 11 must contain anomaly effective vertices generated by the orthogonality of the  $\gamma$ -matrices involved, as illustrated in Fig. 12.

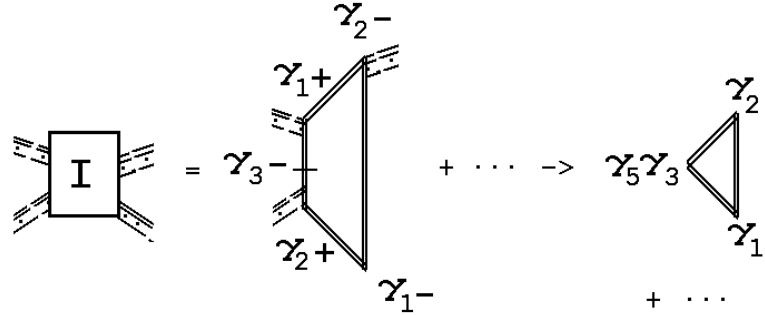


Fig. 12 A Background Effective Vertex Containing an Anomaly

If there is no anomaly, there will be an exponentiation of the divergences via even signature (BFKL) gluon interactions with the reggeon, as illustrated in Fig. 13, that will produce a zero amplitude. The anomaly vertex of Fig. 12 necessarily couples directly to the wee gluons in the scattering state, and so avoids the exponentiation.

As  $SU(3)$  symmetry is restored, the background wee gluon interaction should become  $SU(3)$  symmetric. As a result, the non-zero  $SU(3)$  color of the reggeon in Fig. 11 should lead to the vanishing of this amplitude. However, when the reggeon is replaced by an electroweak vector boson which does not carry color, as we discuss in Section 5, the corresponding amplitude will not vanish.

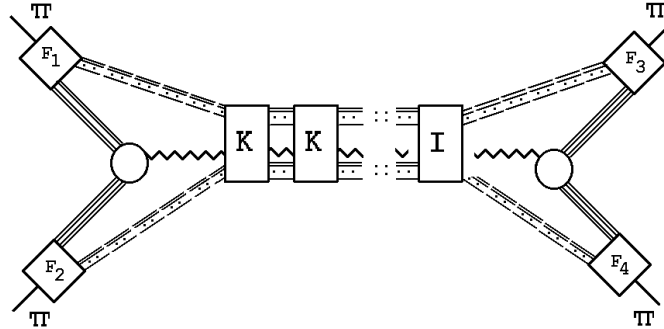


Fig. 13 Potential Exponentiation of the Wee Gluon Interaction

### 3. THE CRITICAL POMERON IN $QCD_S$

If the high-energy behavior of  $CSQCD_S$  is mapped onto supercritical RFT, as discussed in the last Section and in Appendix D,  $SU(3)$  color will be restored via the Critical Pomeron phase transition. As part of this transition, the  $SU(2)$  singlet gluon will become massless and decouple. Simultaneously, the wee gluon condensate will disappear and a corresponding dynamical degree of freedom will appear. That is, the shifting of the Dirac sea will become dynamical. Dynamical, gauge-invariant, infinite number), wee gluon combinations carrying octet color, will produce the chirality transitions illustrated in Fig. 7 (and many more). For this to happen, the longitudinal vector meson interactions, which at first sight should decouple as the color symmetry breaking is removed, must still be present - at zero light-cone momentum.

In fact, the role of zero light-cone momentum, longitudinal, gluons is a major ambiguity of light-cone quantization[21]. When we discuss wee gluons in a pion, as we did in the previous Section, we are essentially invoking light-cone quantization in a frame in which the pion carries light-cone momentum  $k_+$ . For the dynamical wee gluon processes that we are discussing to be present the longitudinal, zero light-cone momentum, gluons must provide the interactions, of the form of (2.17), that are responsible for the occurrence of the chirality transitions (and anomaly poles) in Fig. 7. There is, of course, no vector gluon mass “ $M$ ” in  $QCD_S$ . Consequently, there must be an intrinsic momentum scale  $\mu$  that is generated as part of the symmetry restoration process that will provide the scale for dynamical wee gluon contributions in a hadron. Whether, or not, this scale should simply be identified with the normal dynamical scale of  $QCD_S$  remains to be determined. In any case, by constructing the high-energy behavior of  $QCD_S$  via  $CSQCD_S$  we are, effectively, fixing the ambiguity of the role of zero light-cone momentum, longitudinal gluons.

The dynamical shifting of the Dirac sea produced by wee gluon interactions will, as we said above, no longer correspond to the introduction of a semi-classical gauge field, or condensate, in a fixed direction of the  $SU(3)$  color group. Rather, the chirality transitions, which will be many in any scattering process, will correspond to random gauge field fluctuations within the color group. The transition from a fixed “magnetization” for the gauge field associated with Dirac sea shifts to a randomized, fluctuating, field, characterizes the nature of the “critical phenomenon” that is associated with the high-energy behavior of  $QCD_S$ . The shifting of the Dirac sea is the “order parameter” of the transition. In the supercritical phase this degree of freedom is ordered into a single, semi-classical, wee gluon gauge field contribution, while in the sub-critical phase it is random.

It is obviously essential for the quarks to be massless if the physics of the

Critical Pomeron is to be as we have just described it. The chirality transitions can take place in a “perturbative manner” (i.e. within effective vertex triangle diagrams) only if the quarks are massless. We would expect, however, that the high-energy behavior is independent of the physical states acquiring masses and therefore would expect that the Critical Pomeron remains, at high-energy, even when effective quark masses are added to  $QCD_S$ . To add such masses and preserve the physics involved would appear, nevertheless, to be non-trivial. Perhaps the Dirac sea has to undergo major shifts, as envisaged by Gribov[11], in a random dynamical manner, as part of any scattering process and as part of the creation of asymptotic states. Fortunately, for most of this paper, this obviously complex problem will not concern us.

The large transverse momentum (“short distance”) pomeron will be the least sensitive to the wee gluon phase transition. At large transverse momentum, therefore, the  $QCD_S$  pomeron will be approximately a short-distance (gauge-invariant) reggeized gluon combined with a color compensating dynamical, anomalous, wee gluon contribution. Also, at large transverse momentum, both triplet and sextet pions will have a wee gluon component that is the same as the pomeron, but with a short-distance quark-antiquark pair replacing the reggeized gluon. It can be shown that the quark-antiquark state in a pion reggeizes and so becomes gauge-invariant, like the reggeized gluon in the pomeron, but we will not discuss it in this paper.

As we said in the last Section, we also will not attempt to follow the formation of baryons as  $SU(3)$  color is restored. However, there is one very important feature of baryon formation which is clear. Namely, there are no “hybrid states” formed, for example, by a sextet quark  $Q$  combining with a  $\bar{q}\bar{q}$  triplet state that is a “nucleon” in  $CSQCD_S$ . This combination is possible in principle. But, for the complete  $SU(3)$  invariant state to be formed it would be necessary to also have a  $\bar{q}Q$  state in  $CSQCD_S$  combining with an  $SU(2)$  singlet  $\bar{q}$  (as the symmetry is restored) and, in the previous Section, we already argued that there are no  $\bar{q}Q$  Goldstone boson states. We conclude, therefore, that the only new baryon states formed by the sextet sector are the sextet proton - the  $P_6$ , and the sextet neutron - the  $N_6$ . The importance of this conclusion will become apparent in later Sections.

We can enumerate the formation of the asymptotic states of  $QCD_S$  from those of  $CSQCD_S$ , as follows.

1. “pions”  $\leftrightarrow \{q\bar{q} + \text{wee gluons}\} \rightarrow$  normal meson spectrum in  $QCD_S$
2. “Pions”  $\leftrightarrow \{Q\bar{Q} + \text{wee gluons}\} \rightarrow \Pi^\pm, \Pi^0$ , in  $QCD_S$
3. “nucleons”  $\leftrightarrow \{qq / \bar{q}\bar{q} + \text{wee gluons}\} + \{q / \bar{q}\}$ ,  $\rightarrow$   $SU(3)$  color singlet  $\rightarrow$  normal nucleon spectrum in  $QCD_S$
4. “Nucleons”  $\leftrightarrow \{QQ / \bar{Q}\bar{Q} + \text{wee gluons}\} + \{Q / \bar{Q}\}$ ,  $\rightarrow N_6, P_6^\pm$  in  $QCD_S$

In Section 5 we will discuss hard diffractive interactions of the pomeron with either a photon or an electroweak vector boson. In these interactions the wee gluon component has only a limited role and, most importantly, there are no wee gluon interactions. In these circumstances, we can continue to represent the wee gluon component as a zero transverse momentum “condensate”. Even though, in reality, it is a much more complicated dynamical contribution of wee gluons over a range of infra-red transverse momenta. As we will see, the effective vertices involved will not contain a longitudinal vector interaction and so, as a consequence, the scale of wee gluon couplings will be an important effect. It will be crucial that, as we determine from the electroweak mass scale in the next Section, the wee gluon couplings for triplet and sextet quarks are very different. This will be represented by distinct condensate couplings for triplets and sextets.

With the wee gluons treated as semi-classical, we will be able to use the anomaly pole mechanism to obtain a limited understanding of the production of sextet pions and the resultant production of  $W$ ’s and  $Z$ ’s in hard diffractive processes. Not surprisingly, the minimal representation of the dynamics of the wee gluon component will have major limitations. Most significantly, we will be able to apply the “condensate anomaly mechanism” only at large  $k_\perp$  and then, directly, only to the production of an “on-shell” sextet pion carrying light-like momentum. Dynamical wee gluons can, presumably, produce sextet pions at both small  $k_\perp$  and off-shell, but we will not try to discuss this explicitly. Instead, we first use the kinematic form given directly by the anomaly amplitude to go “off-shell”. This leads to rough order-of-magnitude estimates and (some) qualitative kinematic features of hard diffractive phenomena. We can then combine the knowledge of hard diffraction that we obtain, with regge theory, to discuss expectations for soft diffraction. We will argue that, at the LHC, the most immediate place to see that new physics is in evidence is likely to be the double pomeron exchange cross-section!

## 4. ELECTROWEAK VECTOR BOSONS AND THE SEXTET QCD SCALE

We consider, now, the addition of the electroweak vector boson sector to  $QCD_S$ . We first add a triplet  $\{W^\pm, W^0\}$  of massless  $SU(2)$  gauge bosons with Standard Model left-handed couplings (with coupling constant  $g_w$ ) to both triplet and sextet quarks. Later we will add a massless hypercharge gauge field  $Y$  (with coupling constant  $g_y$ ) that also has Standard Model couplings to all quarks. We define “Standard Model” couplings for sextet quarks by recognizing that sextet antiquarks have the same  $SU(3)$  triality as triplet quarks. It is natural, therefore, for sextet antiquarks (quarks) to have the same electroweak couplings as triplet quarks (antiquarks). In fact, this is also what occurs when both kinds of quarks originate from an underlying unified theory[22]. In massless  $QCD_S$  there will be three flavor doublets of color triplet quarks that each produce a triplet of “pions” that have the quantum numbers to couple directly to the  $W$ ’s. The triplet of Pions produced by the single sextet doublet similarly has the quantum numbers to couple directly to the  $W$ ’s. We begin in  $CSQCD_S$  because this will enable us to understand the generation of a vector boson mass in terms of anomaly pole pions and Pions. We will see how the wee gluon component of a scattering, infinite momentum, pion generates a mass for an exchanged vector boson, as we would expect if the universal wee gluon component of infinite momentum states is able to reproduce vacuum properties.

### 4.1 Background Wee Gluon Interactions

To obtain an infra-red divergent scattering amplitude involving  $W$  exchange, there must be a wee gluon exchange accompanying (but not interacting with) the  $W$ , as illustrated in Fig. 14.

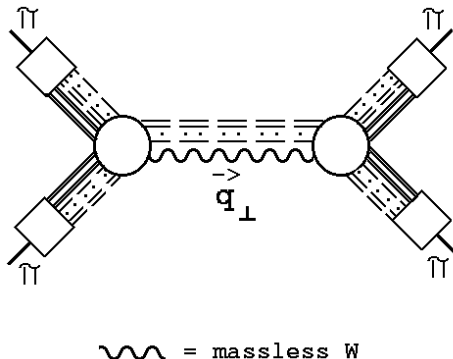


Fig. 14 Scattering via  $W$  exchange.

(Apart from the exchanged vector boson, the notation is the same as in Section 2.) However, because of the left-handed coupling, there will be interaction kernels, analogous to that of Fig. 3, for the  $W$  to interact with multi-gluon states that carry both normal and anomalous color charge parity. As a consequence, all infra-red divergent amplitudes will be exponentiated to zero, except for those produced by background wee gluons. Although the underlying multi-regge calculations remain to be carried out, we expect that there will be amplitudes analogous to that of Fig. 11, but with the gluon reggeon replaced by a (reggeized) vector boson. In this case, we expect that the full anomaly vertices, of the kind illustrated in Fig. 12, will not survive the exponentiation analogous to Fig. 13. Instead, the left-handed component of the axial-vector coupling shown in Fig. 12 will, because of the left-handed  $W$  coupling, contribute to an exponentiation of the form of Fig. 13. Implying that perturbative  $W$  exchange will be accompanied by a background, “right-handed”, wee gluon interaction. In  $QCD_S$ , with  $SU(3)$  color restored, this background interaction will be  $SU(3)$  symmetric.

## 4.2 $W$ Mass Generation

A priori, we anticipate that the existence of Goldstone boson  $\Pi$ ’s will lead to the  $W$ ’s aquiring a mass via the mixing illustrated schematically in Fig. 15.



Fig. 15 The Anticipated Mass Generation.

We will show that, in the regge limit, the first interaction term is produced (when  $q_{\perp}^2 \rightarrow 0$  ) by wee gluons in one, or the other, of the scattering pions. The wee gluon anomaly interactions involved are illustrated in Fig. 16.

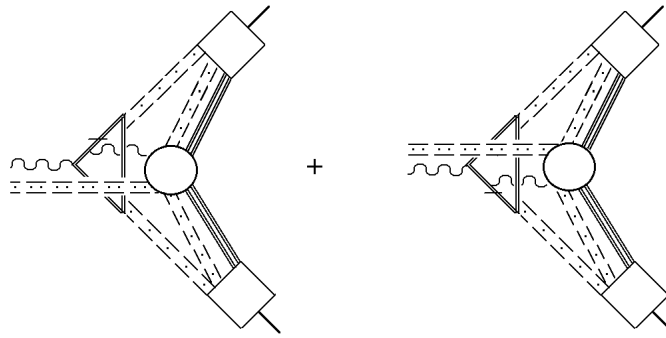


Fig. 16 Anomaly interactions.

For the moment, the quark loop involved can be either sextet or triplet. We will not attempt to identify the higher-order terms in Fig. 15. Identifying the first term will give us sufficient information for our purposes.

With the wee gluon kinematics used in Section 2, the first interaction in Fig. 16 gives, as  $q_\perp^2 \rightarrow 0$ , the anomaly pole contribution shown in Fig. 17.

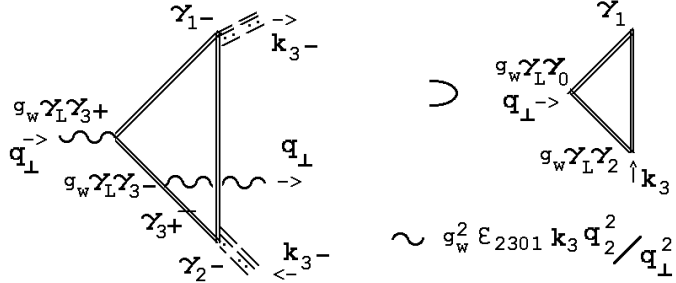


Fig. 17 The anomaly pole contribution.

(Again the notation is the same as in previous diagrams, except that we have introduced  $\gamma_L = 1 + \gamma_5$ .) The  $g_w \gamma_L \gamma_{3\pm}$  couplings appear because the  $W$  is exchanged over a large rapidity interval. The  $\gamma_{1-}$  and  $\gamma_{2-}$  couplings are similarly determined by the wee gluon kinematics.

If we add the two diagrams shown in Fig. 16, and integrate over the wee gluon momentum  $k_3$ , we produce a  $W$  mass of the form

$$M_W^2 \sim \frac{q_1^2 + q_2^2}{q_\perp^2} g_W^2 \int dk_3 k_3 = g_W^2 \int dk_3 k_3 \quad (4.1)$$

That there is actually no pole at  $q_\perp^2 = 0$  is consistent with our argument in Section 2 (and Appendix B) that the on-shell residue of an anomaly pole is finite only in an infinite momentum frame. Nevertheless, the quantum numbers at each vertex of the triangle diagram producing the denominator pole are identical to those of the effective triangle diagrams discussed in Section 2. Therefore, the masss generation can be interpreted as due to the direct coupling of a  $W$  to a Pion (or pion) just as anticipated in Fig. 15.

As discussed in the previous two Sections, wee gluon momentum factors are generally scaled by a mass factor ( $M$  in  $CSQCD_S$  or  $\mu$  in  $QCD_S$ ). However, because the diagrams of Fig. 16 contain only perturbative  $W$  vertices in addition to the wee gluon couplings (with no longitudinal interaction of the form of (2.17) ), the wee gluon momentum factor produced by the coupling to the anomaly diagram is not scaled by such a mass factor. As a result, the mass (4.1) that is obtained is a direct reflection of the wee gluon momenta involved together with an overall normalization factor that will be determined by the color factors associated with the sum over all wee gluon couplings to the quark loop involved. Since this color factor will be different for triplets and sextets, we can write the mass obtained from all quark loop interactions

of the form of Fig. 16 as

$$M_W = g_w^2 F_\Pi^2 + \Sigma_{\pi'} g_w^2 F_\pi^2 \quad (4.2)$$

and consider this to be a definition, for our purposes, of both  $F_\Pi$  and  $F_\pi$ .

We will discuss the relative magnitude of  $F_\Pi$  and  $F_\pi$  shortly. First, however, we note that the mass (4.2) appears only for vector bosons with a purely left-handed coupling. The “LLV” structure of the triangle diagram in Fig. 17 gives an anomaly, whereas if the  $W$  couplings were purely vector we would have a “VVV” structure and no anomaly. Similarly, if the coupling were purely axial vector we would have an “AAV” structure and, again, no anomaly. Hence, if we now introduce the Standard Model hypercharge gauge field  $Y$ , with couplings as discussed above, the above mass generation mechanism will apply also to the left-handed component of  $Y$ . We, therefore, obtain exactly the mass generation pattern of the Standard Model and there is no mass for the photon. (Note that photon exchange exchange will be accompanied by a background axial vector wee gluon interaction.)

To discuss the contribution of wee gluon color factors to  $F_\Pi$  and  $F_\pi$ , it will be simpler to make the transition from  $CSQCD_S$  to  $QCD_S$ . As we have discussed in the previous Section, the wee gluons will no longer be a simple condensate and the  $W$  mass generated by wee gluon interactions will be a much more complicated dynamical effect. Nevertheless, we can continue to define  $F_\Pi$  and  $F_\pi$  by (4.2).

The large sextet color factors surely imply that  $F_\Pi$  is much larger than  $F_\pi$ . A common expectation, based on Feynman graph color factors, is that triplet and sextet quark momentum scales for gluon interactions will be related (approximately) by the “Casimir Scaling” rule. This rule would say that  $F_\Pi$  and  $F_\pi$  should be related by

$$C(6) \alpha_s(F_\Pi^2) \sim C(3) \alpha_s(F_\pi^2) \quad (4.3)$$

where  $C(3)$  and  $C(6)$  are Casimirs for triplet and sextet quarks respectively. For  $SU(3)$  there are two Casimir operators which are (representation dependent) multiples of the identity. In terms of the generators  $G_a$ , these operators can be written as

$$C_2 = G^2 \sim f_{abc} G_a G_b G_c, \quad C_3 \sim d_{abc} G_a G_b G_c \quad (4.4)$$

and since

$$C_2(6)/C_2(3) = 5/2, \quad C_3(6)/C_3(3) = 7/2 \quad (4.5)$$

we can say

$$C(6)/C(3) \approx 3 \quad (4.6)$$

To apply (4.3) to the real world we must use the physical  $\alpha_s$  that is defined via “low-energy” QCD, with the sextet sector integrated out and with the physical quark

masses in place. In this case, if  $\alpha_s$  evolves as slowly as is commonly believed (e.g.  $\alpha_s(F_\pi^2) \sim 0.4$  ), the order of magnitude of  $F_\Pi$  will indeed be the electroweak scale! We conclude, also, that the sextet quark Pions will dominate the mass generation for  $W$  bosons, as anticipated in Fig. 15, and we can effectively ignore the triplet quark contribution.

We can look at the Casimir scaling rule (4.3) in two complimentary ways. We can use it, as we just did, to obtain directly the relative magnitude of triplet and sextet factors with a momentum dimension, on the basis that this is entirely controlled by the evolution of  $\alpha_s$ . More directly, we can say that in going from triplet to sextet graphical contributions,  $\alpha_s$  is effectively replaced by  $\{C(6)/C(3)\} \alpha_s$ . (An explicit example of this is provided by the  $\beta$ -function calculations described in Appendix A.) In this case, we can say that the large factor of  $F_\Pi^2$  that appears in the  $W$  mass results from the color factors associated with the product of the two wee gluon couplings, in the diagrams of Fig. 16, to the sextet quark loop involved. Since, essentially, the same color factors and wee gluon interactions will be involved, we conclude that the wee gluon coupling that provides the coupling of the wee gluon component of the pomeron to a sextet quark loop (in an anomaly pole amplitude) similarly, has the order of magnitude of  $F_\Pi$ . This tells us, as we shall see explicitly in the following, that the pomeron will couple very strongly to the electroweak sector, even though the states are very massive.

## 5. SEXTET PIONS AT HERA

We now begin our discussion of the hard diffractive production of vector bosons ( $W$ 's and  $Z$ 's) via sextet pions. In this Section and the next we will discuss processes that might be seen (or may have already been seen) at current accelerators and could provide evidence for the existence of the sextet sector. As we emphasized in the Introduction, diffractive processes are always a relatively small fraction of the total cross-section. However, as we showed in the previous Section, the strong coupling of the sextet sector to gluons is directly evident in the coupling of this sector to the pomeron and, as we show below, we can begin to estimate the cross-section by utilising the generation of a sextet pion via an anomaly pole. Therefore, diffractive processes might be particularly distinctive in the evidence they provide. (In Section 8 we will argue, very strongly, that this is the case for double pomeron exchange at the LHC.)

We will discuss deep-inelastic diffractive scattering in this Section. At moderate and low  $Q^2$  deep-inelastic scattering is dominated by photon exchange. Because the photon couples to sextet quarks, it can be diffractively excited to a  $Z^0$ , via sextet pion production, and this should be a very striking process to look for. However, to see this process at HERA we will be limited to large  $x$  and  $Q^2$  and, in fact,  $Q^2$  will be sufficiently large that  $Z^0$  exchange, in the neutral current, and  $W$  exchange, in the charged current will give equally large (or even larger) contributions. As we will discuss, all three exchanges similarly produce a final state vector boson via sextet pion production (a  $Z^0$  in the neutral current cross-section and a  $W$  in the charged current cross-section.) If we were at the level of predicting cross-sections it would be important to keep track of the relative contributions in the neutral and charged currents. However, we are certainly not at this stage and, as will become clear, we really do not know whether we are discussing a phenomenon which can be seen only as a very small (or zero) number of events at HERA or whether it could be at a level where relative cross-sections could be predicted, measured, and compared.

Because the produced vector boson carries a large longitudinal momentum and it is longitudinally polarized it has, as we will explain below, an enhanced probability (compared to a transversely polarized vector boson) for decay to a jet pair that are sufficiently close together, in phase space, to appear as a single massive jet. In the kinematical situation at HERA, this is particularly difficult to detect unambiguously. We are encouraged, nevertheless, by the fact that the features of the most dramatic large  $x$  and  $Q^2$  event presented[18] by ZEUS, in the original paper highlighting such events, are such that we are able to argue that a  $Z^0$  may, indeed, have been produced.

## 5.1 Diffractive Hard Interactions

A sextet pion can be directly produced via a hard interaction of the pomeron with a color neutral  $\gamma$ ,  $Z^0$  or  $W^\pm$ . When no pomeron self-interactions are involved, it should be reasonable to treat the wee gluon component of the pomeron as a condensate, as discussed in Section 3. In this case, as illustrated in Fig. 18, the pomeron can provide directly the wee gluon component that is needed for the sextet pion to appear via an anomaly pole.

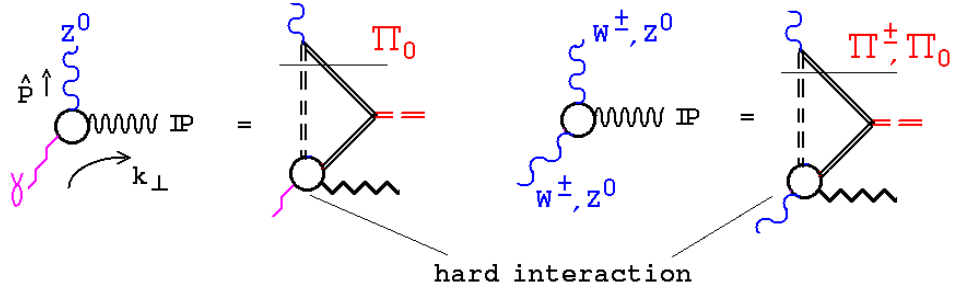


Fig. 18 Hard diffractive interactions.

(We use the same diagrammatic notation as in Section 2.)

In the following we will specifically discuss interactions initiated by a photon and only occasionally refer to the fact that the photon could equally well be a  $W^\pm$  or a  $Z^0$ . The simplest photon interaction that is effectively pointlike at large  $k_\perp$  and has the right  $\gamma$  - matrix structure to produce an anomaly pole, is shown in Fig. 19(a).

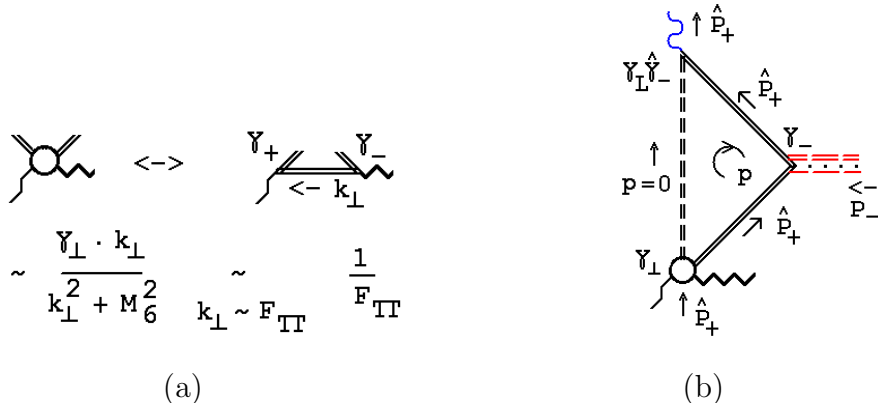


Fig. 19 (a) The hard interaction (b) the anomaly pole diagram.

( $M_6$  is a dynamical sextet quark mass which we take to be  $\sim F_{\Pi}$ .) The resulting anomaly pole diagram is shown in Fig. 19(b). We will see shortly that, in addition

to the large  $k_\perp$ , the hard gluon in the pomeron must also carry a large light-like momentum.

To obtain an anomaly pole amplitude via a finite on-shell residue we should, in principle, go to the infinite momentum frame of the produced pion. In addition, the anomaly pole description is valid only when the  $\Pi$  is on mass-shell, with zero mass. Fortunately, we want to produce a  $Z^0$ , and not a  $\Pi$  on mass-shell. Consequently, it should be reasonable to use the finite momentum anomaly pole amplitude (initially defined close to the Pion mass-shell) and continue that towards the  $Z^0$  pole.

## 5.2 Diffractive Deep-Inelastic Scattering

The anomaly amplitude shown in Fig. 19(b) gives the contribution to deep-inelastic diffractive jet production illustrated in Fig. 20.

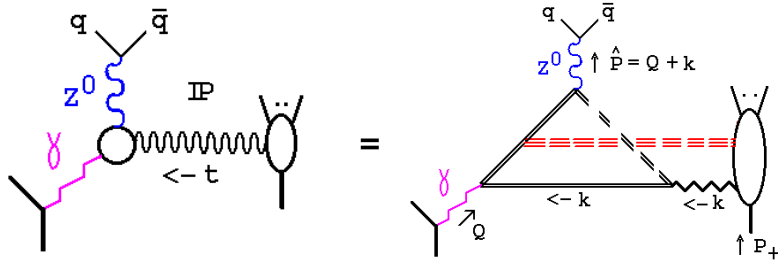


Fig. 20 Deep-inelastic diffractive jet production.

(A  $W^\pm$  or  $Z^0$  can obviously be substituted for the photon in this figure via Fig. 18.) Using the kinematic notation shown in Fig. 19(b) and Fig. 20, we initially take  $\hat{P} = Q + k$  to be light-like ( $= \hat{P}_+$ , as in Fig. 19(b) ) but very importantly, because  $Q$  is spacelike, the light-cone is not parallel to that defining  $P_+$  and  $P_-$ . In this case, with the  $\gamma$ -matrix couplings appearing in Fig. 19(b), the anomaly amplitude has a contribution with the kinematic form

$$\Gamma_{\perp \hat{n}_-} \sim \frac{\hat{P}_+ P_- \hat{P}_+}{P_- \hat{P}_+} = \hat{P}_+ \quad (5.1)$$

where  $\hat{n}_-$  is the light-cone vector orthogonal (in the euclidean sense) to  $\hat{P}_+$ . Again there is no anomaly pole. Instead, the effect of this pole is that the amplitude is independent of the wee gluon momentum  $P_-$ . Therefore, the anomaly pole wee gluon coupling will produce a simple integral over the wee gluon distribution that, for the reasons discussed in the last Section, we take to be  $\sim F_\Pi$ . Combining (5.1) with this

coupling and with the  $Z^0$  propagator and vertices  $g_w$ , and extrapolating away from  $\hat{P}^2 = 0$  by introducing  $\hat{P}_-$ , as a component of  $Q + k$ , gives

$$F_\Pi \hat{P}_+ g_w^2 \frac{(g_{-\nu} - \hat{P}_- \hat{P}_\nu / M^2)}{(\hat{P}^2 - M^2)} = - \frac{\hat{P}_-}{F_\Pi} \frac{\hat{P}^2}{\hat{P}^2 - M^2} \delta_{-,\nu} - \frac{\hat{P}_+}{F_\Pi} \delta_{+,\nu} \quad (5.2)$$

where  $M$  is now  $M_{Z^0}$  (but would be  $M_W$  if we were discussing  $W$  production) and we have used  $M = g_w F_\Pi$ . (All light-cone co-ordinates are now defined relative to the  $\hat{P}$  light-cone.) The first term in (5.2) is present as soon as  $\hat{P}^2 \neq 0$ . It produces a physical, longitudinal,  $Z^0$ .

The second term in (5.2) has no pole, but it is of comparable magnitude away from the pole and (when  $\hat{P}_-$  is small) it gives a direct coupling to fermion final states that is proportional to their mass. Note that there is no explicit  $g_w$  dependence in (5.2) and when  $\hat{P}_+ \sim \hat{P}_- \sim F_\Pi$  both terms are  $O(1)$ . Therefore, at the electroweak scale, the anomaly amplitude produces electroweak final states with no electroweak suppression.

### 5.3 The Angular Distribution of Produced Jets and Leptons

A high momentum longitudinal  $Z^0$  is more likely, than a transversely polarized  $Z^0$ , to produce a jet or lepton pair that are sufficiently close together, in phase space, to appear as a single massive jet. We will show this by comparing infinite momentum limits in the two cases.

If we denote the (four-) momentum vectors of the produced fermions by  $X$  and  $Y$ , then if the  $Z^0$  momentum is

$$P_{Z^0} = (P_+ + P_-, P_+ - P_-, 0, 0), \quad \text{where} \quad 4P_+ P_- = M^2 \quad (5.3)$$

the most general form for  $X$  and  $Y$  is

$$\begin{aligned} X &= (\lambda P_+ + (1 - \lambda) P_-, \lambda P_+ - (1 - \lambda) P_-, p_\perp, 0) \\ Y &= ((1 - \lambda) P_+ + \lambda P_-, (1 - \lambda) P_+ - \lambda P_-, -p_\perp, 0) \end{aligned} \quad (5.4)$$

where  $0 \leq \lambda \leq 1$ . The mass of both fermions is given by

$$m_f^2 = 4\lambda(1 - \lambda)P_+ P_- - p_\perp^2 = \lambda(1 - \lambda)M^2 - p_\perp^2 \quad (5.5)$$

This notation will be convenient for our purposes, even though it obscures the fact that we could obtain all momenta via a boost from the rest frame of the  $Z^0$ . In this frame, the only variable would be the angle between the transverse momenta of the

fermion pair and the direction in which the  $Z^0$  is to be boosted. This is, of course, why  $p_\perp$  and  $\lambda$  are related via (5.5).

We consider first a transverse coupling which, for the purpose of  $\gamma$ -matrix manipulations, we write in the form

$$\langle Y|n_\perp \cdot \gamma_\perp|X\rangle \quad (5.6)$$

where  $n_\perp$  is a unit transverse vector. Suppose, first, that  $P_+$  is so large that both  $P_-$  and  $p_\perp$  can be neglected. Using the Dirac equation for  $|X\rangle$  then gives

$$\begin{aligned} \langle Y|n_\perp \cdot \gamma_\perp|X\rangle &\sim \langle Y|n_\perp \cdot \gamma_\perp \lambda \gamma_- P_+ / m_f|X\rangle \\ &\sim -\langle Y|\lambda \gamma_- P_+ n_\perp \cdot \gamma_\perp / m_f|X\rangle \\ &\sim \frac{\lambda}{1-\lambda} \langle Y|n_\perp \cdot \gamma_\perp|X\rangle \end{aligned} \quad (5.7)$$

$$\implies \langle Y|n_\perp \cdot \gamma_\perp|X\rangle = 0 \quad (5.8)$$

except, possibly, when  $\lambda = (1-\lambda) = 1/2$ . Not surprisingly, we have to add transverse momentum in order to get substantial information about how a transversely polarized  $Z^0$  will decay.

If we repeat the above manipulation keeping the transverse momentum dependence we obtain

$$\begin{aligned} \langle Y|n_\perp \cdot \gamma_\perp|X\rangle &\sim \langle Y|n_\perp \cdot \gamma_\perp (\lambda \gamma_- P_+ + \gamma_\perp \cdot p_\perp) / m_f|X\rangle \\ &\sim -\langle Y|(\lambda \gamma_- P_+) n_\perp \cdot \gamma_\perp / m_f|X\rangle + \langle Y|n_\perp \cdot \gamma_\perp (\gamma_\perp \cdot p_\perp) / m_f|X\rangle \\ &\sim \frac{\lambda}{(1-\lambda)} \langle Y|n_\perp \cdot \gamma_\perp|X\rangle - \frac{\lambda}{(1-\lambda)} \langle Y|(\gamma_\perp \cdot p_\perp) n_\perp \cdot \gamma_\perp|X\rangle / m_f \\ &\quad + \langle Y|n_\perp \cdot \gamma_\perp (\gamma_\perp \cdot p_\perp) / m_f|X\rangle \\ &\sim \frac{\lambda}{(1-\lambda)} \langle Y|n_\perp \cdot \gamma_\perp|X\rangle + \frac{(1-2\lambda)}{(1-\lambda)} \langle Y|p_\perp \cdot n_\perp|X\rangle / m_f + \dots \end{aligned} \quad (5.9)$$

The additional terms cancel if we add the corresponding equation obtained by reversing the roles of  $\lambda$  and  $(1-\lambda)$ . (Note that  $(1-2\lambda)$  changes sign under  $\lambda \leftrightarrow (1-\lambda)$  but, also,  $m_f \leftrightarrow -m_f$ .) We then obtain the simple result

$$\langle Y|n_\perp \cdot \gamma_\perp|X\rangle \sim -\langle Y|p_\perp \cdot n_\perp|X\rangle / m_f \quad (5.10)$$

We learn from (5.10) that a transverse  $Z^0$  decays to fermions with transverse momenta determined by the polarization. The amplitude is a maximum when  $|p_\perp|$

is a maximum which, from (5.5) occurs when  $\lambda = 1/2$ . In this case, the fermions symmetrically carry one half of the light cone momenta of the  $Z^0$ . It is a smooth maximum, however, and so there is a significant probability that the  $Z^0$  will decay into an asymmetric configuration.

If we repeat the above discussion for the longitudinal polarization we obtain a non-zero contribution already in the first manipulation, i.e.

$$\begin{aligned} \langle Y | \gamma_+ | X \rangle &\sim \langle Y | \gamma_+ \lambda \gamma_- P_+ / m_f | X \rangle \\ &\sim - \langle Y | \lambda \gamma_- P_+ 2\gamma_+ / m_f | X \rangle \\ &\sim \frac{\lambda}{1-\lambda} \langle Y | \gamma_+ | X \rangle - 2\lambda \langle Y | P_+ | X \rangle / m_f \end{aligned} \quad (5.11)$$

giving

$$\langle Y | \gamma_- | X \rangle \sim - \frac{2\lambda(1-\lambda)}{m_f(1-2\lambda)} \langle Y | P_+ | X \rangle \quad (5.12)$$

Now the symmetric case, with  $\lambda = 1/2$ , is strongly enhanced. Although, because terms that are non-leading as  $P_+ \rightarrow \infty$  will also be singular as  $\lambda \rightarrow 1/2$ , we can use (5.12) only if we stay away from  $\lambda = 1/2$ . It is, nevertheless, sufficient for us to conclude that, at large momentum, the symmetric configuration with two jets (or leptons) close together in phase space is enhanced for a longitudinal  $Z^0$  decay, compared to the transverse case. In general, the final result may often look like a broad single jet. Therefore, although it is usually only possible to definitively detect a  $Z^0$  via a leptonic decay, it seems that when it is produced longitudinally and is carrying a large light-like momentum, as will be the case in the deep-inelastic scattering kinematics that we consider, we could instead try to identify it as a single massive jet.

#### 5.4 Comparison With a Jet Amplitude

In this sub-section we introduce an argument that will form the general basis for, potentially at least, obtaining order of magnitude estimates for hard diffractive sextet pion amplitudes. In sub-section 5.5 we will give a further general argument for extending such estimates to soft diffractive amplitudes.

At first sight, as illustrated in Fig. 19(a), the hard interaction that helps produce the anomaly amplitude is  $O(1/F_\Pi)$  at the electroweak scale and does give a suppression. However, as we discuss now, this is the natural order of magnitude for a normal two jet amplitude that does not involve sextet pion production. We consider the two jet amplitude involving gluon exchange shown in Fig. 21(a), and consider the two production vertices shown in Fig. 21(b). (Once again the photon could be replaced by either a  $Z^0$  or a  $W^\pm$ .) The first vertex shown is a lowest-order amplitude involving quark exchange. The second is a loop amplitude that gives

the lowest-order triplet sector vertex for  $Z^0$  production. Considering (5.2) to simply give a factor that is  $O(1)$ , if we compare the the quark exchange amplitude with the anomaly amplitude of Fig. 20, the first difference is that in the jet amplitude a triplet quark propagator, carrying momentum  $P_j$ , replaces the hard interaction in the triangle diagram amplitude. However, provided  $|P_j| \sim |k_\perp|$ , this will simply give the “natural” order of magnitude for a jet amplitude that we referred to above.

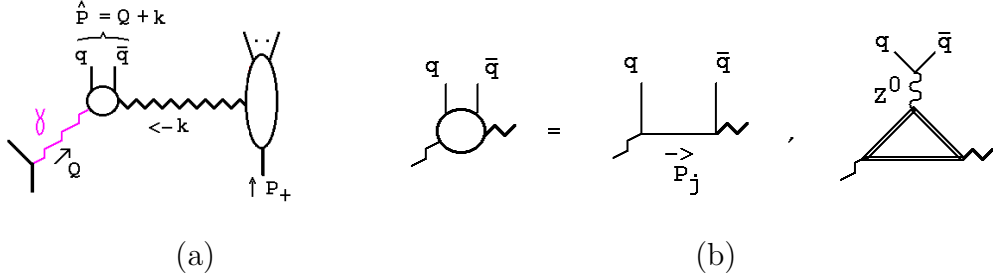


Fig. 21 (a) A two jet amplitude (b) production vertices

The second, and only other, difference between the lowest-order jet amplitude and the anomaly amplitude is that a regular gluon (parton) vertex replaces the pomeron vertex (that is the reggeized gluon plus wee gluons vertex). Since deep-inelastic diffractive hard cross-sections are about 10% of the corresponding full cross-section, we can expect the pomeron vertex to give a reduction of a factor of  $1/3$  in the amplitude. However, this will be compensated for, in part, by the fact that  $\alpha_s$  for a sextet quark coupling is involved. Since our discussion of orders of magnitude is certainly not accurate to within factors of 3, we conclude that (to the limited accuracy that we can achieve) when all the momenta involved are electroweak scale in magnitude, the diffractive production of jet pairs via  $Z^0$  production will give a comparable cross-section to that for conventional (non-diffractive) two jet production.

To emphasize the (relatively) large magnitude of the diffractive production amplitude we are discussing, we consider corresponding cross-sections for  $Z^0$  production when only the triplet sector is present. First, we consider the anomaly pole mechanism. In this case, the factor of  $F_\Pi$  in the numerator of the left side of (5.2) is replaced by  $F_\pi$  and there is a reduction in cross-section of  $\gtrsim O(10^6)$ . If we instead consider the one loop production vertex of Fig. 21(b), the factor of  $F_\Pi \hat{P}_+$  in the left side of (5.2) is replaced by a factor of  $\mu^2$ , where  $\mu$  is the triplet sector momentum scale, leading to a much greater reduction of the cross-section.

The most immediate question is, of course, whether there could be observable events at HERA? Not surprisingly, it is very difficult to realize the appropriate kinematics with the available energy. However, as we discuss below, if we invoke regge

theory to amplify our discussion we can argue that, at large  $x$  and  $Q^2$ , there could be events that are due to the diffractive  $Z^0$  production that we are discussing.

## 5.5 HERA Kinematics

For most of our discussion we will take both the proton and the positron to be massless. We denote the momentum of the proton beam by  $E_p$  and the momentum of the positron beam by  $E_e$ . If we write the photon (or  $Z^0$ , or  $W^\pm$ ) momentum as

$$Q = (Q_+ + Q_-, Q_+ - Q_-, Q_\perp) \quad (5.13)$$

then the light-cone components  $Q_+$  and  $Q_-$  are determined, at fixed  $x$  and  $Q^2$ , by the mass-shell condition for the scattered positron, i.e.

$$0 = 4p_- Q_+ - Q^2 \quad (5.14)$$

and

$$x = \frac{Q^2}{4P_+ Q_-} \quad (5.15)$$

Solving for  $Q_\perp^2$ , we obtain

$$Q_\perp^2 = Q^2 - \frac{Q^4}{Sx} = (1 - y)Q^2 \quad (5.16)$$

where  $S = 4P_+ p_-$  and  $xyS = Q^2$ .

(5.16) shows that large  $Q_\perp$  requires both large  $x$  and  $Q^2$ . With  $E_p = 820$  GeV and  $E_e = 27.5$  GeV (the original HERA values) we can obtain  $Q_\perp \sim 100$  GeV with  $Q^2 \sim 30,000$  GeV $^2$  and  $x \sim 0.5$ . However, if (in the notation of Fig. 20) we also require that  $k_\perp \sim 100$  GeV and  $\hat{P}^2 \sim M_{Z^0}^2$  then, not surprisingly, it is very difficult to have all conditions satisfied. First, it is necessary for  $k$  to have a very large light-cone component to put the  $Z^0$  on-shell. We then find that to keep the diffractively excited proton state physical we must have  $|k^2| = |t| \gtrsim 2k_\perp^2 \sim 20,000$  GeV $^2$ . In this case, the jet cross-section we are comparing with will be far too small to be observable.

## 5.6 Small $t$ Scattering

We can extend the foregoing discussion with an argument that we will also apply to other diffractive amplitudes in later Sections. According to our analysis, the  $QCD_S$  pomeron is essentially a regge pole and so has, approximately, the factorization properties of a regge pole all the way from electroweak scale values of  $|t|$  down to  $|t| \sim 0$ . The regge behavior is manifest at large  $|t|$  via the reggeized

gluon that gives the kinematic properties of the hard pomeron that we have been discussing and this will match smoothly with a soft pomeron regge pole picture as  $|t|$  decreases. (Note that  $t$  can be small even though a large light-like momentum is exchanged.) Since we anticipate that the “non-perturbative”  $\gamma Z^0 \text{IP}$  vertex is entirely due to electroweak scale dynamics it should vary only slowly with  $|t|$  (with a scale determined by  $F_\Pi$ ). However, the proton/pomeron coupling will be the normal hadronic coupling and will increase exponentially fast as  $|t|$  decreases. It is difficult to know how large this increase will be, since there are no measurements of this coupling for  $|t| \sim 20,000 \text{ GeV}^2$  ! We do know that the cross-section for proton elastic scattering, which involves the square of the coupling that we are interested in, decreases by five orders of magnitude between zero and  $|t| \sim 1 \text{ GeV}^2$ , and by another five orders of magnitude between  $|t| \sim 1 \text{ GeV}^2$  and  $|t| \sim 10 \text{ GeV}^2$ .

Presumably, the largest cross-section at HERA would be the extreme case in which the initial proton scatters elastically and  $|t|$  is at it’s kinematic minimum. (The mass-shell condition for the proton gives a lower limit for  $|t|$  when a longitudinal momentum is exchanged, but it is relatively small  $\lesssim 2 - 3 \text{ GeV}^2$  ). Knowing that the cross-section should increase by orders of magnitude as  $|t|$  decreases, if we are also close to the  $Z^0$  pole, it is surely possible that the resulting jet cross-section could be observable.

## 5.7 A Model Event

To illustrate, specifically, the situation described in the last sub-section we can take the following set of momenta as potentially describing an event at HERA. We take

$$\begin{aligned} P_p &\sim (820, 820, 0, 0), & P_e &\sim (27.5, -27.5, 0, 0) \\ Q &\sim (-263, -297, 105, 0), & k &\sim (560, 560, 0, 0), \\ \hat{P} &= Q + k = (297, 263, 105, 0) \end{aligned} \quad (5.17)$$

giving

$$\begin{aligned} Q^2 &\sim -30,000 \text{ GeV}^2, & x &\sim 0.54, & Q_\perp &\sim 105 \text{ GeV}, \\ |t| &= k^2 \sim 0, & \hat{P}^2 &= \sim 8,000 \text{ GeV}^2 & \sim M_{Z^0}^2 \end{aligned} \quad (5.18)$$

Although  $k$  has a very large light-cone component,  $t$  is very close to zero. ( $|t| = 0$  only because we have not taken the mass of the proton into account). The scattered positron will have momentum

$$P_e - Q \sim (290.5, 269.5, -105, 0) \quad (5.19)$$

and so, comparing with  $\hat{P}$  in (5.17), we see that (because  $|t| \sim 0$ ) the positron and the  $Z^0$  emerge with opposite, but equal in magnitude, transverse momentum. Moreover,

in this example they make (very close to) the same angle ( $\theta$ ) with the proton beam, where

$$\tan \theta \sim \frac{105}{270} \sim 0.39 \implies \theta \sim 21^\circ \quad (5.20)$$

Since all invariants are large compared to  $t$  (although not compared to  $Q^2$ ) the kinematics described by (5.17)-(5.20) correspond to a Regge limit in which pomeron exchange could appear. Indeed, if the  $Z^0$  were a stable particle, there would also be a rapidity gap that, because of the special HERA kinematics, would be small and very far forward - between  $0^\circ$  and  $21^\circ$ . (In the center of mass frame of the positron and the proton, the  $Z^0$  would actually be produced in the backward hemisphere compared to the final state proton.) In reality, of course, the  $Z^0$  is not stable and the decay products can fill in a large part of the rapidity gap that would exist if it were stable.

## 5.8 What Can be Seen at HERA ?

In the original ZEUS paper[18] five events were highlighted which all had relatively large  $x$  and  $Q^2$ . We have identified an electroweak scale  $|Q_\perp|$  as necessary for sextet pion  $Z^0$  production and four events had  $|Q_\perp| \gtrsim 100$  GeV. We have considered the five ZEUS events in some detail, mainly because full kinematics of the events have been published in the form that we need. Although subsequent ZEUS data[23] appear to show that the  $e^+p$  cross-section at large  $x$  and  $Q^2$  (up to, and including,  $Q^2 = 30,000$  GeV $^2$ ) is not substantially above that predicted by the Standard Model, H1 data seem to give a different impression. The published H1 cross-section[24] for the neutral current at  $Q^2 = 30,000$  GeV $^2$  (and the charged current at lower  $Q^2$ ) seems to be significantly above the Standard Model value. Therefore, it remains possible that some fraction of the original five events (particularly at  $Q^2 > 30,000$  GeV $^2$ ) and, presumably, subsequently observed events, are due to a non Standard model process. In fact, according to our arguments, of the five ZEUS events, only the largest  $Q^2$  event clearly has a high probability to have resulted from  $Z^0$  production.

In each event there is a clear jet and the essential question we have to discuss is whether there is reason to identify it as a massive jet produced by a  $Z^0$ . To this end, we consider first the particular event shown in Fig. 22. At first sight, this event is very tantalizing because, if the observed jet could indeed be identified as a  $Z^0$ , the event has (almost exactly) the kinematic properties illustrated by (5.17)-(5.20).  $Q^2 \sim -25,000$  GeV $^2$ ,  $x \sim 0.55$  and  $Q_\perp \sim 110$  GeV. In addition, the transverse momenta of the positron and the jet balance almost perfectly and they are both produced at an angle of  $\sim 28^\circ$  with the beam. Unfortunately, perhaps, this event is the one in which it is most clear that the jet could not have been a  $Z^0$ , as we now discuss.

We will make essential use of the fact that two, a priori independent, recon-

strucion methods are used to measure both  $Q^2$  and  $x$  and the results from both are quoted separately, as in Fig. 22.

$$\theta_e = 27.8^\circ \quad \gamma = 26.7^\circ \quad \rightarrow \quad x_{DA} = 0.570 \pm 0.029 \quad Q_{DA}^2 = 25200 \pm 700 \text{ GeV}^2$$

$$E'_e = 236 \text{ GeV} \quad \rightarrow \quad x_e = 0.536 \pm 0.048 \quad Q_e^2 = 24400 \pm 1100 \text{ GeV}^2$$

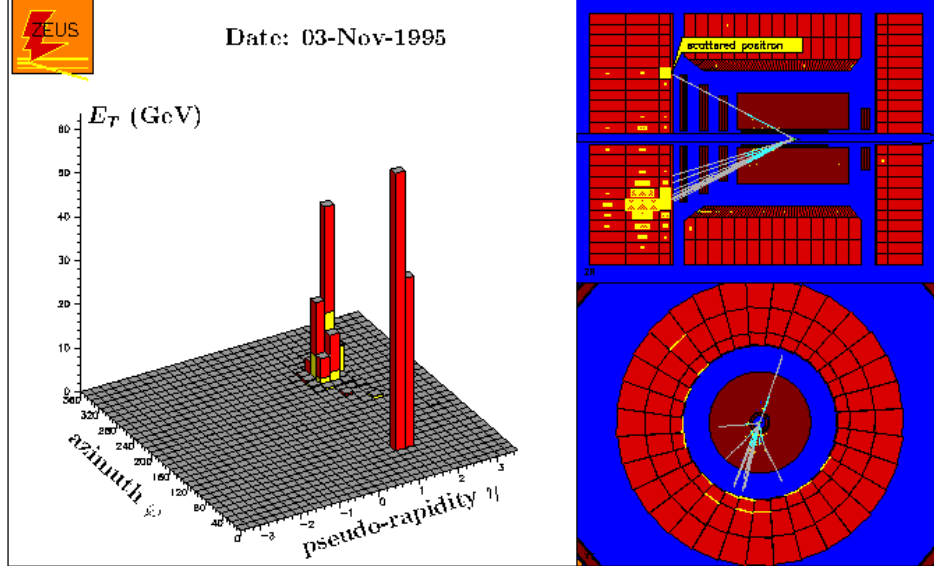


Fig. 22 A tantalizing ZEUS event.

The first method, called the “double-angle” (DA) method uses only the measured angles of the jet ( $\gamma$ ) and the electron ( $\theta_e$ ), together with the formulae

$$x_{DA} = \frac{E_e}{E_p} \frac{\sin \gamma}{(1 - \cos \gamma)} \frac{\sin \theta_e}{(1 - \cos \theta_e)}$$

$$y_{DA} = \frac{\sin \theta_e (1 - \cos \gamma)}{\sin \gamma + \sin \theta_e - \sin(\gamma + \theta_e)} \quad (5.21)$$

$$Q_{DA}^2 = s x_{DA} y_{DA}$$

The other “positron” method uses only the measured positron energy  $E'_e$  and the angle  $\theta_e$ , together with the formulae

$$x_e = \frac{E_e}{E_p} \frac{E'_e (1 + \cos \theta_e)}{2E_e - E'_e (1 - \cos \theta_e)}$$

$$y_e = 1 - \frac{E'_e}{2E_e} (1 - \cos \theta_e) \quad (5.22)$$

$$Q_e^2 = s x_e y_e$$

Although this second method is much more direct, because of the difficulty of measuring  $E'_e$  reliably, the double angle method is generally regarded as more reliable for discussing large  $Q^2$  deep-inelastic events. Note that the value of  $E'_e$  quoted in Fig. 22 is a corrected value that differs from the number originally quoted in [18]. It is, however, the number that gives the quoted values of  $Q_e^2$  and  $x_e$  from (5.22).

As can be seen from the numbers in Fig. 22, the two reconstruction methods give very similar results for both  $Q^2$  and  $x$ . Indeed, if we reconstruct the full four-momentum  $Q$  from (5.13)-(5.16) we obtain

$$Q_{DA} = (-215.5, -242.5, 111, 0) \quad (5.23)$$

and

$$Q_e = (-208.5, -235.5, 110, 0) \quad (5.24)$$

That there is no significant difference between (5.23) and (5.24) is very important for our purposes because the double angle method is predicated[25] on the assumption that the jet mass can be neglected. As a result, (5.21) correctly gives  $x$  and  $Q^2$  only when the jet is (at least approximately) massless. Therefore, the agreement between (5.23) and (5.24) can be regarded as explicit confirmation that the jet mass is, in fact, small or zero.

It is also significant that the jet angle  $\gamma$  is actually  $26.7^\circ$  and not  $21^\circ$ , as it was in the example we constructed in sub-section 5.6. Because of its large mass, the  $Z^0$  has to be produced relatively far forward ( $21^\circ$  is not very far from the maximum possible angle if  $Q^2 \sim 30,000 \text{ GeV}^2$  and  $|Q_\perp| \sim 100 \text{ GeV}$ ). This is, in itself, a potential difficulty in looking for a  $Z^0$  jet. If the jet is very broad it might not be well separated from the beam pipe. We will consider this possibility more seriously when we discuss another event below. To have the  $Z^0$  produced at a maximally large angle, maximally large  $Q^2$  is necessary. We should also note that if the  $Z^0$  decays into two distinct jets (a decay that we have argued is less likely because the  $Z^0$  is longitudinal), one jet could go very close to the beam pipe and become indistinguishable from the proton remnant. While it is, perhaps, possible that some of the ZEUS events could be of this kind, we do not think it is very likely and will not discuss the possibility seriously.

We conclude that, although the event shown in Fig. 19 has many of the features of the diffractive  $Z^0$  production that we are looking for, the jet involved can not be a  $Z^0$ . For the largest  $Q^2$  event, however, the situation is very different.

## 5.9 The Largest $Q^2$ Event

This event is shown in Fig. 23. We immediately notice that, for both  $Q^2$  and  $x$ , the results for the two reconstruction methods differ significantly, with the differences

being outside of the quoted errors. As we implied above, a possible reason for this

$$\theta_e = 15.4^\circ \quad \gamma = 38.6^\circ \quad \rightarrow \quad x_{DA} = 0.709 \pm 0.034 \quad Q_{DA}^2 = 46100 \pm 1600 \text{ GeV}^2$$

$$E'_e = 380 \text{ GeV} \quad \rightarrow \quad x_e = 0.605 \pm 0.060 \quad Q_e^2 = 41000 \pm 3000 \text{ GeV}^2$$

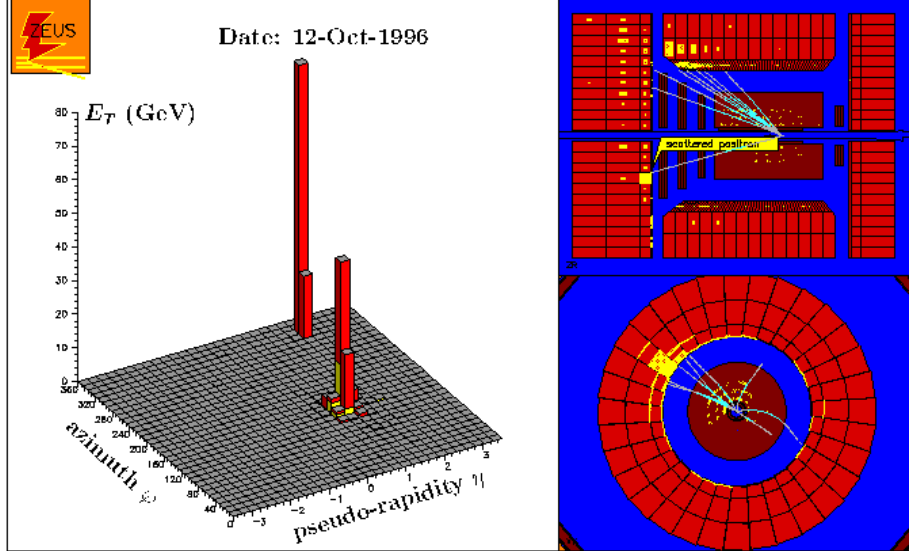


Fig. 23 The largest  $Q^2$  ZEUS event.

discrepancy is that a large mass for the produced jet invalidates[25] the double-angle method. If we again reconstruct the full four-momentum  $Q$  from (5.13)-(5.16) we obtain

$$Q_{DA} = (-399, -439, -113, 0) \quad (5.25)$$

and

$$Q_e = (-352.5, -393.5, 101, 0) \quad (5.26)$$

Clearly, the results are significantly different.

We can regard the double-angle method as projecting the experimentally measured calorimeter energies and momenta onto the combination of a massless jet and an additional momentum projected onto the measured direction of the positron. In effect, this is what is done by the process of eliminating the energy of the positron and assuming that only the angle is well determined experimentally. The jet angle  $\gamma$  is determined directly (under the assumption that the jet is massless). Following the procedure used in the ZEUS paper we determine the jet energy by using the fact that  $p_\perp$  is approximately conserved (as is recorded in Fig. 23). As a result, the  $p_\perp$  of the jet must balance that given by  $Q_e$ . With  $\gamma = 38.6^\circ$ , this determines the four-momentum of the (assumed to exist) massless jet to be

$$P_j = (167, 126.5, 101, 0) \quad (5.27)$$

Taking the directly measured  $Q_e$  to be correct, the additional momentum projected along the positron direction is

$$Q_e - Q_{DA} = (46.5, 45.5, -12, 0) \quad (5.28)$$

Adding this back to  $P_j$  to, potentially, obtain the true four momentum of the produced hadronic state we obtain

$$P_j + Q_e - Q_{DA} = (213.5, 172, 89, 0) \quad (5.29)$$

which has a mass squared of

$$8,077.25 \text{ GeV}^2 = (89.9 \text{ GeV})^2 \quad (5.30)$$

suggesting that a massive  $Z^0$  jet was indeed produced. The production angle would have been

$$\gamma_{Z^0} = 27.4^\circ \quad (5.31)$$

That the production angle can be this large is only possible because  $Q^2$  is so large.

Although the detector region involved includes the gap between two components of the calorimeter (and so may not be reliable), looking at the raw visual display in the top right corner of the event display shown in Fig. 23, and magnified in Fig. 24, it is (perhaps) plausible that the true axis of the jet was not so far from  $27.4^\circ$ . To guide the eye, lines are drawn at  $27.4^\circ$  and  $38.6^\circ$  in Fig. 24. Of course, the “lego plot” of the jet would have to be shifted along the pseudorapidity axis. (The current plot actually seems at odds with the raw event display in that no  $E_T$  is recorded for  $\eta > 1.4$  (corresponding to angles less than  $28^\circ$ ) even though there are clearly tracks in the event display.

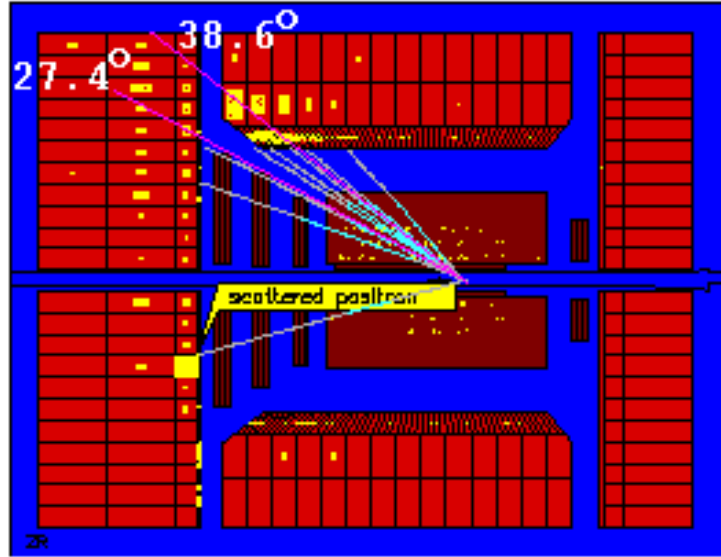


Fig. 24 The event display from Fig. 23.

If, comparing with (5.17), we compute the momentum transfer  $k$  using (5.29) for the momentum  $\hat{P}$  of the  $Z^0$  we obtain

$$k = P_{Z^0} - Q_e = (566, 565.5, 12, 0) \quad (5.32)$$

implying (more exactly than is surely justified by all the reconstruction involved) that the squared momentum transfer may have indeed been small. Thus allowing the interpretation of the event as diffractive  $Z^0$  production.

While our reconstructive argument can only be regarded as suggestive, it should, presumably, be possible to study properties of the event more directly to determine whether it can really be interpreted as a  $Z^0$ .

## 5.10 The Other ZEUS Events

If we consider the remaining three ZEUS events we find that in two cases the agreement between the results obtained for the two reconstruction methods is good enough to, essentially, eliminate the possibility that the jet involved was a massive  $Z^0$ . In the third case it is not so clear. The event involved is shown in Fig. 25

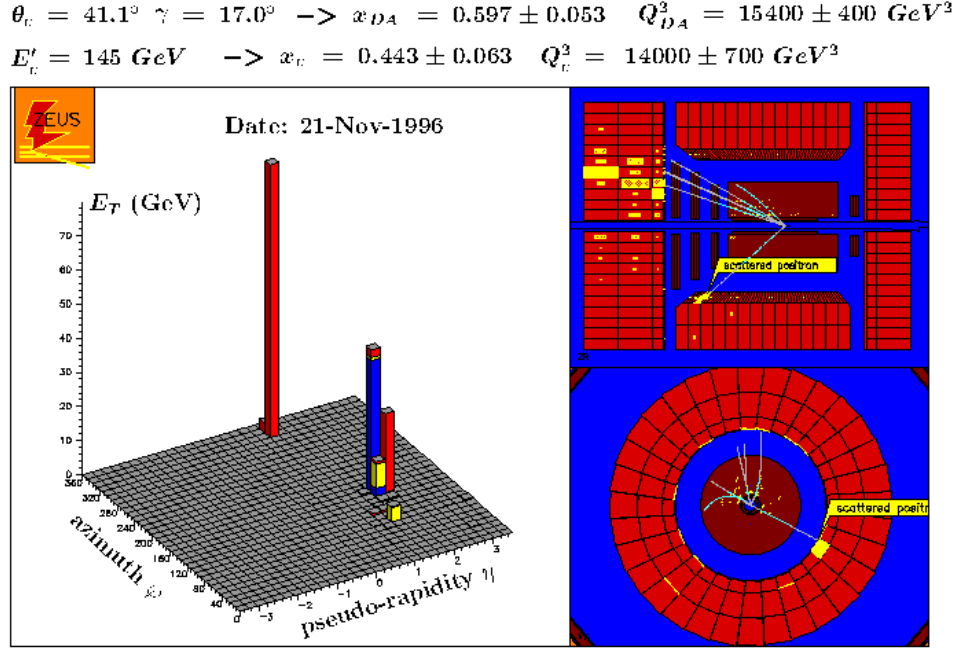


Fig. 25 A ZEUS event with reconstruction problems.

Again the disagreement in the values of  $x$  and  $Q^2$  is outside of the quoted errors.  $|Q_\perp| \sim 95 \text{ GeV m}$  which is probably large enough. However,  $Q^2 \sim 14,000 \text{ GeV}^2$  and

so is much smaller than that of the previous event. If we follow the same procedure as we used in discussing Fig. 23 we arrive at a candidate  $Z^0$  four momentum

$$P_j + Q_e - Q_{DA} = (339.5, 322.5, 85, 0) \quad (5.33)$$

which has a mass squared of

$$4029 \text{ GeV}^2 = (63.5 \text{ GeV})^2 \quad (5.34)$$

Because of the much smaller  $Q^2$ , the production angle for the candidate  $Z^0$  is only  $14.8^\circ$  and, looking at the raw event display, the possibility that some significant part of the jet (or rather a “slow jet” component of the  $Z^0$ ) went down the beam pipe is probably difficult to eliminate. However, since we have no way of evaluating this possibility, we have to conclude that the probability that there was a  $Z^0$  in the event of Fig. 25 is not high. Thus, the large  $Q^2$  event of Fig. 23 is clearly the most serious candidate for diffractive  $Z^0$  production.

### 5.11 Other Events

It will be very interesting to determine whether the foregoing analysis can reveal further HERA events that might be consistent with diffractive  $Z^0$  production. Although the H1 events, that were presented in the paper[26] that was contemporaneous with the ZEUS paper, carried large  $Q^2$  they were selected with different criteria and were presented from a different viewpoint. There was an emphasis on the possibility of a large mass intermediate state in the electron + jet channel that led to the presentation of the kinematics of the events in a way that makes it impossible to directly apply our analysis. Also the search for a large mass intermediate state produced an emphasis on large  $y$ , and hence low  $Q_\perp^2$ , that is counter to our purpose. In particular, the two largest  $Q^2$  events presented (with  $Q^2 \sim 31,000 \text{ GeV}^2$ ) both had relatively small  $x$  ( $\sim 0.45$ ) and consequently had lower  $Q_\perp^2$  ( $\sim 80 \text{ GeV}$ ) than we would prefer for our analysis.

Presumably, both ZEUS and H1 have further candidate events from runs subsequent to 1997. However, cross-sections for  $Q^2 > 30,000 \text{ GeV}^2$  have yet to be published, as have any corresponding event pictures.

## 6. SEXTET PHYSICS AT FERMILAB

In this Section we discuss evidence for the existence of the sextet sector, both diffractive and non-diffractive, that might be seen (or may have been seen) at Fermilab. We begin with diffraction.

### 6.1 Single Diffraction

The interactions shown in Fig. 18 will also take place in a hadron collider when a  $Z^0$ ,  $W^\pm$ , or photon is emitted from a quark in a hadron. Unfortunately, it will be very difficult to isolate these processes because of the small cross-section involved. Single diffractive production of a  $W$  or  $Z$  can proceed as illustrated Fig. 26(a). The comparable two jet amplitude, analagous to Fig. 21, is shown in Fig. 26(b)

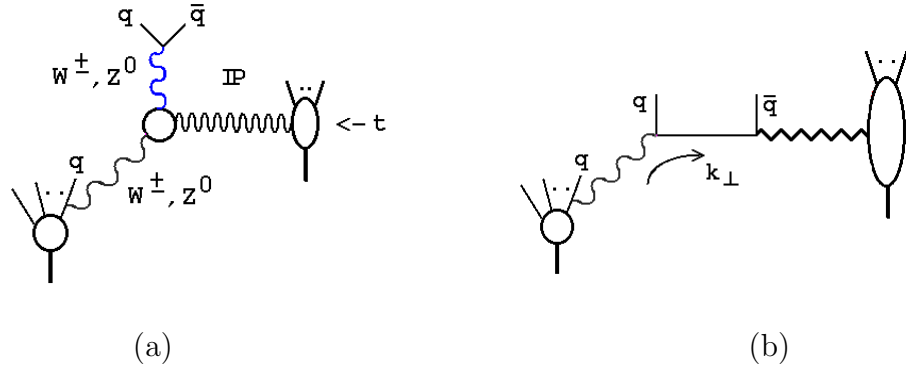


Fig. 26 (a) Diffractive  $W$  and  $Z$  production (b) comparable jet production.

The jet amplitude and sextet pion amplitude will be comparable, but small, when  $k_\perp$  is electroweak scale, say  $|k_\perp|^2 \sim 10,000 \text{ GeV}^2$ . However, as in our discussion of deep-inelastic scattering in the previous Section, the  $t$  dependence of the pomeron/hadron vertex implies there should be a “relatively large” forward amplitude. In fact, this interaction could explain the push towards larger rapidities, that is apparently observed[27] at the Tevatron, when a  $W^\pm$  or  $Z^0$  is produced in association with a large  $E_T$  jet.

Diffractive production of vector boson pairs should also take place as illustrated in Fig. 27, although it is not clear whether there are anomaly pole vertices of this form. Apparently[28], there is already an anomalously large  $W$  pair cross-section at the energy of the  $S\bar{p}pS$  collider. Since, as we discuss in the next Section, we expect this cross-section to be really large at the LHC, it seems that an “anomalous” (although still relatively small) cross-section should surely be observed at the Tevatron. A

complication is that detection of events in which one of the pair decays hadronically is much more difficult at the Tevatron than it was at the  $S\bar{p}pS$  because of the large background from the QCD production of  $W$  (or  $Z$ ) plus two jets. In addition, the vector boson pairs will be produced with much greater momentum at the Tevatron (than at the  $S\bar{p}pS$ ) and so the problem of the close together decays of longitudinal bosons will be much more significant.

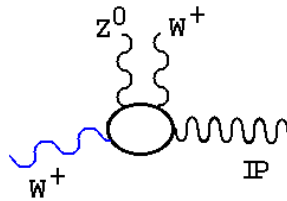


Fig. 27 Diffractive production of a  $W^+Z^0$  pair.

Other anomalous events, related to the single diffractive interactions, may also be observed. In particular, a connection between diffractive cross-sections and events with twice the average multiplicity density (in rapidity) is required by the AGK cutting rules. In addition, the Wilson lines attached to sextet quarks should also generate higher associated multiplicities than triplet quark lines. Anomalously low multiplicity events may also anticipate the higher energy rapidity gap cross-sections that we expect to appear.

## 6.2 Double Pomeron Exchange at the Tevatron

Double pomeron production of  $W^\pm$  and  $Z^0$  pairs which, as we discuss in the next Section, we expect to be a very clean signal of sextet quark physics at the LHC, is (probably) inaccessible kinematically at the Tevatron. However, a  $Z^0$  can also pair with a photon to give a state with zero sextet quark flavor. Since double pomeron production of  $Z^0\gamma$  is accessible kinematically, although there is not an obvious anomaly pole vertex, there could be a significant (although small, because an electromagnetic coupling is involved) anomalous cross-section for this process at the Tevatron. Since there are two hadron/pomeron couplings there should also be a major increase of the cross-section at smaller  $t$ . Assuming that the photon can simply play the role of introducing sextet quark quantum numbers, it need not carry electroweak scale transverse momentum.

## 6.3 The $\eta_6$ , $t\bar{t}$ , and Large $E_T$ Jets.

We turn now to non-diffractive sextet quark physics that might be seen (or may have already been seen) at the Tevatron.

As illustrated in Fig. 28, the  $\eta_6$  has two anomaly couplings to wee gluons in

$CSQCD_S$ . There is both a  $Q\bar{Q}$  and an  $SU(2)$  singlet gluon coupling (where the gluon has a non-leading helicity). Therefore, in  $QCD_S$ , the  $\eta_6$  mixes with a pure glue state



Fig. 28 Anomaly couplings for the  $\eta_6$ .

and, as a result, we expect that it will have an electroweak scale mass, with the sextet quark and antiquark carrying electroweak scale constituent masses. The  $\eta_6$  will also mix, via the gluon state, with the triplet flavor singlet (the  $\eta_3$ ) that will be dominated by  $t\bar{t}$  at the electroweak scale.

We can characterize the  $\eta_6$  as having an electroweak scale short-distance component which carries octet color that is compensated by wee gluons. This short distance component can be produced via gluon production and, since sextet quarks are stable, it will decay, primarily, through  $t\bar{t}$ . Assuming that the major disparity in scales leads to a minimal dynamical role for the wee gluons in the process,  $t\bar{t}$  production at Fermilab could be due to the  $\eta_6$ , and could be, essentially, “perturbatively” calculable. This would imply that  $m_{\eta_6} \sim “2m_t”$ .

That top production is due to resonance production would, of course, resolve the paradox that the production of a confined, colored, quark can, apparently, be observed experimentally. Theoretically, and “philosophically”, it would surely be attractive if an electroweak scale mass, i.e.  $2m_t \sim 350 \text{ GeV}$ , is explained as the (dynamical) mass of a sextet quark/antiquark bound state, rather than as (twice the value of) a lagrangian parameter of the triplet quark sector. Whether a well-determined top quark “mass” should still be, experimentally, identifiable is not clear.

Within  $QCD_S$ , the existence of a non-perturbative QCD sector above the “mass” of the top quark makes it very unlikely that the concept of a perturbative, electroweak scale, current quark mass can be well-defined enough to be directly measured. There would be a large dynamical mass generated above the electroweak scale that, most likely, would make the concept of the current quark mass very elusive. Alternatively, if we identify the  $\eta_6$  as responsible for top production then we can identify  $m_t$  as the sextet quark constituent mass scale. This would imply that the sextet neutron  $N_6$  has a relatively low mass of  $500 - 600 \text{ GeV}$ . As we will discuss in the next Section, this maximises the possibility that the Cosmic Ray spectrum knee is associated with the appearance of sextet quark states.

As detailed in Appendix A, the contribution of the sextet quark doublet to the QCD  $\beta$ -function is equivalent to the contribution of ten triplet quarks. Consequently at the scale where (non-chiral) sextet quarks enter the dynamics, they will halt the

evolution of  $\alpha_s$  entirely. If the top quark mass is actually the sextet constituent mass scale, as we have suggested, then the evolution of  $\alpha_s$  will halt at  $E_T \sim m_t$ . In Fig. 29 we show a CDF analysis[29] which translates the observed (Run 1) jet excess at large  $E_T$  into the (non-)evolution of  $\alpha_s$ . As can be seen,  $\alpha_s$  does indeed stop evolving just at  $E_T \sim m_t$ .

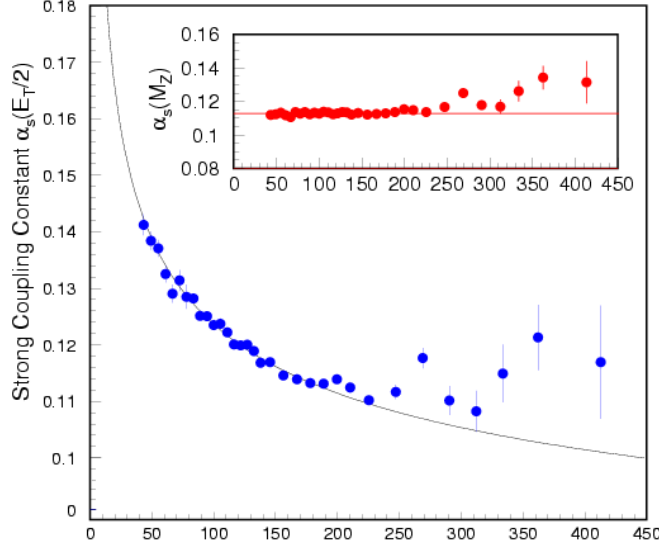


Fig. 29 CDF measurement of  $\alpha_s$  at large  $E_T$ .

Measurement of the jet cross-section in Run 2 appears, at present, to be entangled by the very real problem of systematic experimental errors. However, in spite of this, we can make a few general observations. First we consider the “raw data” shown in Fig. 30.

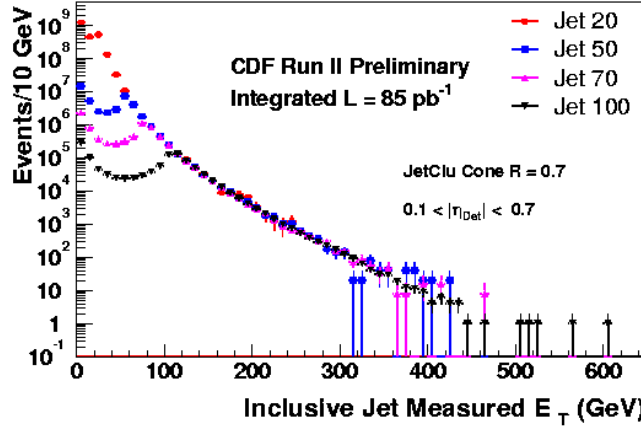


Fig. 30 CDF raw data for the inclusive jet cross-section.

The accumulation of events at the largest  $E_T$  hints at a leveling of the  $E_T$ -dependence of the cross-section which we will argue in Section 8 is also suggested by Cosmic Ray data. It is also an indication that a new mass scale is appearing that will halt the perturbative decrease of cross-sections.

In Fig. 31 we show the current comparison of data with theory[30].

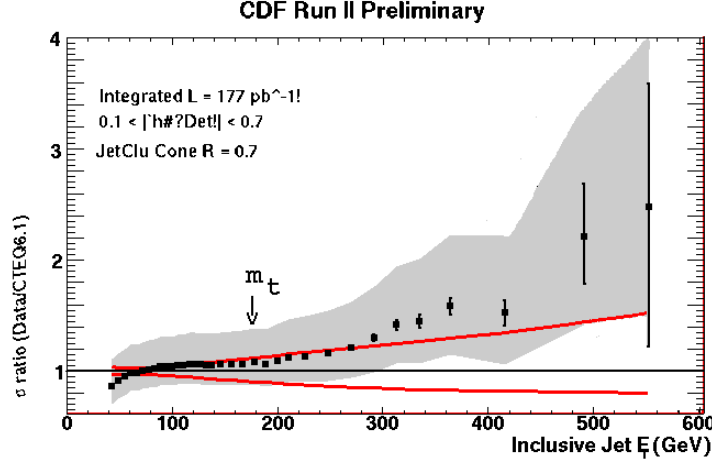


Fig. 31 Current CDF jet data compared with theory.

Note that ‘‘theory’’ in this case includes a gluon distribution that was chosen to best fit the Run 1 excess cross-section. As can be seen, if we ignore the experimental error problem, the data again pull away from theory, for  $E_T \sim m_t$  upwards, with the effect clearly growing with  $E_T$ . In Fig. 32(a) we show the energy dependence involved when Run 2 and Run 1 cross-sections are compared[30]. Clearly, this is also way off from theory for  $E_T > m_t$ .

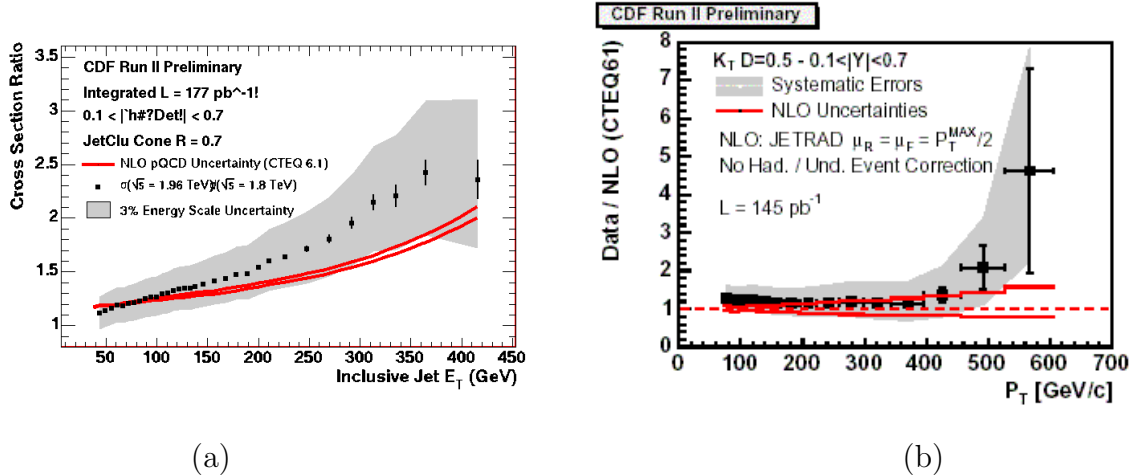


Fig. 32 (a) Comparison of Run II and Run I data (b) using  $k_T$  clustering.

Finally, in Fig. 32(b), we show the result obtained[31] by using a  $k_T$  clustering algorithm for jets. A match with theory for  $p_t \sim 200 - 400 \text{ GeV}$  can be achieved, but at the cost of a poor fit at lower and higher  $p_T$ . The highest  $p_T$  point being (ignoring error bars) almost five times the theoretical value.

From the above discussion, it seems hard to avoid the conclusion that, above the electroweak scale, QCD jet physics is breaking down in just the manner that we would expect from  $QCD_S$ . Indeed, if the top mass has the significance that we have just discussed, then the sextet sector has fully entered the theory at this scale. In addition to halting the evolution of  $\alpha_s$ , the increasing entry of sextet sector states into the dynamics should imply that the “excess” continues to grow as  $E_T$  increases. Indeed, we would expect that in the highest  $E_T$  excess region there is an enrichment of longitudinal  $W^\pm$  and  $Z^0$  jets with  $M_{jet} \approx M_{W/Z}$ . As we discuss in the next Section, at the LHC such events will have become a major part of the cross-section.

#### 5.4 Non-perturbative Decay Modes

If the  $\eta_6$  is indeed responsible for  $t\bar{t}$  production, then we would also expect to see “non-perturbative” decay modes. To discuss these modes, the best we can do is to exploit the parallel between the  $\{\Pi^\pm, \Pi^0, \eta_6\}$  sextet states, corresponding to  $\{W^\pm, Z^0, \eta_6\}$ , and the familiar  $\{\pi^\pm, \pi^0, \eta\}$  triplet quark states. Although the width should be large, if we take  $m_{\eta_6} \sim 2m_t \sim 350 \text{ GeV}$ , the relative couplings and masses of the vector mesons, and the photon, imply that the primary non-perturbative decay mode should be (in parallel with  $\eta \rightarrow \pi^+ \pi^- \pi^0$ )

$$\eta_6 \rightarrow W^+ W^- Z^0 \quad (6.1)$$

which, when  $Z^0 \rightarrow b\bar{b}$ , would give the same final state as  $t\bar{t}$ . The next most significant mode

$$\eta_6 \rightarrow Z^0 Z^0 Z^0 \quad (6.2)$$

(in parallel with  $\eta \rightarrow \pi^0 \pi^0 \pi^0$ ) should have a smaller branching ratio, because of the larger  $Z^0$  mass. In addition, (6.2) would be indistinguishable from (6.1) when the  $Z^0$ ’s decay hadronically, as they do most of the time. Because the  $\eta_6$  mass is so large, decay modes involving an electromagnetic coupling, such as

$$\eta_6 \rightarrow W^+ W^- \gamma, \quad Z^0 Z^0 \gamma, \quad Z^0 \gamma \gamma, \quad \gamma \gamma \quad (6.3)$$

would be expected to have smaller branching ratios but should be present at some level.

Unfortunately, because the non-perturbative decay modes proceed via sextet pion interactions, the produced vector mesons will be longitudinally polarized and so, as we discussed in the previous Section, when they carry large momentum they will have close together jet and lepton decay modes that are difficult to detect.

## 6.5 What if $m_{\eta_6} \gg 2m_t$ ?

For the sextet higgs mechanism to be operative, sextet quarks can not have a current quark mass. How the dynamically generated sextet mass scale compares with the top quark mass is, therefore, crucial. As we have already indicated, the attractions of having the sextet dynamical mass scale be  $m_t$  will become clear in the next Section.

Could the sextet dynamical scale be such that the  $\eta_6$  mass is too large for it to be seen at the Tevatron (say 1 TeV)? In this case we could, perhaps, assume that all effects of the sextet sector, apart from those in which sextet pions are involved, can be integrated out at the top quark mass scale. This would imply that standard perturbative QCD could be applied to top quark production and the only evidence of the sextet quark sector would be in the vector boson production cross-sections that we have already discussed. For consistency  $\alpha_s$  should, presumably, evolve as usual up to and beyond the top mass. Therefore, a jet excess would have to be entirely due to the multiple production of  $W$ 's and  $Z$ 's, as the only phenomenon that would be outside of the standard perturbative calculation. The excess would appear above  $E_T \sim 2M_W$ . Although there is little difference between  $E_T \sim 2M_W$  and  $E_T \sim m_t$ , we would not expect the chiral scale,  $M_W$ , to appear in the evolution of  $\alpha_s$  and would not expect the jet excess to be interpretable as due to the halt of this evolution.

## 6.6 Top Quark Physics Versus Diffractive $W/Z$ Production

Since top quark physics at the Tevatron is very complex, with elaborate analyses needed to make a connection between theory and experiment, it is clear that it may not be an easy place to look for new physics of the kind we have discussed. Whether or not  $W^+W^-$ ,  $Z^0\gamma$ , and  $Z^0Z^0$ , production conform to Standard Model expectations may be a much more straightforward issue to determine. If, however, significant evidence for sextet quark physics begins to accumulate at the Tevatron then, obviously, all possible discovery directions should be pursued intensely.

## 7. DARK MATTER, COSMIC RAY PHENOMENA, AND LARGE CROSS-SECTION LHC PHYSICS

If the sextet sector exists, the LHC will most probably be the discovery machine, at least as far as accelerator physics is concerned. Although it is possible that the phenomena that we have suggested are already occurring at HERA and at the Tevatron may come to be viewed as definitive evidence, it seems most likely that they will remain as hints of what is to come. In the next Section, we will give direct theoretical arguments as to why definitive effects should be seen at the LHC. However, we will not be able to predict, theoretically, the magnitude of the major phenomena we expect with any great certainty. Nevertheless, if there is “a major change in the strong interaction above the electroweak scale”, it surely should be visible in Cosmic Ray physics and, more generally, in other cosmic phenomena. As we will discuss in this Section, there are candidate phenomena of this kind and, if they are interpreted as we will suggest, they indicate that large cross-section effects are to be expected at the LHC. In order to be able to make comparisons with cosmic phenomena, we first give a brief, qualitative, discussion of why we expect the sextet sector to appear with high-energy cross-sections that are larger than hadronic in size and what we expect the major effects of these cross-sections to be. We will discuss LHC physics more specifically in the next Section.

### 7.1 Larger Than Hadronic Size Cross-Sections

If  $QCD_S$  existed in isolation, without the electroweak sector, then, because of the larger Casimirs, the sextet sector would constitute a stronger coupling sector of the theory. Just how significant the casimir effect is, we do not know. In general, it is clearly present in perturbation theory but is less significant in conventional non-perturbative formalisms. In  $QCD_S$ , because of the “almost perturbative” form of confinement that is present, we expect the effect to be maximal. Most importantly, though, we do not know how the wee gluon distribution contributes to the pomeron couplings that determine the size of asymptotic cross-sections, although sextet couplings should surely be larger. Therefore, the best we can say is that sextet pions will be massless and have asymptotic cross-sections that are (probably considerably) larger than their triplet counterpart. The sextet nucleon mass scale will be larger than the triplet scale but, nevertheless, sextet nucleon asymptotic cross-sections should also be larger. In general, therefore, although the asymptotic mass scale will be much larger, the size of asymptotic cross-sections, including multi-pomeron cross-sections, should be larger for the sextet sector, than the triplet sector, in  $QCD_S$ .

Adding the electroweak sector transforms the massless sextet pions into massive vector mesons. Effective current quark masses also have to be added. At asymptotic energies neither effect should matter, but such effects do matter for determining

the scale above which asymptotia sets in. In addition, if we start (in the real world) with initial triplet states we will only be able to produce the large cross-section sextet states via multiple gluon exchange and therefore, to obtain large cross-sections, via the pomeron. This does not mean, however, that only double pomeron production processes can be involved. We will discuss the double pomeron cross-section in more detail in the next Section. Here we note only that, if the double pomeron amplitude for the production of a sextet state, such as the  $W^\pm$  pair amplitude shown in Fig. 33(a), is large then the associated “cut-pomeron” amplitude, shown as the first diagram in Fig. 33(b), should also be large. (This amplitude is, however, entirely non-perturbative in that it can not be obtained by an anomaly pole method.)

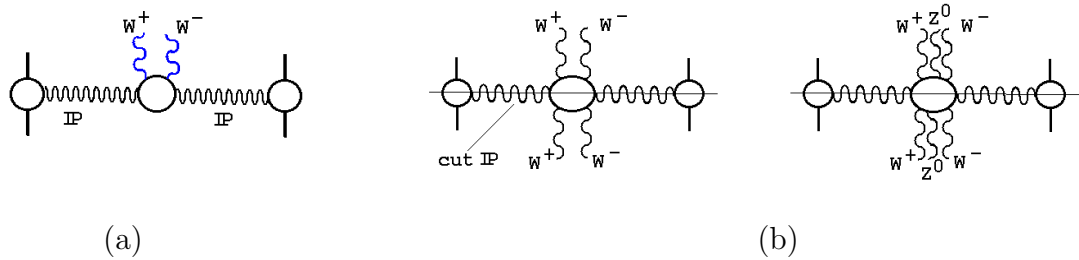


Fig. 33 (a) The double pomeron  $W$  pair amplitude (b) cut-pomeron amplitudes.

The cut-pomeron amplitude describes the full, central region, inclusive cross-section for production of a  $W^\pm$  pair. Like the total cross-section, a significant part of the inclusive cross-section should be describable by pomeron exchange, even when only a relatively small rapidity range is effectively available for one cut-pomeron or the other. Therefore, if the cut-pomeron amplitude is large it implies that  $W^\pm$  pairs (and, similarly,  $Z^0$  pairs) will be strongly, and multiply, produced inclusively across a larger part of the rapidity axis than is covered by the double pomeron produced state. The second cut-pomeron amplitude shown in Fig. 33(b) describes the inclusive production of three boson states which requires, of course, a bit more energy, and so on for higher cut-pomeron amplitudes. Once there is enough energy for cut-pomeron exchange to begin describing significant production of the sextet sector then the larger cross-sections of this sector should imply that sextet states actually come to dominate the inelastic (triplet state) hadronic cross-section at a (not too much) higher energy.

We expect, therefore, that the initial “major change in the strong interaction above the electroweak scale” will be that multiple vector boson states are produced, with large cross-section, across most of (but not all of) the rapidity axis - in close analogy with pion production at much lower energies. Sextet nucleon production will set in at higher energies, depending on the mass of these states. If the pomeron provides the gateway to the asymptotically dominant sextet sector, then we could expect that to produce a sextet state with mass  $M$  requires at least

$$\sqrt{S} > 10 M \quad (7.1)$$

and so if  $M \sim 400 \text{ GeV}$ , to be safely above the threshold for vector boson pair production, then we would need

$$\sqrt{S} > 4 \text{ TeV} \quad (7.2)$$

which is just above the Fermilab energy. Such states will be produced at lower energy, with much smaller cross-section, via gluon production. This would be the origin of  $W$  and  $Z$  pair contribution to the large  $E_T$  jet cross-section at Fermilab, discussed in the previous Section.

(7.2) is, of course, very approximate, but it does tell us that large sextet cross-sections should start to appear at an energy not too far above the Tevatron energy. As we now discuss, if we assume that sextet physics is involved, we can obtain additional information from the cosmic phenomena referred to above.

## 7.2 The $N_6$ and Dark Matter

That the (triplet quark) proton is lighter than the neutron is entirely due to the fact that the current mass of the  $u$  quark is less than that of the  $d$  quark. Electromagnetic effects, alone, would make the proton heavier. Remarkably, the current quark mass difference produces an effect that is of the same order of magnitude, but is just a little larger, and of the opposite sign, than the electromagnetic mass difference.

Because of the absence of hybrid triplet/sextet states, for the reasons discussed in Sections 2 and 3, the lightest of the sextet nucleons must be stable (assuming there is no grand unification). However, sextet quark current masses must be zero. If not, sextet pions would be massive and could not mix with the massless  $W$  and  $Z$  states to give them masses, as discussed in Section 5. Therefore, the sextet nucleon mass difference has to be entirely electromagnetic in origin, and so it is the  $N_6$  that is stable. If the sextet quark dynamical mass is given by the top quark mass, as discussed in the last Section, then the  $N_6$  mass should be  $\approx 500 \text{ GeV}$  and the  $P_6$  mass should be just a little higher. Since triplet and sextet quarks do not combine to form bound states it is, presumably, reasonable to assume that sextet nucleons also do not form bound states with triplet nucleons. More particularly, perhaps, if pion exchange provides the binding force for nucleons to form nuclei, the distinct quark content of sextet and triplet nucleons implies that there is no common “pion” that can bind them.

The  $N_6$  is, therefore, neutral, stable, and (because of the dominance of sextet states) will be the dominant, heavy, stable state produced in high energy cross-sections. Consequently, it will be dominantly produced in the high energy interactions that are believed to have been responsible for the formation of the early universe. If it does not form bound states with normal quark matter it will abundantly form cold dark matter, in the form of (sextet) nuclei, clumps, etc. (Perhaps sextet pions can exist inside sextet nuclei and provide the binding force.) As a result, the existence of the sextet nucleon sector provides a natural explanation for the dominance of dark

matter in the universe. Conversely, once we establish that the  $N_6$  will form dark matter, the dominance of dark matter in the universe can be regarded as evidence confirming that sextet quark states dominate high energy cross-sections.

We have not discussed at all, in this paper, the leptonic sector that should accompany the sextet sector if the electroweak interaction is to be anomaly free. The simplest possibility is two generations of heavy leptons although other  $SU(2) \otimes U(1)$  quantum numbers could be involved. Clearly, a leptonic sector of this kind could also contribute, in some way or other, to dark matter. A more subtle possibility is suggested by the unified theory of [22]. In this case, the anomaly is cancelled by color octet quarks with lepton-like properties.

The dominance of dark matter in the universe does not (at least not immediately) tell us at what energy scale this dominance appears in total cross-sections. Although, given the extensive production of triplet quark matter at energies, up to and including the Tevatron, it should probably not be too many orders of magnitude above this energy. Specific evidence for the relevant scale is, however, provided by the cosmic phenomenon that we discuss next.

### 7.3 The Knee in the Cosmic Ray Spectrum

The “knee” in the cosmic ray spectrum is an extraordinary, well-established and very well-known, phenomenon. As shown in Fig. 34,

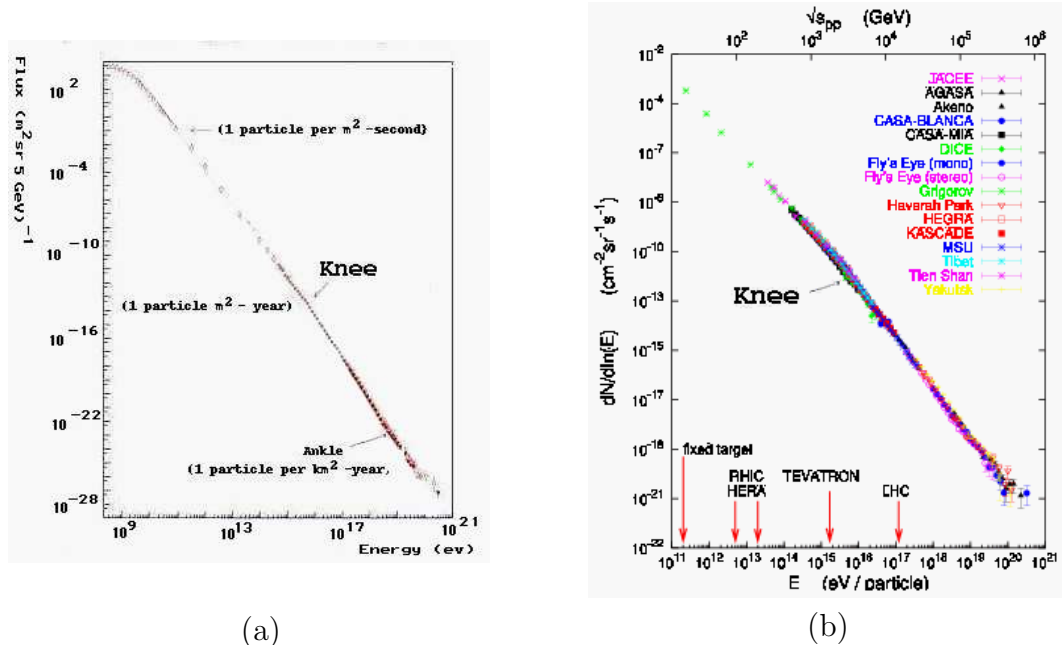


Fig. 34 The full cosmic ray spectrum (a) early data (b) recent data

it appears as a break in the slope of the spectrum that stands out, as a distinctive feature, as the energy increases over some ten orders of magnitude and the flux decreases by thirty orders of magnitude. In first approximation there is as is most evident in the early data of Fig. 34(a), one single slope as the energy increases from  $10^{10} \text{ eV}$  to  $10^{16} \text{ eV}$  and a second slope as the energy increases from  $10^{16} \text{ eV}$  to  $10^{20} \text{ eV}$ . It is called the knee because, as is clear from the larger scale plot shown in Fig. 35 (the dashed lines are for a later discussion), it is not simply a break in slope but rather a “bump” in which, for a short energy range, it looks like the slope has decreased before it settles at an increased value.

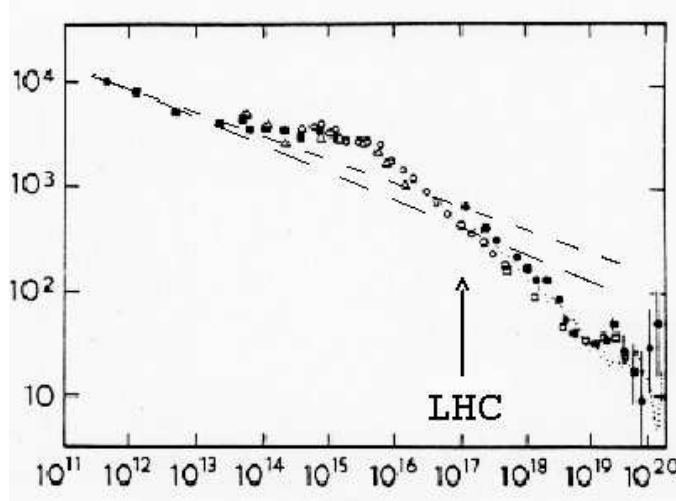


Fig. 35 A larger scale view of the knee.

It is widely believed by cosmic ray physicists that the origin of the knee is cosmic, even though there is no consensus on what the cause could be. *A priori*, it seems almost inconceivable that a conspiracy of external phenomena could produce such a pronounced local effect, in a spectrum that (naively at least) is arriving from all directions and all distances of the universe. It seems far more plausible that the cause of the effect is in the atmospheric interaction. Indeed, right from its earliest discovery, it was suggested[32] that the knee could be the threshold for a new interaction that produces (stable or relatively stable) neutral particles which are not observed in the ground level detectors. This would produce an underestimation of the shower energy above the threshold and would lead to a pile-up of events below the threshold energy which, together with a depletion of the spectrum above the threshold, would be observed as a “knee”. However, as we discuss further below, the major part of the cross-section has to be affected by this threshold. Since there was no serious idea what the neutral particle(s) could be and there was no reason to expect such a dramatic effect in the strong interaction, particularly after the discovery that this interaction is described by QCD, there was no general acceptance of the proposal.

For our part, we have previously proposed[8] that the knee is the threshold for the appearance of the sextet sector in  $QCD_S$ . However, at the time, we did not have the understanding of the phenomena that could be involved, that we now have, as we discuss below. Presumably because of the absence of such details, our proposal had little impact. In the meantime, other authors have emphasized the difficulty of explaining the knee as an effect of cosmic physics and have made various proposals[32, 33, 34] for a threshold effect that could be involved. That a large fraction of the cross-section (increasing as the energy increases) has to be involved, is a problem for all threshold proposals. As the discussion in **7.1** shows, the sextet sector threshold has (perhaps uniquely) the potential, at least, to play this role.

The plot in Fig. 35, although it appears in the most recent NASA release on Cosmic Rays, corresponds to Fig. 34(a) and is now fairly out of date. In recent years many different experiments have studied the knee and the results, already shown in Fig. 34(b), are shown in the region of the knee in Fig. 36 (the horizontal and vertical lines are again for the later discussion).

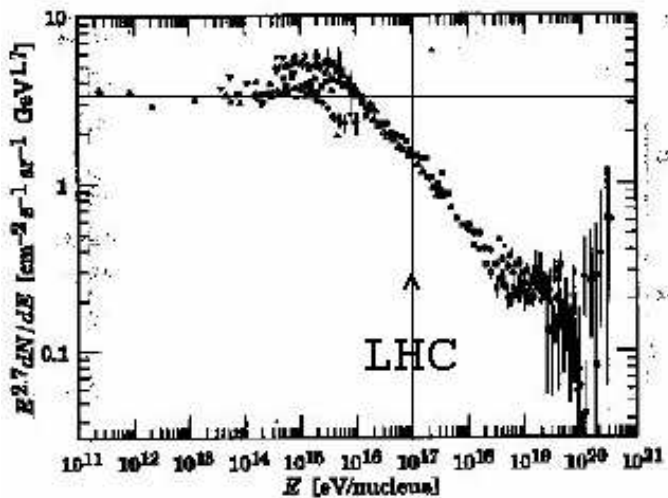


Fig. 36 Recent knee data.

In fact, the mass of new data has, if anything, confused the situation. Particularly, if we wish to extract information about the threshold effect that could be involved.

Because the data from different experiments do not agree about the absolute value of the flux and also cover different energy ranges, it is difficult to be sure exactly where the threshold is and how much of the cross-section has to be involved. It will be helpful to first consider Fig. 35 alone, since it has the virtue that the data looks relatively unambiguous (because there is much less of it) and the nature of the knee is more apparent. If we draw the extrapolation of the lower energy data as the lower

dashed line (consisting of longer dashes) in Fig. 35, it seems that the flux at the LHC energy ( $E_0 \sim 10^{17} \text{ eV}$ ) could be consistent with the extrapolation from lower energies. Indeed, it then appears that the problem is with events above the LHC energy and that is only their energies which have been underestimated. If a threshold is involved, however, this can not be the case, because there would not be a sufficient number of missing events above  $E_0 \sim 10^{17} \text{ eV}$  for the full knee to be formed by their movement (into the knee). If, instead, we draw the extrapolation of the lower energy slope as the upper dashed line (consisting of shorter dashes) in Fig. 35 then, according to most data points, there is already a problem at the LHC, although perhaps at a level that could be as low as 10%. In addition, it now looks reasonable that the missing higher-energy events could fill the knee.

If we consider the more recent compilation of data in Fig. 36, the lower energy slope has been extracted and so the extrapolation of the lower energy data should be drawn as a horizontal line. The horizontal line drawn in Fig. 36 is (close to) the upper dashed line of Fig. 35 and if we use this our extrapolation we reach essentially the same conclusion for the LHC. In this case, a loss of 20% of the cross-section at the LHC looks, perhaps, to be the best estimate. However, the spread of the data in the neighborhood of the knee makes it completely impossible to determine where the horizontal line should be drawn in Fig. 36 in order that missing high energy events should be just enough to fill the knee. Since this is an essential element of the threshold explanation, it should clearly be an important part of determining where the threshold is located.

The most reasonable conclusion from the above discussion is that the threshold should be below the LHC energy and that the physics involved should be visible at the LHC as a significant part of the hadronic cross-section. However, wherever the exact location of the threshold is, there is no way to avoid the conclusion that, at energies significantly above the LHC energy, the majority of the cross-section must be involved in the underestimation of cosmic ray energies. As we now describe, the major changes that we expect the sextet sector to bring can surely contribute the needed effects. (7.2) and the foregoing discussion suggests that the result can be as big and as immediate an effect as is needed.

The first effect produced by the sextet sector, i.e. the prolific production of vector bosons, will increase the average transverse momentum of events enormously and lead to such an increase of the shower spread that a much greater fraction (than expected) of the shower particles will be undetected. At the LHC, ten or more vector bosons could be produced, kinematically, via the cut-pomeron cross-section. The major consequence will, of course, be a huge increase of the large  $E_T$  jet cross-section. (The effective increase due to the non-evolution of  $\alpha_s$  will be just a small part of this effect). There will also be marked changes in the distributions of leptons produced. In particular, there will be a much larger fraction of (undetected) neutrinos in the

ground level particles.

The second effect is the production of “dark matter” (sextet neutron/antineutron pairs). This will straightforwardly take away undetected energy and the effect will be maximal if the sextet neutron mass is as low as possible. If  $m_{N_6} \sim 500 \text{ GeV}$ , as we argued for in the previous Section, it is reasonable to expect a relatively large inclusive cross-section (described by cut pomeron amplitudes) at the LHC. At higher energies the inclusive production of  $N_6$  pairs will surely become more and more significant and, necessarily, be a major contribution to the loss of detected energy by most of the total cross-section.

In general, it is clear that, to produce as strong an effect as is needed to explain the knee, the combination of all sextet amplitudes has to become dominant at high energies, just as we have suggested should be the case in 7.1. This being the case, and given the ambiguity in the implications of the data, it seems very likely that consistency can be achieved. We should emphasize, however, that for the sextet processes to play the role we have described the cross-sections involved (particularly the multiple vector boson cross-sections) have to rise to very large values over a relatively small energy range. It is interesting that the production of  $N_6$  pairs is not so different from the original proposal[32] of the production of neutrals to explain the knee. Of course, the existence of dark matter was unknown and the link between the two phenomena, that we are proposing as a consequence of the existence of a sector sector, could not have been imagined.

#### 7.4 Cosmic Ray Dijets and Ultra High Energy Events

There are a number of distinct effects that have been seen in cosmic ray showers with energies above the knee, for example those discussed in [32]. Collectively, they all suggest that new physics appears above the knee. We catalogued the effects, and offered explanations of the phenomena involved, in [8]. However, in most cases, the explanations we offered would surely be modified by our current understanding. In addition, other effects have been discovered since. We will not attempt a recataloguing here, but instead will concentrate on one of the, by now, most well-established effects and will also discuss what has since become one of the most interesting phenomena.

There are very significant anomalies in the rate of high  $E_T$  jets (“cores”) in experiments such as Chacaltaya and Kanbala [35]. A QCD Monte Carlo was tuned to jet data at fixed target and collider energies (including the  $Spp\bar{S}$  and Tevatron). The prediction for  $\chi_{12}$ , which is basically the product of the jets’  $E_T$  and the jet-pair separation  $R_{12}$ , was then compared with the cosmic ray data. As shown in Fig. 35, for energies above  $\sqrt{s} \approx 5 \text{ TeV}$  (i.e. above the knee) the jet rate for  $\chi_{12} \gtrsim 1000 \text{ TeV.cm}$  exceeds the QCD expectation by as much as two orders of magnitude. If we interpret this is an extension, to higher energies, of the large  $E_T$  jet excess observed at Fermilab, then it shows that there is an (orders of magnitude) increase of just the

kind that we expect.

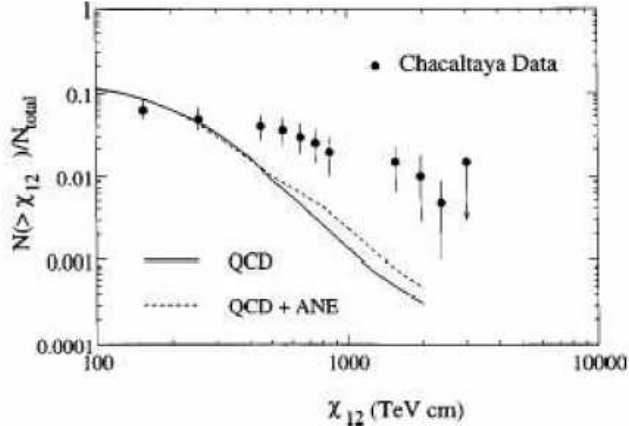


Fig. 35 Excess large  $E_T$  dijets (“cores”).

Ultra high-energy cosmic ray events, with  $E_0 \gtrsim 10^{20} \text{ eV}$ , have attracted great attention because the energy exceeds the GZK cut-off produced by the interaction of a proton with the cosmic background radiation. This suggests, of course, that the particles involved can not be protons. On the other hand, it is believed that the high velocities involved imply the particles must have traveled a long way and so should be stable. Within the Standard Model there is no other candidate besides the proton. As a result, both the origin and the nature, of the high-energy events is regarded as a mystery.

Within the sextet sector, there is an obvious candidate for producing the ultra high-energy events. Sextet neutrons are stable and will avoid the GZK cut-off, both because they are neutral and because they are massive. Also (because they have a large coupling to the pomeron) they will have a large high-energy hadronic cross-section. Clearly they could be responsible for the ultra high-energy cosmic rays. Indeed, they are probably responsible for an increasing fraction of the spectrum from energies lower than  $10^{20} \text{ eV}$  upwards. Since they would simply be very high energy dark matter, which is omnipresent in the universe, their origin would (presumably) not be a mystery.

To the extent that the existence of the ultra high-energy events is evidence for a stable, massive, particles that are strongly interacting (and preferably neutral), they could actually be regarded as evidence that dark matter is strongly interacting.

## 8. WHAT SHOULD BE SEEN AT THE LHC ?

As we have emphasized several times. the major evidence for the sextet sector, in the LHC high luminosity mode, is likely to be that, in general, both multiple vector boson and large  $E_T$  jet cross-sections are much larger than expected, producing a dramatic rise in the average  $|p_\perp|$ . Because large momentum longitudinal bosons that preferentially decay to jet or lepton configurations with isolation problems, will be dominantly produced, the size of the diboson cross-section may not be recognized (at least at first) to be as large an effect as it really is. Instead the major, observed, effect of this cross-section may be to contribute to the increased magnitude of large  $E_T$  jet cross-sections. Quite possibly, this increase will not be immediately identified as due to a sextet quark sector.

A priori, the neutral  $N_6$  will also be quite difficult to detect, since missing energies of several hundred  $GeV$  will be common. The  $P_6$ , assuming it is not too unstable (for some unknown reason), should be seen. Although a massive, charged, particle with a large production cross-section will surely cause much general interest, it also may not be immediately identified with the sextet sector. For the reasons we now outline, it seems that the double pomeron cross-section may well be the most definitive early evidence for the existence of the sextet sector.

### 8.1 Double Pomeron Exchange.

Vector bosons can be pair-produced directly in double pomeron exchange, via the sextet pion anomaly mechanism, as illustrated in Fig. 36.

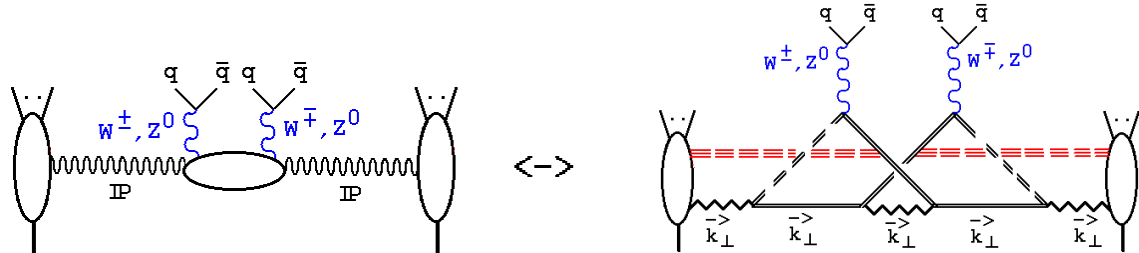


Fig. 36 Double pomeron production of  $W$  and  $Z$  pairs via sextet pions.

The kinematics needed for the derivation of this amplitude, as a straightforward extension of the argument of 5.2, are easily satisfied at the LHC. A parallel argument to that of 5.4 and 6.2 can then be used to obtain an order of magnitude estimate for the cross-section. The jet amplitude, analagous to Fig. 18(a), that has, apart from the anomaly loops, the same propagators and couplings as Fig. 36 is shown in Fig. 37(a). When the transverse momentum is electroweak scale, i.e.  $|k_\perp| \gtrsim 100 \text{ GeV}$ ,

the cross-sections given by Fig. 36 and Fig. 37(a) are comparable. That is to say, at large  $k_\perp$ , the  $W^+W^-$  and  $Z^0Z^0$  pairs will give jet cross-sections that are as large as those predicted by standard QCD. In Fig. 37(b) we show the lowest-order triplet sector amplitude that would comparably produce a vector boson pair decaying to jets, and would also involve the gluon exchanges necessary for pomeron exchange.

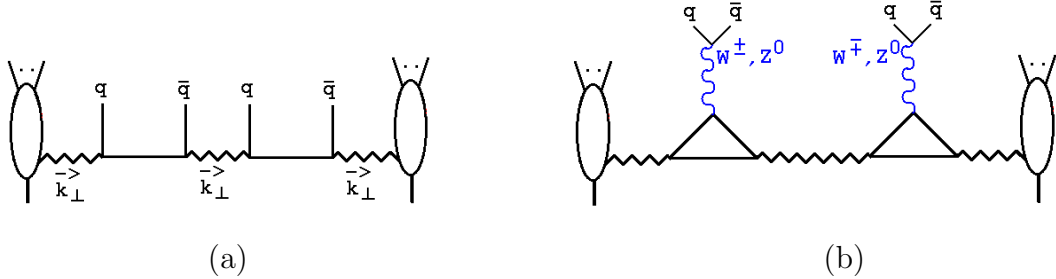


Fig. 37 (a) The comparable jet amplitude (b) a triplet sector amplitude

Extending the argument of 5.4, since there are two sextet pions involved, and therefore two factors of  $F_\Pi$ , the cross-section given by Fig. 36(b) would be smaller by a factor of  $\gtrsim O(10^{12})$ .

Repeating the argument of 5.6 in the present context, we note that the central double pomeron vertex of Fig. 36 should vary only slowly with  $k_\perp$  (with an electroweak scale), while the external hadron/pomeron vertices will have strong  $k_\perp$  - dependence and give a large increase as  $|t|$  decreases. As was the case in our discussion of HERA events, we will obtain the maximum increase if the scattering protons are not diffractively excited. In this case, the increase will be given by the same product of hadron/pomeron couplings that is present in the elastic cross-section. When combined with a large  $|t|$  amplitude that is larger than its triplet sector counterpart by  $\gtrsim O(10^{12})$ , this should imply a large double pomeron cross-section when  $|t|$  is at the minimum kinematically allowed value, in agreement with the general argument of 7.1.

## 8.2 LHC Kinematics

If we consider, as illustrated in Fig. 38, the (symmetric) central region production of a state with mass  $4M^2$  by colliding proton beams with momentum  $\sqrt{S}/2$ , then this corresponds to a (symmetric) minimum  $t$  value of

$$t \sim -\frac{4M^2 m_p^2}{S} \quad (8.1)$$

If we consider  $W^\pm$  (or  $Z^0$ ) pair production then, in analogy with the double pomeron cross-section for pion pairs we might expect the maximal cross-section to be at  $M \sim$

$2M_W \sim 170 \text{ GeV}$ . In this case, with  $\sqrt{S} = 14 \text{ TeV}$  and the proton mass set to  $1 \text{ GeV}$ , we obtain from (8.1)

$$t \sim 4 \left( \frac{0.17}{14} \right)^2 \sim 5 \times 10^{-4} \text{ GeV}^2 \quad (8.2)$$

which is close to the minimum value that is expected to be achieved by TOTEM in the initial low luminosity running at the LHC. Therefore, it should be possible to detect the cross-section very close to its maximal value.

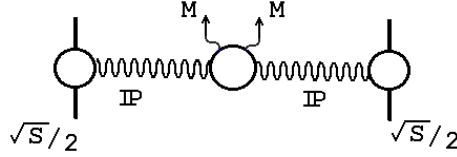


Fig. 38 Double pomeron kinematics.

If CMS/TOTEM have the central detector operational during the initial “soft physics” running period, then it should be straightforward to look for  $W^\pm$  and  $Z^0$  pairs in the central detector, in combination with very forward scattered protons in the Roman pots. The cross-section will be maximal when  $t$  is at its minimum but should, of course, be observable over a range of  $t$  values. However, it will also be preferable to be as close as possible to threshold to minimize problems caused by the asymmetric decays of high momentum longitudinal vector bosons. In fact, with this in mind, it could be that at larger  $|t|$  values multiple  $W^\pm$  and  $Z^0$  pairs will be easier to detect because they are closer to threshold. Perhaps, since we expect the cross-sections to be so large, there could be spectacular events in which the far-forward protons are tagged and only (a multitude of) large  $E_T$  leptons are seen in the central detector!

A large double pomeron cross-section for  $W^\pm$  and  $Z^0$  pairs immediately implies that the longitudinal components have direct strong interactions. Therefore, the observation of such a cross-section would be an immediate confirmation of the existence of the sextet sector and the sextet higgs mechanism. In addition, this cross-section can be looked for as soon as the LHC turns on. Consequently, we regard it as the top signature to be looked for as evidence for the sextet sector.

If we consider sextet neutrons and, to be appropriately above threshold, set  $M = 1 \text{ TeV}$  in (8.1) we obtain a minimum  $|t|$  value of

$$t \sim 4 \left( \frac{1}{14} \right)^2 \sim 2 \times 10^{-2} \text{ GeV}^2 \quad (8.3)$$

which will be detectable, if the cross-section is large enough. It would also be a spectacular process. The deflection of the tagged protons would determine that a

very massive state was produced, while no charged particles would be seen in any of the detectors. Comparison with charged lepton production should allow a clear separation between this process and the multiple production of neutrinos by  $Z^0$ 's.

As we have said earlier, it could even be that the sextet nucleon double pomeron cross-section is so extraordinarily large that it will be detectable in the low luminosity run of the LHC. If not, it could very well be seen by the high luminosity detector set up that is envisaged to look for the double pomeron production of the Standard Model higgs particle.

### 8.3 Inclusive Cross-Sections for Sextet States.

As we noted in the previous Section, we expect cut-pomeron amplitudes of the form of Fig. 31(b) to be responsible for the inclusive production of mutiple vector bosons across most of the rapidity axis. This should be a major effect when the LHC is in high luminosity mode. However, as we already implied above, it is likely to take time to determine that this phenomenon is indeed taking place, since the main effect will be the contribution to jet cross-sections. Note that since we showed above that the double pomeron production of jets via vector bosons will be comparable with the total jet rates that are expected, we would obviously expect the inclusive production of jets via vector bosons to be orders of magnitude larger (as we argued for, more generally, in the previous Section).

For the leptonic decays, the association of multiple leptons and missing  $E_t$  to multiple  $W$ 's will have obvious problems, which the close together decays of longitudinal bosons will only make worse. Multiple  $Z^0$  states should be the easiest to detect, but the close together decays will also be a problem. Nevertheless, since the cross-sections should be so dramatically large, they should eventually provide emphatic evidence for the sextet sector.

If the  $N_6$  and  $P_6^\pm$  pairs (and also  $\eta_6$  pairs) are indeed too massive to be seen in double pomeron exchange, the central region inclusive cross-sections could (as we have already said) still be relatively large via cut-pomeron amplitudes. The problem then becomes how to detect such states. How, and if, the  $N_6$  will eventually be detected is difficult to speculate on, particularly, given that missing  $E_T$  will actually be far more common than in the Standard Model, because of the strong  $W$  pair production. Assuming the lifetime is long enough, it should be possible to detect  $P_6$ 's.

### 8.4 Large Jet Cross-Sections and the Evolution of $\alpha_s$

If the influence of the sextet sector on  $\alpha_s$  is that the evolution stops at  $E_T \sim m_t$ , as we discussed in Section 6, then the LHC jet cross-sections will be further enhanced. Even ccording to conventional QCD predictions, the LHC jet cross-section persists for an order of magnitude in  $E_T$  beyond  $E_T > m_t$  and so the lack of evolution would be straightforwardly evident, if it were the only phenomenon involved. In

effect, Fig. 35, together with the large  $E_T$  jet excess at the Tevatron, are existing experimental evidence that the jet cross-section will be much larger than anticipated from conventional QCD, for almost all of the  $E_T$  range. As we have emphasized, we expect the enhancement by the production of vector boson states to be an orders of magnitude effect. If it is, indeed, as big as we are anticipating, it will be very hard to imagine an alternative explanation besides the existence of the sextet quark sector.

## ACKNOWLEDGEMENTS

I am grateful to Mike Albrow, Malcolm Derrick and Geoff Bodwin for valuable discussions

## Appendix A. Infra-red and Ultra-violet Properties of $QCD_S$ and $CSQCD_S$

In this Appendix we summarize, briefly, the properties of  $QCD_S$  and  $CSQCD_S$  that we use in the main body of the paper.

### A.1 The Infra-red Fixed-Point in $QCD_S$

We write the  $QCD_S$   $\beta$ -function in the form

$$\beta(\alpha_s) = -\frac{g^4}{(4\pi)^2} \beta_0 - \frac{g^6}{(4\pi)^4} \beta_1 - \frac{g^8}{(4\pi)^6} \beta_2 + \dots \quad (A.1)$$

The three loop calculation of [36] gives, for  $n_f$  triplet flavors,

$$\beta_0 = 11 - \frac{2}{3}n_f, \quad \beta_1 = 102 - \frac{38}{3}n_f, \quad \beta_2 = \frac{2857}{2} - \frac{5033}{3}n_f + \frac{325}{54}n_f^2 \quad (A.2)$$

When  $n_f = 6$ , we obtain

$$\beta_0 = 7, \quad \beta_1 = 26. \quad (A.3)$$

When the two sextet flavors are included we obtain[36]

$$\beta_0 = 7 - 4T(R)n_f^6/3 = 7 - 4(\frac{5}{2})2/3 = 1/3, \quad (A.4)$$

and

$$\beta_1 = 26 - 20T(R)n_f^6 - 4C_2(R)T(R)n_f^6 = 26 - 100 - 66\frac{2}{3} = -140\frac{2}{3} \quad (A.5)$$

where  $T(R) = C(R)/C(3) = 5/2$  and  $C_2(R) = 10/3$  for sextet quarks. Therefore,  $QCD_S$  is (just) asymptotically-free and also has an infra-red fixed point at

$$\alpha_s \approx \frac{1}{34} \quad (A.6)$$

(There is a sense in which this can be argued to be present to all orders[37]). In addition, between the ultra-violet and infra-red fixed points the  $\beta$ -function remains very small ( $< 10^{-6}$ ). As a result the massless theory evolves only very slowly and is almost scale-invariant.

### A.2 Asymptotic Freedom in $CSQCD_S$

As in the body of the paper, we use  $CSQCD_S$  to denote the “color superconducting” version of  $QCD_S$  obtained by adding a scalar field and using the usual

higgs mechanism. (Note that, in this context, the “higgs mechanism” is a technical manipulation that has nothing to do with electroweak symmetry breaking.) It is a special property of  $QCD_S$  that a (complex) color-triplet Higgs scalar sector can be added[38, 39] - with both the gauge-coupling *and* the Higgs self-coupling asymptotically free. We can illustrate this as follows.

Let  $g(t)$  and  $h(t)$  be the respective scale-dependent couplings, then

$$\frac{dg}{dt} = \beta(g, h) \quad (A.7)$$

$$= -\frac{1}{2}b_0 t^3 + \dots \quad (A.8)$$

where, now,

$$b_0 = \frac{1}{8\pi^2} \left[ \beta_0 - \frac{1}{6} \right] \quad (A.9)$$

$\beta_0$  is calculated from the quark content, as above, and the  $1/6$  is due to the triplet scalar. Similarly

$$\frac{dh}{dt} = \tilde{\beta}(g, h) \quad (A.10)$$

$$= Ah^2 + Bg^2 + Cg^4 + \dots \quad (A.11)$$

where

$$A = \frac{7}{8\pi^2}, \quad B = -\frac{1}{\pi^2} \quad \text{and} \quad C = \frac{13}{48\pi^2}. \quad (A.12)$$

We can have  $h \rightarrow 0$  consistently in (3.5) if  $h = xg^2 + 0(g^3)$ . This gives a stability equation for  $x$ , that is

$$\frac{dx}{dt} = g^2 (Ax^2 + B'x + C) \quad (A.13)$$

where  $B' = B + b_0$ . When the stability condition  $(B')^2 > 4AC$  is satisfied there are two fixed-points of (3.7) and the smaller is stable for  $t \rightarrow \infty$ . The stability condition gives

$$(1 - \pi^2 b_0)^2 > \frac{91}{96} \quad (A.14)$$

which for  $b_0$  small gives

$$\frac{5}{24} > 8\pi^2 b_0 \quad (A.15)$$

If there are 16 color triplet quarks, or six color triplets and two sextets, then

$$8\pi^2 b_0 = \frac{1}{6} < \frac{5}{24} \quad (A.16)$$

For comparison, if there are 15 color triplet quarks then

$$8\pi^2 b_0 = \frac{5}{6} > \frac{5}{24} \quad (A.17)$$

We conclude that, only when the number of quark flavors is “saturated”, as in  $QCD_S$ , can we use the Higgs mechanism to break the  $SU(3)$  gauge symmetry to  $SU(2)$ , and so smoothly introduce a (single) massive vector into the theory, while *maintaining* the short-distance asymptotic freedom of the theory.

## Appendix B. Properties of the Triangle Anomaly

In this Appendix we summarize the various properties of the triangle diagram that are used in the paper. We consider the contribution of the massless fermion loop, shown in Fig. B1,

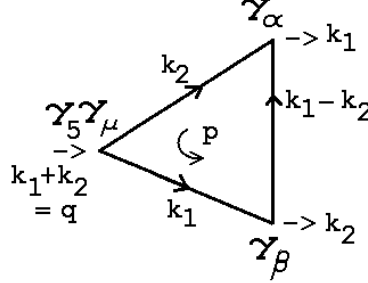


Fig. B1 The Fermion Loop Contribution to  $T_{\mu\alpha\beta}(k_1, k_2)$

to an axial-vector/two-vector three current vertex, i.e.

$$\Gamma_{\mu\alpha\beta}(k_1, k_2) = \frac{i}{(2\pi)^4} \int \frac{d^4 p \operatorname{Tr}\{\gamma_5 \gamma_\mu (\not{k}_1 + \not{p}) \gamma_\alpha \not{p} \gamma_\beta (-\not{k}_2 + \not{p})\}}{p^2 (k_1 + p)^2 (p - k_2)^2}$$

A general decomposition of the symmetrized vertex

$$T_{\mu\alpha\beta}(k_1, k_2) = \Gamma_{\mu\alpha\beta}(k_1, k_2) + \Gamma_{\mu\beta\alpha}(k_2, k_1) \quad (B.1)$$

into invariant amplitudes is

$$\begin{aligned} T_{\mu\alpha\beta}(k_1, k_2) &= A_1 \epsilon_{\sigma\alpha\beta\mu} k_1^\sigma + A_2 \epsilon_{\sigma\alpha\beta\mu} k_2^\sigma + A_3 \epsilon_{\delta\sigma\alpha\mu} k_{1\beta} k_1^\delta k_2^\sigma \\ &+ A_4 \epsilon_{\delta\sigma\alpha\mu} k_{2\beta} k_1^\delta k_2^\sigma + A_5 \epsilon_{\delta\sigma\beta\mu} k_{1\alpha} k_1^\delta k_2^\sigma + A_6 \epsilon_{\delta\sigma\beta\mu} k_{2\alpha} k_1^\delta k_2^\sigma \end{aligned} \quad (B.2)$$

with

$$\begin{aligned} A_1(k_1, k_2) &= -A_2(k_2, k_1) \\ A_3(k_1, k_2) &= -A_6(k_2, k_1) \\ A_4(k_1, k_2) &= -A_5(k_2, k_1) \end{aligned} \quad (B.3)$$

The large momentum region ‘‘anomaly’’ contribution to  $A_1$  and  $A_2$  gives

$$A_1 = \frac{1}{4\pi^2} + \dots, \quad A_2 = \frac{-1}{4\pi^2} + \dots, \quad (B.4)$$

leading to the “anomalous” divergence equation

$$(k_1 + k_2)^\mu T_{\mu\alpha\beta} = \frac{1}{2\pi^2} \epsilon_{\delta\sigma\alpha\beta} k_1^\delta k_2^\sigma \quad (B.5)$$

It is well-known[40] that (B.4) can be understood as the consequence of a large momentum shift of the Dirac sea, during the interaction, that does not conserve axial charge.

As is also well-known, the numerical value of (B.4) is fixed by requiring that the vector Ward identities hold, i.e.

$$k_1^\alpha \Gamma_{\mu\alpha\beta} = 0, \quad k_2^\beta \Gamma_{\mu\alpha\beta} = 0 \quad (B.6)$$

and so vector charge is conserved. For the invariant amplitudes  $A_i$ , the Ward identities require that

$$A_2 = k_1^2 A_5 + k_1 \cdot k_2 A_6 \quad (B.7)$$

and

$$A_1 = k_2^2 A_4 + k_1 \cdot k_2 A_3 \quad (B.8)$$

These identities imply, in turn, an inter-relation between the ultra-violet anomaly contribution and the infra-red structure of the other  $A_i$ . For example, when  $k_1^2 = 0$ , (B.7) becomes

$$A_2 = k_1 \cdot k_2 A_6 = \frac{q^2 - k_2^2}{2} A_6 \quad (B.9)$$

suggesting that there is a pole in  $A_6$ . In particular, if we insert the ultra-violet anomaly term (B.4) into (B.9), we obtain

$$A_6 \underset{k_1^2 \rightarrow 0}{\sim} \frac{1}{2\pi^2 (k_2^2 - q^2)} + \dots \quad (B.10)$$

which appears to determine that, when  $k_1^2 = 0$ , there is a pole in  $A_6$  at  $k_2^2 = q^2$ .

In fact, explicit expressions for the  $A_i$  can be given when  $k_1^2 = 0$  (references to the original calculations can be found in [13]), i.e.

$$\begin{aligned} A_1 &= \frac{1}{4\pi^2} \left( \frac{k_2^2}{k_2^2 - q^2} \ln \frac{k_2^2}{q^2} + 1 \right) \\ A_2 &= \frac{1}{4\pi^2} \left( \frac{k_2^2}{k_2^2 - q^2} \ln \frac{k_2^2}{q^2} - 1 \right) \\ A_3 = -A_6 &= \frac{1}{2\pi^2} \frac{1}{k_2^2 - q^2} \left( \frac{k_2^2}{k_2^2 - q^2} \ln \frac{k_2^2}{q^2} - 1 \right) \end{aligned} \quad (B.11)$$

(While  $A_4$  can be obtained from (B.8),  $A_5$  is undetermined by (B.7) and is considerably more complicated.) Both (B.4) and (B.10) are clearly present in (B.11). However, it can easily be checked that there is no pole at  $k_2^2 = q^2$  in  $A_6$ . The logarithms of  $k_2^2$  and  $q^2$  are due to the “normal thresholds” in these channels, while the pole at  $k_2^2 = q^2$  is a (triangle diagram) “anomalous threshold”. In general anomalous thresholds are hidden by normal thresholds. Consistent with this, the pole at  $k_2^2 = q^2$  is present only if the expressions in (B.11) are continued to unphysical sheets of the logarithms.

In special kinematic configurations, the “anomaly pole” does appear on the physical sheet. In particular, with  $k_1^2$  already set to zero,

$$k_2^2 = 0 \implies A_3 = -A_6 = \frac{1}{2\pi^2 q^2} \quad (B.12)$$

while

$$k_1 = 0 \equiv k_2^2 = q^2 \implies A_3 = -A_6 = \frac{1}{4\pi^2 q^2} \quad (B.13)$$

In both of these kinematic configurations the invariant functions containing the anomaly pole reduce to just the pole term with the residue determined entirely by the anomaly. In (B.13) the thresholds actually produce a partial cancelation of the pole. This partial cancelation is related to the property that, if  $q^2$  is integrated over, the real part of the anomaly pole cancels and only the imaginary part  $\delta$ -function remains. As we discuss in Section 2, this is important for the contribution of the U(1) anomaly in pomeron vertices.

If the massless fermions are actually confined, the anomaly pole can be interpreted as a Goldstone boson pole signaling chiral symmetry breaking. As we showed explicitly in [13], and briefly describe below, the pole is generated in the infra-red internal momentum region. Consequently, the Ward identities (B.7) and (B.8) involve a direct cancelation between the large internal momentum region generating anomaly contributions of the form (B.4) and the small internal momentum region giving the anomaly pole contribution. In effect, there are two distinct consequences of the presence of the ultra-violet anomaly (B.4). The first is the anomalous Ward identity (B.5). The second is that, for general momenta, the vector Ward identities require a cancelation between separate contributions (with different kinematic structure) from large and small internal momentum regions. If an internal large transverse momentum cut-off is introduced, (B.4) will be modified and the vector Ward identities will no longer hold. The contribution, to the vector current divergences of the anomaly pole terms will survive, however, since they are generated in the infra-red transverse momentum[13].

If we keep just the anomaly pole contributions of  $A_3$  and  $A_6$  to  $T_{\mu\alpha\beta}$  we can write

$$T_{\mu\alpha\beta}(k_1, k_2) = -\frac{1}{2\pi^2} \frac{(\epsilon_{\delta\sigma\alpha\mu} k_{1\beta} - \epsilon_{\delta\sigma\beta\mu} k_{2\alpha}) k_1^\delta k_2^\sigma}{(k_1 + k_2)^2} + \dots \quad (B.14)$$

This expression does not satisfy the vector Ward identities and does not have the axial current anomaly. When  $k_1^2 = k_2^2 = 0$ , and  $q^2 \rightarrow 0$ , we can rewrite (B.14) as

$$T_{\mu\alpha\beta}(k_1, k_2) \sim \frac{1}{2\pi^2} \frac{-q_\mu [\epsilon_{\delta\sigma\alpha\beta} k_1^\delta k_2^\sigma]}{q^2} \quad (B.15)$$

which now satisfies both vector Ward identities and also gives the anomalous divergence (B.5). We conclude that, by itself, the anomaly pole contribution violates the vector Ward identities, except at  $k_1^2 = k_2^2 = 0$ .

The ultra-violet anomaly contribution (B.4) is absent in (B.15) and yet the anomaly is present. To understand how the anomalous divergence can be due to the anomaly pole we must first discuss the internal momentum configuration that generates the pole. The analysis of [13] shows that, if external light-like momenta  $k^+$  and  $k^-$  are directed as shown in Fig. B2, and  $p$  is the internal loop momentum, the pole is generated at  $p = 0$ .

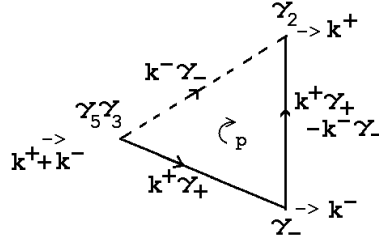


Fig. B2 Generation of the anomaly pole.

The  $\gamma$  matrices shown give an anomaly pole term

$$\Gamma_{32-} = -\frac{[\epsilon_{\sigma\delta32} k_1^\sigma k_2^\delta] k_{1-}}{2\pi^2 q^2} = -\frac{k_+^2 k_-}{2\pi^2 q^2} \quad (B.16)$$

If  $k^- \rightarrow 0$  then  $q^2 = 2k^+k^- \rightarrow 0$ . The finite light-like momentum  $k^+$  then flows along two of the internal lines while the third, the dashed line in Fig. B2, carries zero momentum. Because both poles of the zero momentum propagator participate in generating the anomaly pole, there is effectively a particle/antiparticle “chirality transition”, that is equivalent to an infra-red shift of the Dirac sea, during the interaction. This is how the anomaly pole produces an infra-red non-conservation of axial

charge that parallels that produced by the ultra-violet Dirac sea shift. The infra-red effect is present only when the fermions involved are massless and then only in the infra-red region where (B.15) is valid.

If the  $1/q^2$  factor in (B.15) is to be interpreted as a Goldstone boson particle pole then  $q_\mu$  must provide the coupling to the axial current while  $[\epsilon_{\delta\sigma\alpha\beta} k_1^\delta k_2^\sigma]$  provides, potentially, a coupling to physical currents. There is a problem, however, in that  $k_1$  and  $k_2$  are both light-like and so  $q^2 = 0$  implies that they are also parallel. Therefore, because of the  $\epsilon$ -tensor, the pole residue vanishes, as is seen explicitly in (B.16). This should be expected, of course. Otherwise we would be able to obtain a coupling of a pion to finite momentum gluons. Nevertheless, we can avoid the vanishing of the pole residue if, as we go to the pole, we simultaneously go to an infinite-momentum frame. If we make a boost  $a_3(\zeta)$  along the 3-axis and consider  $\Gamma_{32-}$  defined in the new frame, we can use either (B.15) or (B.16) to obtain

$$\Gamma_{32-} \sim \frac{k_+ \cosh \zeta [-k_+ k_- \sinh \zeta]}{\sqrt{2} q^2} \quad (B.17)$$

Since we still have  $q^2 = 2k_+k_-$ , the limit  $k_- \rightarrow 0$  again gives  $q^2 \rightarrow 0$ . However, the coupling  $[k_+ k_- \sinh \zeta]$  is finite if  $k_- \cosh \zeta$  is kept finite, i.e. if the mass-shell and infinite momentum limits are combined. As discussed in Section 2, the anomaly then provides a coupling to infinite momentum wee gluons. This is very important because, on general grounds, we expect to see wee-partons carry vacuum properties in the infinite momentum frame !!

## Appendix C. Reggeon Diagrams and Transverse Momentum Kernels

In this Appendix we define, and describe the properties of, the transverse momentum kernels whose properties we exploit in Section 2 and in the following Appendix. A very similar, extended, description is given also in [13].

It is well-known from perturbative calculations[41]-[46] that in gauge theories the regge limit is described by transverse momentum diagrams. When all gluons and quarks have a mass there are no infra-red divergences and high-order leading and next to leading log calculations show that these diagrams exponentiate (in momentum space) to produce regge pole and regge cut behavior. Both gluons and quarks lie on regge trajectories, i.e. they “reggeize”. Reggeization of the gluon corresponds to the exponentiation

$$\frac{s}{t - M^2} \equiv \frac{1}{t - M^2} \int \frac{dJ \, S^J}{(J - 1)} \rightarrow \frac{s^{1-\Delta(t)}}{t - M^2} \equiv \frac{1}{t - M^2} \int \frac{dJ \, S^J}{(J - 1 + \Delta(t))} \quad (C.1)$$

where  $1 - \Delta(t)$  is the (massive) gluon regge trajectory given (in the leading log approximation) by

$$\Delta(-Q^2) = \frac{(Q^2 + M^2)}{16\pi^2} \int \frac{d^2 k_1}{k_1^2 + M^2} \frac{d^2 k_2}{k_2^2 + M^2} \delta^2(Q - k_1 - k_2) \quad (C.2)$$

As is illustrated by (C.1), momentum space exponentiation corresponds to power series summation in the  $J$  - plane ( $J$  = complex angular momentum). We can further illustrate this by considering an amplitude for which the leading high-energy behavior is given by the regge-cut corresponding to two reggeized gluons. In this case the lowest-order result is (apart from a normalization factor)

$$A_0(J, t) = \frac{1}{J - 1} \int \frac{d^2 k_1}{k_1^2 + M^2} \frac{d^2 k_2}{k_2^2 + M^2} \delta^2(Q - k_1 - k_2) \quad (C.3)$$

where  $t = Q^2$ . The momentum space exponentiation corresponding to reggeization of the gluons is now described by replacing the fixed pole at  $J = 1$  by the two-reggeon propagator

$$\Gamma_2 = \frac{1}{J - 1 + \Delta(k_1^2) + \Delta(k_2^2)} \quad (C.4)$$

giving

$$A_0(J, t) \rightarrow A(J, t) = \int \frac{d^2 k_1}{k_1^2 + M^2} \frac{d^2 k_2}{k_2^2 + M^2} \frac{\delta^2(Q - k_1 - k_2)}{J - 1 + \Delta(k_1^2) + \Delta(k_2^2)} \quad (C.5)$$

Further momentum space exponentiation is provided by reggeon interactions that, in the  $J$  - plane, simply iterate (C.5) - which we identify as a “two-reggeon state”.

In general, it can be shown[47] that the contributions of all logarithms (down to an arbitrary non-leading level) can be described by transverse momentum diagrams. Abstract S-Matrix results[20, 48, 49] on unitarity in the complex angular momentum plane (reggeon unitarity) imply that the transverse momentum diagrams can be organized into an elaborate exponentiation phenomenon in which a complete set of reggeon diagrams appears, involving all possible  $J$ -plane multi-reggeon states.

When  $M \rightarrow 0$ , infra-red divergences appear in both the reggeon trajectories and the (integrated) reggeon interactions. At first sight the divergence

$$\begin{aligned} \Delta(Q^2) &\longrightarrow \ln M^2 \\ M^2 \rightarrow 0 \end{aligned} \tag{C.6}$$

exponentiates to zero all reggeon amplitudes via the regge pole exponentiation (C.1). However, since divergences also appear in the reggeon interactions, to discuss the  $M \rightarrow 0$  limit in detail, it is advantageous to undo the reggeon diagram organization and go back to transverse momentum diagrams. The reggeon interactions and reggeon trajectory contributions can be combined into “kernels”  $K_N^I(\dots, k_i, \dots, k_j', \dots)$ , where  $I$  denotes SU(2) color. If the kernels are defined to include a transverse momentum conserving  $\delta$ -function they are dimensionless (in transverse momentum) and describe the iteration of dimensionless lowest-order “multigluon transverse momentum states”  $T_N$  where

$$T_N = \frac{1}{J-1} \int \prod_{i=1}^N \frac{d^2 k_i}{k_i^2} \tag{C.7}$$

We refer to  $T_N$  as a “multigluon state”. A multigluon state is the lowest-order transverse momentum diagram contributing to a multi-reggeon state. As such, it carries the color and signature properties of the parent multi-reggeon state. Note that gauge invariance (in the form of reggeon Ward identities[50]) implies that the kernels  $K_N^I$  have zeroes (when any  $k_i$  or  $k_j'$  vanishes) which, at fixed  $Q^2$ , prevent the poles in the  $T_N$  from producing divergences. At fixed  $Q^2$ , therefore, the divergences come only from the trajectory and interaction terms contained in the kernels.

When the  $t$ -channel color of an  $N$ -gluon state is non-zero, the interaction divergences do not cancel the trajectory divergences and, in general,

$$T_N K_N^I = \frac{1}{J-1} \int \prod_{i=1}^N \frac{d^2 k_i}{k_i^2} = K_N^I(\dots, k_i, \dots, k_j', \dots) \rightarrow \infty, \quad Q^2, I \neq 0 \tag{C.8}$$

As a result, the sum of all diagrams in any colored channel exponentiates to zero, as illustrated in Fig.C1.

$$\sum \quad \text{Diagram} \quad \rightarrow \quad 0$$

The diagram consists of a sum symbol followed by a sequence of three boxes. Each box contains a 'K\_I' label. Between the first and second boxes is a 'T\_N' label. Between the second and third boxes is another 'T\_N' label. Dashed lines connect the boxes. To the right of the third box is a condition 'I ≠ 0'.

Fig. C1 Iteration of a Massless Gluon Kernel.

When  $I = 0$  and  $Q^2 \neq 0$ , the trajectory and interaction divergences do cancel. As a result there is no exponentiation of divergences. The disappearance of all colored multigluon states is not confinement since, in the color zero diagrams the gluon poles in the states remain. Confinement is produced when the  $Q^2 = 0$  singularity is absorbed into a “condensate”, as described in Section 2.

In leading-log calculations the infra-red finiteness property of the dimensionless kernels leads directly to conformal scale invariance. In general non-leading log contributions the introduction of a scale for the gauge coupling destroys all scale-invariance properties. When there is an infra-red fixed point for the gauge coupling, as in  $QCD_S$ , the scale invariance properties are still present in the infra-red region. In this case, the kernels  $K_N^0$  scale canonically as  $Q^2 \rightarrow 0$  so that

$$\int_{|k_i|^2, |k'_j|^2 < \lambda} \prod_i \frac{d^2 k_i}{k_i^2} \prod_j \frac{d^2 k'_j}{k'_j^2} K_N^0(k_1, \dots, k_N, k'_1, \dots, k'_N) \sim \int^{\lambda_\perp} \frac{dQ^2}{Q^2} \quad (C.9)$$

where, as in the above,  $Q = \sum k_i = \sum k'_j$ . If (C.9) is obtained via the limit  $M^2 \rightarrow 0$ , this divergence would appear as a factor of  $\ln [M^2/\lambda_\perp]$ .

To understand the implications of this last divergence we formally rewrite (C.9), analogously to (C.8), as

$$(J-1)^2 T_N T'_N K_N^0 \quad (C.10)$$

and note that infra-red finiteness implies firstly that  $(J-1) T'_N K_N^0$  is finite when the  $k_i$  are finite and, also, that  $(J-1) T_N K_N^0$  is finite when the  $k'_j$  are finite. Consequently, there are two contributions to the divergence in (C.9), depending on whether the  $Q^2$  - integration is performed as part of the integration over the  $k_i$  or as part of the integration over the  $k'_j$ . In the first case the divergence is obtained from the region  $\{ k_i \ll k'_j \ \forall i, j \}$ , whereas in the second case it is the region  $\{ k'_j \ll k'_i \ \forall i, j \}$ . In effect, either the  $T_N$  or the  $T'_N$  integration produces the divergence, but not both.

If a color zero multigluon state is coupled without the Ward identity zero (involving the transverse momentum of the complete state) that is (normally) a consequence of gauge invariance, (C.9) is a potential source of an infra-red divergence. As the kernel  $K_N^0$  is iterated a divergence always occurs when  $Q^2 \rightarrow 0$ , but the degree of divergence does not increase. Rather, in an integral involving a product of many

ernels, there is a distinct contribution from each  $T_N$ . The divergent  $T_N$  can then be isolated and the remaining integrations organized, in the complete set of diagrams, as illustrated in Fig. C2.

$$\left( \sum \text{Diagram with } \mathbf{T}_N \text{ and } \mathbf{K}_N^0 \right) \text{---} \mathbf{T}_N \text{---} \left( \sum \text{Diagram with } \mathbf{T}_N \text{ and } \mathbf{K}_N^0 \right)$$

Fig. C2 Isolation of the Divergence Associated with  $T_N$ .

It follows that the residue of the logarithmic divergence can be written in the factorized form

$$\frac{1}{J-1} \int \frac{dQ^2}{Q^2} \int \prod_i \frac{d^2 k_i}{k_i^2} \delta^2(Q - \sum k_i) |M_N^0(J, k_1, \dots, k_N, \lambda_\perp)|^2 \quad (C.11)$$

where  $M_N^0$  is given by the sum of diagrams shown in Fig. C3.

$$M_N^0 = \left( \sum \text{Diagram with } \mathbf{T}_N \text{ and } \mathbf{K}_N^0 \right)$$

Fig. C3 Diagrams Contributing to  $M_N^0$

We can also discuss the interaction between massless multigluon states and massive (reggeized) gluons. For  $SU(2)$  color zero we can distinguish two classes of multigluon states. For a gluon field, with color matrix  $A_{\alpha\beta}^i$ , color charge conjugation  $C$  gives

$$A_{\alpha\beta}^i \rightarrow - A_{\beta\alpha}^i \quad (C.12)$$

We can also define the signature  $\tau$  of a multigluon state as  $\tau = \pm 1$  for an even/odd numbers of gluons. There are, essentially, two distinct color zero combinations of gluon fields, i.e.

$$Tr\{\delta_{ij} A^i A^j\}, \quad Tr\{\epsilon_{ijk} A^i A^j A^k\} \quad (C.13)$$

which both have  $C = +1$  but can, respectively, create  $\tau = +1$  and  $\tau = -1$  states.

In the absence of anomalies, all external couplings of color zero multigluon states have  $P = +1$ . In this case, since  $\tau = CP$ , only even signature  $SU(2)$  color zero combinations of gluons can couple.  $P = -1$  corresponds to “abnormal” parity. Odd signature multigluon states can couple only via the abnormal parity properties of anomaly couplings. Since the kernel describing the interaction of massless and massive gluons does not contain any anomaly, it will vanish for odd-signature combinations of massless gluons as illustrated in Fig. C4.

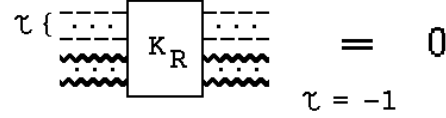


Fig. C4 Interaction of Massive and Massless Gluons.

Therefore, if the odd signature gluons couple initially and finally via anomalies, an infra-red scaling divergence will be produced as illustrated in Fig. C5.

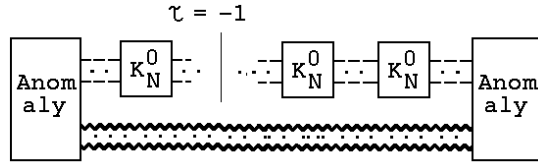


Fig. C5 Producing an infra-red scaling divergence.

In the next Appendix we make extensive reference to multi-reggeon diagrams[50] that are the extension to multiparticle amplitudes of the elastic scattering diagrams we have described above. For our present purposes it will be sufficient to understand only that, in the multi-reggeon diagrams, there are several distinct reggeon channels (each described by a separate “J” and “t”) in which the elastic scattering kernels again appear - with all the same properties. It is very important, however, that the vertices which couple the distinct reggeon channels contain anomalies that can not be present in the interactions of (vector) gluon reggeons within the elastic scattering diagrams. In the next Appendix, details of these vertices and the anomalies that occur are described, when necessary, in the context of the discussion.

## Appendix D. The Multi-Regge Program

In this Appendix we provide a general description of the multi-regge program that we have formulated over the years which, as we note often in the main body of the paper, should ultimately provide the best framework for a complete derivation of the high-energy solution of  $QCD_S$ . We include some historical background in order to explain the original motivation for the development of the program and to show why we have been led to connect  $QCD_S$  to the Critical Pomeron. More technical descriptions of the arguments we give can, for the most part, be found in our recent papers.

The asymptotic freedom of QCD almost certainly implies that total cross-sections must rise asymptotically if perturbation theory is to have any validity. The Critical Pomeron description of rising cross-sections was discovered[3] thirty years ago. While its derivation as a renormalization group solution of Reggeon Field Theory (RFT) implied that it satisfied full multiparticle  $t$ -channel unitarity, it was soon established that it also satisfies all known  $s$ -channel unitarity constraints. It remains today the only known rising cross-section solution of unitarity in the regge limit. In a sense, it is a fixed point solution of the regge limit (necessarily expressed in terms of physical degrees of freedom) that is analogous to the asymptotically-free fixed-point solution of the short-distance limit. The Critical Pomeron is, however, much more difficult to realize in a physical theory than is asymptotic freedom.

The critical solution of RFT was found via the well understood sub-critical theory (essentially the multiperipheral model plus unitarity corrections). The physical significance of the supercritical theory was the subject of much dispute and conflicting proposals were put forward. The solution we proposed[1, 2, 20] has the advantage that it is described by an explicit diagrammatic expansion that clearly satisfies reggeon unitarity. The supercritical diagrams are generated (as in a normal supercritical phase) by introducing a pomeron condensate in the critical RFT lagrangian. The condensate generates new classes of RFT diagrams, a simple example of which is shown in Fig. D1.

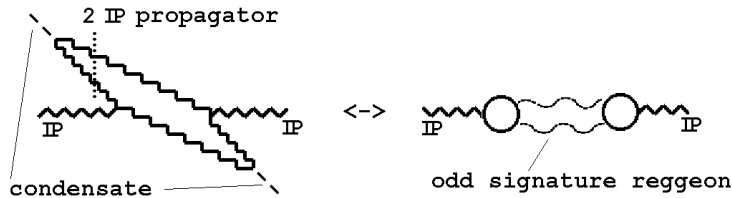


Fig. D1 A new RFT diagram generated by the pomeron condensate

The two pomeron propagators produced by the condensate give  $k_\perp$  poles that have to be interpreted as particle poles, implying that there is a pomeron transition to a two

vector reggeon state as shown. Reggeon states involving many vector particle poles similarly appear in higher-order diagrams. Consequently, the RFT phase transition can be characterized by saying that divergences in rapidity produced in the subcritical graphical expansion (because the bare pomeron intercept is above one) are converted to vector particle divergences in  $k_\perp$  in the supercritical expansion. That is to say, the supercritical phase is characterized by the “deconfinement of a vector particle on the pomeron trajectory”.

We soon realized[2] that the deconfinement of a vector particle is exactly what should happen if it is possible to make a smooth transition from QCD to CSQCD. This strongly suggested that the Critical Pomeron occurs, in particular circumstances, in QCD. It also suggested that a transition from perturbative reggeized gluon diagrams, that describe a spontaneously-broken gauge theory, to non-perturbative pomeron diagrams that describe a confining theory, could be followed within RFT. For this to be the case, confinement would have to be produced by the infra-red divergences of reggeized gluon diagrams.

We proposed[52], therefore, starting with the gluon and quark reggeon diagrams of QCD, but with the gauge symmetry completely broken so that all gluons are massive. (A brief description of reggeon diagrams is given in the previous Appendix.) The aim was to first restore the gauge symmetry to  $SU(2)$ , to obtain CSQCD, and to show that the diagrams obtained could be identified with those of supercritical pomeron RFT. We anticipated that infra-red divergences would produce confinement of  $SU(2)$  color and a pomeron, while the broken part of the gauge group would provide the accompanying massive vector meson. Restoring the symmetry to  $SU(3)$  would then be done within RFT and the result would be the Critical Pomeron. We gave arguments, based on complimentarity, that with a transverse momentum cut-off imposed the symmetry restorations should take place smoothly and, over the years[50, 51], made a number of attempts to implement our proposal.

The derivation of our supercritical RFT solution involved many subtleties that we eventually realized implied that the nature of the scattering hadron states has to be closely related to that of the pomeron. In particular, the “pomeron condensate” that defines the supercritical phase has to be associated with a (“wee parton”) component of the scattering hadrons. To derive the solution in a well-defined way, it had proved necessary[20] to consider a multi-regge amplitude in which regge pole hadrons scatter via pomeron exchange. As a result we believed we should consider an analagous amplitude in QCD. That is, we should consider a “many-body” scattering amplitude, in an appropriate multi-regge region[50] of phase-space, in which regge pole pions and the pomeron could emerge together, as illustrated schematically in Fig. D2. Starting with the appropriate multi-regge perturbative reggeon diagrams, we would look for infra-red divergences that could produce pions and the pomeron as the gluons become massless. That, a priori, very complicated diagrams were to be considered is not as

bad as it seems because the general structure of high-order diagrams is determined[50] from that of lower-order diagrams by reggeon unitarity.

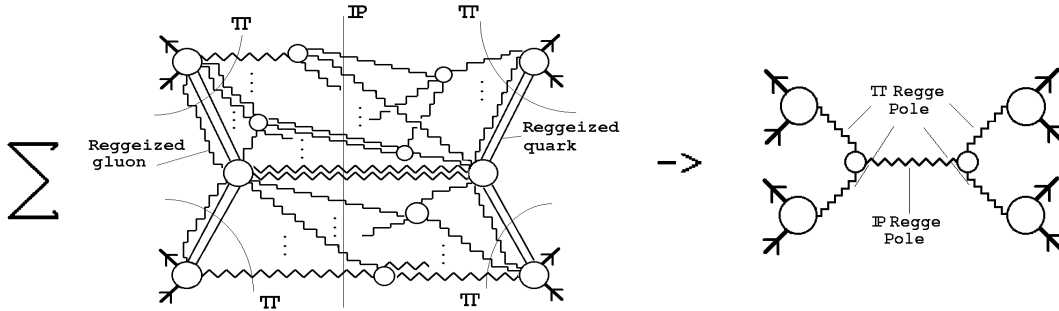


Fig. D2 The transition from perturbative reggeon diagrams to reggeized pions scattering via pomeron exchange.

In the multiperipheral sub-critical theory it was apparent that the criticality of the pomeron should depend on the number of hadron states and, therefore, on the number of quark flavors. Consequently, “saturating” the asymptotic freedom constraint, as in  $QCD_S$ , would be most likely to produce the critical behavior. The only physically realistic way to do this was[52] to add two sextet flavors and have the sextet higgs mechanism operative. It also became clear, rather quickly, that the special infra-red scaling properties of reggeon interaction kernels in  $QCD_S$ , which follow from the presence of an infra-red fixed-point, would have to be an essential ingredient of the infra-red divergence structure[52]. In addition there would, somehow, have to be (anomaly related) interactions to which divergences produced by the scaling properties would have to couple. Finally we realized that, because the Higgs mechanism scalar field is asymptotically free in  $CSQCD_S$ , the restoration of  $SU(3)$  color (which is to give the Critical Pomeron) can be carried out without a transverse momentum cut-off.

It soon seemed, therefore, that if Fig. D2 was to be implemented fully then, most likely, we would have to specifically consider  $QCD_S$ . There was, however, a major problem that, for a long time, prevented us from systematically developing a program to implement Fig. D2. If we consider  $QCD_S$  in isolation, then we can not find suitable external scattering states to provide a perturbatively well-defined starting amplitude within which pions and the pomeron could emerge as in Fig. D1. Without this we can not determine, for sure, whether anomaly related divergences occur. Consequently, the anticipated mapping onto supercritical RFT can not be carried out. We initially supposed[52] that the external states could be multi-quark states. However, as will soon become clear, the pions and pomeron, that we are led to, do not couple to such states. In [50] we assumed the existence of external couplings with particular properties but, in this case, it was clear that the nature of the infra-red divergences that occurred depended on these assumptions.

Only recently[12, 13], have we understood that adding the electroweak vector boson sector of the Standard Model to  $QCD_S$  solves the problem of the external states for Fig. D2. As illustrated in Fig. D3, the desired pion amplitude should appear in a multi-regge limit[50] of an amplitude for multiple vector boson scattering.

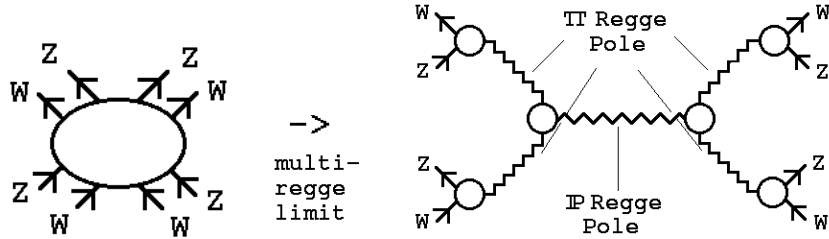


Fig. D3 The pion amplitude within a multiparticle vector boson amplitude.

Conversely, since  $W$ 's and  $Z$ 's have explicit perturbative couplings, this amplitude also has a perturbative reggeon diagram description. Most importantly for our program, because of the presence of elementary left-handed couplings, the perturbative reggeon vertices of the external  $W$  and  $Z$  states contain[12] anomalies that can give (with the cut-off manipulation that we discuss below) the infra-red divergences that we are looking for. We want, of course, to add the vector boson sector of the Standard Model to  $QCD_S$  in order to study the sextet higgs mechanism. Clearly, the fact that electroweak vector bosons provide the perfect external states for our multi-regge program could be related to the actual validity of the solution of  $QCD_S$  that we find. That is to say, our solution of  $QCD_S$  is effectively induced by the presence of the electroweak vector bosons and may, perhaps, only be valid in their presence. Note that, if the sextet higgs mechanism is operative, then the initial perturbative amplitude we calculate will have massless external vector bosons and the process of obtaining the physical on-shell amplitude will be intricately intertwined with the general infra-red divergence analysis.

For massless gluons, the individual reggeon diagrams in Fig. D1 have well-known infra-red divergences (that we will return to later) but, if the scattering states are color zero vector bosons, we expect that (as described in the previous Appendix) these divergences will cancel in the sum over all diagrams of a given order. Therefore, there must be an additional divergence phenomenon, if  $CSQCD_S$  reggeon diagrams are to be mapped on to the pomeron diagrams of supercritical RFT via divergences. In fact, we now understand well that it is the appearance[13, 14] of chiral anomalies in, high order, multi-regge vertices that produces the divergences that we are looking for. The anomalies occur because these vertices contain triangle diagrams that result from the contraction (in the regge limit) of larger loop feynman diagrams. Even though there are no axial vector currents in the elementary QCD interaction,  $\gamma_5$  couplings are generated within these vertices by products of orthogonal  $\gamma$ -matrices.

We anticipate that, without a transverse momentum cut-off, the anomalies appear as a large transverse momentum phenomenon that produces (non-unitary) power enhancement of the high energy behavior. We have shown this explicitly in our analysis[12] of elastic vector boson scattering. The enhancement is avoided by the introduction of a cut-off but there is then a violation of gauge invariance Ward identities for the anomaly generating vertices (in analogy with our discussion of the elementary triangle diagram in Appendix B). As a result, as we will discuss more explicitly below, infra-red transverse momentum divergences appear which couple directly to the part of the anomaly diagrams which, because the quarks involved are massless, contain the infra-red “anomaly pole”. (The anomaly pole contribution to a triangle diagram is discussed briefly in Appendix B and, at much greater length, in [13].) In effect, introducing a transverse momentum cut-off removes ultra-violet chirality violation produced by the anomaly and replaces it with infra-red chirality violation that produces anomaly poles. Since an anomaly pole can be interpreted as a Goldstone boson particle pole, this provides a crucial mechanism for a bound-state, Goldstone boson, spectrum to appear out of reggeon diagrams via infra-red divergences. Indeed, we will assume that anomaly poles survive higher-order corrections only when they are associated with a chiral symmetry.

Understanding that the infra-red divergence phenomenon that we are looking for should appear as a consequence of anomalies if a transverse momentum cut-off is imposed, the first step of our program is to look for this phenomenon within the multi-regge diagrams of  $CSQCD_S$  obtained by setting the mass of an  $SU(2)$  subgroup of gluons to zero.  $CSQCD_S$  contains an  $SU(2)$  triplet of massless (reggeized) gluons, plus two  $SU(2)$  doublets and one singlet of massive (reggeized) gluons. Each  $SU(3)$  triplet quark gives one  $SU(2)$  doublet and one singlet quark. Each  $SU(3)$  sextet quark gives one  $SU(2)$  triplet, one doublet, and one singlet quark. The color symmetry breaking can be done, as we discussed above, by initially adding a scalar field and using the usual Higgs mechanism (this is a technical manipulation that has nothing to do with electroweak symmetry breaking).

The main infra-red divergence of massless gluon reggeon diagrams is that associated with reggeization. Independently of the transverse momentum cut-off, this divergence exponentiates to zero all amplitudes with non-zero  $SU(2)$  color (in the reggeon channel), while leaving finite color zero amplitudes. As described in more detail in Appendix C, when an infra-red fixed point is present[21], the reggeon interaction kernels of color zero massless gluons have a crucial infra-red scaling property (the ultra-violet version of which produces the leading-order BFKL pomeron). This scaling is an essential component of the anomaly related infra-red divergences that we are looking for, as we now discuss.

We consider reggeon states which contain both an  $SU(2)$  color zero massless gluon component and an additional  $SU(2)$  color zero component - either a massive

gluon or a quark-antiquark pair. We consider the possibility of an infra-red divergence from the infra-red region where all the transverse momenta of the massless gluons scale uniformly to zero. If the massless gluons carry, overall, normal color parity (= the signature) they will interact with the additional color zero component and, as a result, any divergence that occurs will be exponentiated via reggeization effects, giving a zero amplitude. If, however, the massless gluon component carries anomalous ( $\neq$  the signature) color parity the divergence will not exponentiate. This is because, as explained in Appendix C, a gluon component of this kind can only couple to an anomaly vertex and anomalies can not occur in vector reggeon interactions that take place within a reggeon state. Consequently, the massless gluon component will have only self interactions, as illustrated in Fig. D4.

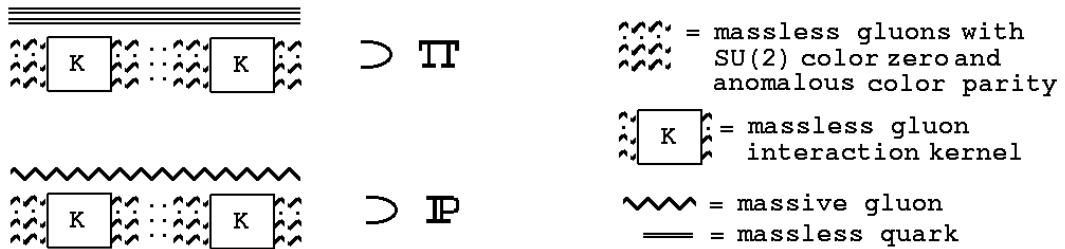
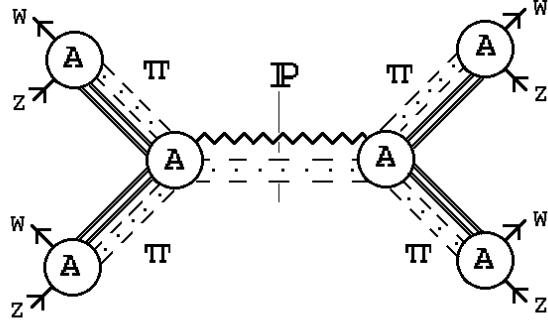


Fig. D4 Pomeron and pion reggeon states in  $CSQCD_S$ .

Provided there are external (to the reggeon state) anomaly vertices to which the complete reggeon states shown in Fig. D4 can couple the scaling property of the gluon self-interactions will produce a divergence (at zero transverse momentum for the gluons). The residue of this divergence contains a reggeon state that we can potentially identify as either a “pion” or a “pomeron”, as shown. If we can absorb this divergence into a “reggeon condensate”, this condensate will be an essential, zero transverse momentum, part of both the pion and the pomeron in  $CSQCD_S$ . Since “anomalous gluons” with  $SU(2)$  color zero necessarily have odd signature (three is the minimal number), the pomeron given by Fig. D4 will be an even signature regge pole that is exchange degenerate with an odd signature, massive gluon, reggeon. This, together with the existence of a “pomeron condensate”, are crucial features of supercritical RFT. Also, since all amplitudes have  $SU(2)$  color zero, if pion anomaly poles appear as we anticipate, we will have a spectrum with confinement and chiral symmetry breaking.

For the pion and pomeron to appear as in Fig. D4, via infra-red divergences, Fig. D2 has to be realized by the appearance of a “lowest-order” amplitude, of the form shown in Fig. D5, in which an anomaly that can couple the reggeon states appears in each vertex (as indicated by the  $A$ ). The notation for Fig. D5 is the same as that for Fig. D4 except that a new notation is introduced to indicate that each of the massless gluons now carries zero transverse momentum.



 = vertex containing an anomaly  
 = massless gluons with zero  $SU(2)$  color, anomalous color parity, and zero transverse momentum

Fig. D5 Anomaly vertices that must appear in the pion amplitude.

The external anomaly vertices needed for Fig. D5 are identical to those that appear in our recent paper[12] deriving elastic scattering amplitudes of electroweak vector bosons. In that paper we demonstrated that anomalous color parity gluons have the needed coupling. In the elastic scattering context, it is very clear how the use of a cut-off removes bad, large transverse momentum based, high-energy behavior produced by the anomalies and, instead, introduces anomaly dominated infra-red divergences that potentially produce “non-perturbative” anomaly pole Goldstone bosons. Although we did not discuss the generation of the anomaly pole explicitly in [12], we did give a brief summary of how the anticipated infra-red divergences should be mapped onto RFT and the amplitude for pion exchange obtained.

The anomaly vertices obtained in [12] contain triangle diagrams resulting from the contraction of larger loop feynman diagrams as illustrated in Fig. D6.

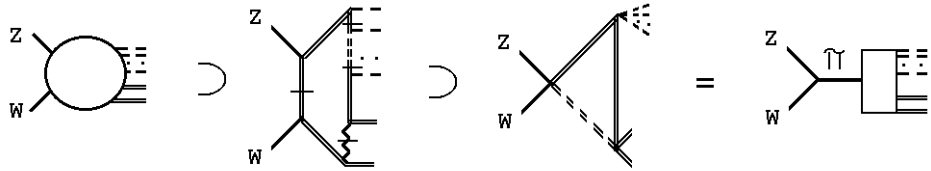


Fig. D6 Generation of an effective triangle diagram containing an anomaly pole.

(A hatch on a line indicates that it is on-shell.) As described in Appendix B, an anomaly pole is generated in the triangle diagram by a zero momentum quark line (the partially broken line in Fig. D6). It is important that it is the longitudinal polarization of the on-shell massive vector boson that produces the quark/antiquark

coupling in the anomaly triangle diagram. Note that, in the calculation of [12], the on-shell massive gluon in Fig. D6 was replaced by a massive electroweak vector boson.

The anomaly that occurs in diagrams that contribute to the pion/pion/pomeron vertex in Fig. D5 is discussed in [14] and [53]. The reduction to a triangle diagram is as illustrated in Fig. D7 and it is the U(1) anomaly that is involved.

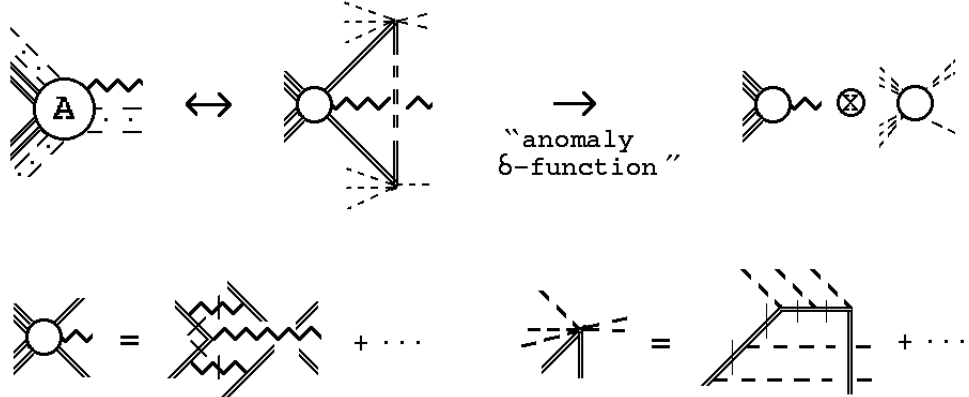


Fig. D7 The reduction to a triangle diagram that involves the U(1) anomaly.

(The notation is the same as in previous diagrams.) The anomaly pole is present but, because it is integrated over, it contributes as an “anomaly  $\delta$ -function” and plays the remarkable role, also illustrated in Fig. D7, that it factorizes off the (zero transverse momentum) anomalous gluon interaction from the remaining “hard interaction”. The anomaly  $\delta$ -function is again generated by a zero momentum quark line (illustrated by a broken line in Fig. D7) which undergoes a chirality transition. The hard interaction production of a massive gluon has an overall axial vector nature that compensates for this transition. To produce the axial coupling it is essential that the exchanged on-shell massive gluons within the hard interaction are longitudinal. (It is also important that these gluons carry zero light-cone momentum in a frame in which the pion carries finite light-cone momentum.)

Because each of the external reduced triangle diagrams that we have discussed contain anomaly contributions, imposing a transverse momentum cut-off will lead to a violation of Ward identities for the gluons coupling to such vertices. A scaling transverse momentum divergence should then appear in each pion channel and generate Fig. D5, as we have discussed above. We anticipate that there will be an overall logarithmic divergence as the transverse momenta in all channels are scaled uniformly to zero and that this is what we will have to factorize off to obtain the physical amplitude. However, to be sure of this and to elaborate the divergence phenomenon in full requires more details of the calculation than we presently have. We have, so far, carried out the full analysis only in the situation described in [13] in which we used

the pion anomaly pole approximation that we describe in Section 2.

For the more general case of the reggeized pion amplitude appearing in Fig. D5, we can say the following. The divergence is at zero transverse momentum, which (in an appropriate frame) should be equivalent to zero four momentum for the gluon vertex of the effective triangle diagram in Fig. D6. From (B.13), we see that in this kinematic configuration the triangle diagram amplitude reduces to a “pion” anomaly pole, as illustrated in Fig. D6. Thus, as we have anticipated, the anomaly pole should provide the mechanism whereby a pion particle pole appears (in the residue of the infra-red divergence) as part of the pion reggeon state.

To obtain the multi-regge amplitudes of  $QCD_S$  from those of  $CSQCD_S$ , via RFT, it is clearly necessary to understand in complete detail how the full set of divergent  $CSQCD_S$  diagrams maps onto super-critical RFT. In higher-orders we expect to find vertices, of the form shown in Fig. 10, in which massive gluons are produced by a wee gluon interaction only. Interactions of this kind should lead to particle pole interactions within pomeron vertices, just as is produced by the pomeron condensate in the supercritical pomeron phase[20].

Although there is every indication that the reggeon diagrams of  $CSQCD_S$  can be mapped onto supercritical RFT, it remains a major challenge to carry out the mapping in full. Our hope is that the (relative) simplicity of the external vector boson couplings, appearing in Fig. D6, will finally make it feasible. It also remains to be determined how a pion anomaly pole, which occurs at zero transverse momentum, combines with reggeization at spacelike momentum transfer. In the anomaly pole vertex method[13], that we use in Section 2, we effectively assume that the on-shell pion couplings can be obtained by an anomaly pole coupling of the form shown in Fig. D7. While the above discussion suggests that this should be a straightforward outcome of the full multi-regge calculation, it remains to be shown.

With the mapping of  $CSQCD_S$  onto supercritical RFT established, it should be straightforward to show that the high-energy behavior of  $QCD_S$  is that of the Critical Pomeron. Critical Pomeron amplitudes can be, and have been, calculated without reference to QCD. There will, however, be much to understand about the limiting process involved, particularly with respect to the formation of baryons. For our present purposes we have, in Sections 2 and 3, concentrated on the underlying physical phenomenon which describes the pomeron in  $QCD_S$ .

## References

- [1] A. R. White, "The Reggeon Field Theory Beyond the Critical Point ...", CERN Preprint TH.2259, January, 1977.
- [2] A. R. White, Proceedings of the Int. Conf. on High Energy Physics, Tokyo (1978).
- [3] A. A. Migdal, A. M. Polyakov and K. A. Ter-Martirosyan, *Zh. Eksp. Teor. Fiz.* **67**, 84 (1974); H. D. I. Abarbanel and J. B. Bronzan, *Phys. Rev.* **D9**, 2397 (1974).
- [4] W. J. Marciano, *Phys. Rev.* **D21**, 2425 (1980).
- [5] E. Braaten, A. R. White and C. R. Willcox, *Int. J. Mod. Phys.*, **A1**, 693 (1986).
- [6] A. R. White, "Sextet Quark Physics at the Tevatron? ", hep-ph/0405190.
- [7] A. R. White, "The Sextet Higgs Mechanism and the Pomeron ". Presented at 34th International Symposium on Multiparticle Dynamics (ISMD 2004) - hep-ph/0409181.
- [8] A. R. White, Proceedings of the 8th International Symposium on Very High Energy Cosmic Ray Interactions, Tokyo (1994).
- [9] A. R. White, hep-ph/9704248 (1997)
- [10] T. E. Clark, C. N. Leung, S. T. Love and J. L. Rosner, *Phys. Lett.* **B177**, 413 (1986).
- [11] For a detailed description of Gribov's confinement picture and for references to the original papers see Y. L. Dokshitzer and D. E. Kharzeev, hep-ph/0404216 (2004).
- [12] A. R. White, *Phys. Rev.* **D69**, 096002 (2004).
- [13] A. R. White, *Phys. Rev.* **D66**, 056007 (2002).
- [14] A. R. White, *Phys. Rev.* **D66**, 045009 (2002).
- [15] V. N. Gribov, *Nucl. Phys.* **B139**, 1 (1978), S. Mandelstam, *Phys. Rev.* **D19**, 2391 (1978).
- [16] C. Ewerz, "The Perturbative Pomeron and the Odderon: Where Can We Find Them?" hep-ph/0403051.

- [17] Y. Iwasaki, K. Kanaya, S. Kaya, S. Sakai, T. Yoshie, *Phys. Rev.* **D69**, 014507 (2004).
- [18] ZEUS Collaboration (M. Derrick et al.), *Z. Phys.* **C74** 207 (1997).
- [19] J. B. Kogut, M. A. Stephanov, D. Toublan, J. J. M. Verbaarschot and A. Zhitnitsky, *Nucl. Phys.* **B582**, 477 (2000).
- [20] A. R. White, *Int. J. Mod. Phys.* **A11**, 1859 (1991).
- [21] A. R. White, *Phys. Rev.* **D29**, 1435 (1984) and references therein.
- [22] K. Kang and A. R. White, *Int. J. Mod. Phys.* **A2**, 409 (1987).
- [23] ZEUS Collaboration (S. Chekanov et al.), hep-ex/0401003.
- [24] H1 Collaboration (C. Adloff et al.), *Eur. Phys. J.* **C30**, 1 (2003).
- [25] S. Bentvelsen, J. Engelen and P. Kooijman, Physics at Hera, Vol. 1, 23.
- [26] H1 Collaboration (C. Adloff et al.), *Z. Phys.* **C74** 191 (1997).
- [27] G. E. Forden, presentation at ISMD94. See also D0 Collaboration (S. Abachi et al.). FERMILAB-CONF-95-218-E (1995), presented at HEP 95.
- [28] UA1 Collaboration (C. Albajar et al.), *Phys. Lett.* **B193** 389 (1987).
- [29] CDF Collaboration (T. Affolder et al.), *Phys. Rev. Lett.* **88** 042001 (2002).
- [30] CDF Collaboration, “CDF-QCD Group Run 2 Results” - <http://www-cdf.fnal.gov/physics/new/qcd/inclusive/index.html>.
- [31] CDF Collaboration, “CDF-QCD Group Run 2 Results” - <http://www-cdf.fnal.gov/physics/new/qcd/ktjets/ktjets.html>.
- [32] See S. I. Nikolsky, *Phys. Atom. Nucl.* **62**, 2048 (1999), for references.
- [33] D. Kazanas and A. Nicolaidis, *Gen. Rel. Grav.* **35**, 1117 (2003) - hep-ph/0109247; “Cosmic Ray Spectrum ”Knee”: A Herald of New Physics?” - astro-ph/0103147.
- [34] S. Barshay and G. Kreyerhoff, *Mod. Phys. Lett.* **A16**, 1061 (2001) - hep-ph/0005022.
- [35] Z. Cao, L. K. Ding, Q. Q. Zhu, Y. D. He, *Phys. Rev.* **D56** 7361 (1997).

- [36] O. V. Tarasov, A. A. Vladimirov and A. Yu. Zharkov, *Phys. Lett.* **B93**, 429 (1980).
- [37] T. Banks and A. Zaks, *Nucl. Phys.* **B196**, 189 (1982).
- [38] D. J. Gross and F. Wilczek, *Phys. Rev.* **D8**, 3633 (1973).
- [39] T. P. Cheng, E. Eichten and L. F. Li, *Phys. Rev.* **D9**, 2259 (1974).
- [40] V. N. Gribov, “Gauge Theories and Quark Cofinement”, published by PHASIS Research and Publishing Corporation, Moscow (2002).
- [41] V. S. Fadin, E. A. Kuraev and L. N. Lipatov, *Sov. Phys. JETP* **45**, 199 (1977); V. S. Fadin and L. N. Lipatov, *Nucl. Phys.* **B406**, *Nucl. Phys.* **B477**, 767 (1996) and further references therein.
- [42] J. B. Bronzan and R. L. Sugar, *Phys. Rev.* **D17**, 585 (1978), this paper organizes into reggeon diagrams the results from H. Cheng and C. Y. Lo, *Phys. Rev.* **D13**, 1131 (1976), **D15**, 2959 (1977).
- [43] V. S. Fadin and V. E. Sherman, *Sov. Phys. JETP* **45**, 861 (1978).
- [44] J. Bartels, *Z. Phys.* **C60**, 471 (1993) and further references therein.
- [45] R. Kirschner, *Nucl. Phys. Proc. Suppl.* **51C**, 118 (1996).
- [46] A. R. White, *J. Mod. Phys.* **A8**, 4755 (1993).
- [47] A. Sen, *Phys. Rev.* **D27** 2997 (1983) and unpublished work on non-abelian gauge theories.
- [48] V. N. Gribov, I. Ya. Pomeranchuk and K. A. Ter-Martirosyan, *Phys. Rev.* **139B**, 184 (1965).
- [49] A. R. White, “The Past and Future of S-Matrix Theory”, hep-ph/0002303, published in “Scattering”, edited by E. R. Pike and P. Sabatier (Academic Press, 2002).
- [50] A. R. White, *Phys. Rev.* **D58**, 074008 (1998). This paper describes all the necessary multi-regge limits, as well as the construction of multi-reggeon diagrams via reggeon unitarity.
- [51] A. R. White, *Nucl.Phys.Proc.Suppl.* **96**, 277 (2001).
- [52] A. R. White, CERN preprint TH.2976 (1980) - a summary of this paper is presented in the Proceedings of the XVIth Rencontre de Moriond, Vol. 2 (1981).

[53] A. R. White, *Phys. Rev.* **D63**, 016007 (2001).

